CARBON DIOXIDE ACTIVATION AND SUBSEQUENT REDUCTION TO VALUE-ADDED CHEMICALS AND FUELS ON GRAPHITIC CARBON NITRIDE SURFACES

Hariprasad N (Reg. No. 4403)
Research Guide: Dr. Harindranathan Nair

School of Environmental Studies,
Cochin University of Science and Technology, Cochin

Presynopsis
(26/07/2023)

Table of Contents

Table of Contents

Table of Contents

Activation of Small Molecules

CO_2, CO, NO, N_2O, N_2, H_2, CH_4, H_2O, O_2

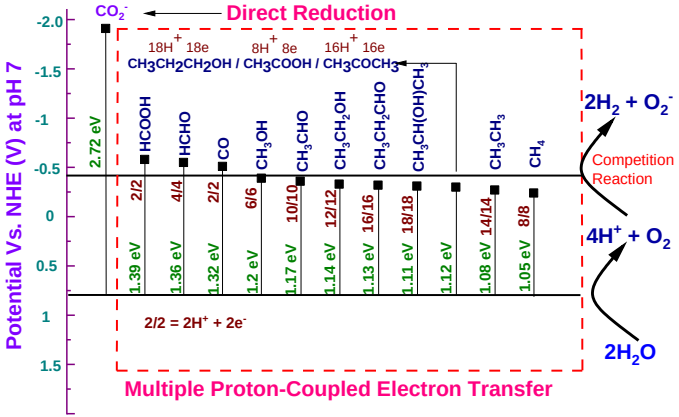

Table of Contents

Experimental

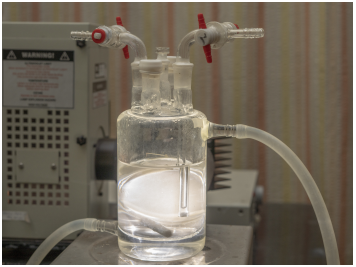

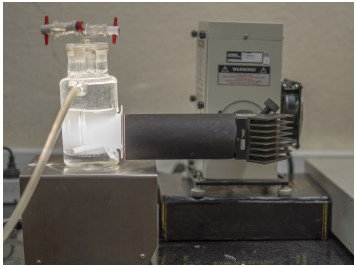

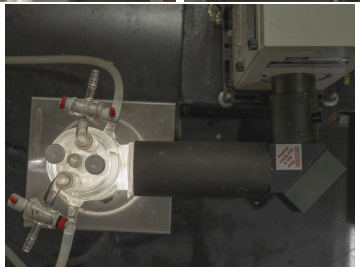

Objectives

1. Revisiting the existing paradigm of carbon dioxide photo-reduction and material design criteria adopted
2. Assess and optimize the catalytic efficiency of graphitic carbon nitride surfaces.
3. Mechanistic Insights: Gaining a comprehensive understanding of the reaction mechanisms involved in carbon dioxide activation and reduction is of paramount importance. This objective seeks to unveil the underlying chemical processes and reaction intermediates responsible for the transformation of carbon dioxide into valuable products.

Table of Contents

Context

- **How the Surface Functionalities and Other Properties Change with the Precursor?** The properties of g-C_3N_4 surface, including surface functionalities and photoreduction activity, can be tuned by changing the precursor used in the synthesis process.
- **How Defect States Will Change?** The defect states of g-C_3N_4 also play an important role in determining its photoreduction activity. The precursor used in synthesis can affect the formation and distribution of defect states on the g-C_3N_4 surface.

Context

- **How it all Affect the Carbon Dioxide Photoreduction?** The changes in the surface functionalities, properties, and defect states of g-C_3N_4 with different precursors can significantly impact its CO_2 photoreduction performance.
- **Importance of the Study and Output to the Scientific Community** This study aims to understand the influence of precursors on the properties of g-C_3N_4 surface towards CO_2 photoreduction, providing valuable insights into the optimization of g-C_3N_4 for CO_2 photoreduction applications. These findings of this study will contribute to the scientific community's efforts to mitigate CO_2 emissions and develop sustainable energy technologies.

Synthesis Procedure

1. Analysis of the precursor: The precursor received is analyzed using XRD to confirm the suitable compound received.
2. Mixing and sonication: 10 g of the precursor is mixed well with 100 mL acetone and sonicated for 15 min for complete mixing in a 250 mL beaker.
3. Recrystallization: The recrystallization procedure for melamine, cyanamide, dicyandiamide, urea, thiourea, and ammonium thiocyanate in acetone was conducted.
4. Heating: The alumina crucible is placed in a SIGMA Laboratory Muffle Furnace for 4 h with a ramping rate of 2 °C min. The samples are removed once the oven reaches room temperature.
5. Grinding: The resultant hard yellow block of graphitic carbon nitride formed is transferred into a mortar and ground well using a pestle.
6. Storage: The delicate yellow powder is transferred into a 25 mL storage amber glass vial with an air-tight cap.

Chemical Structures

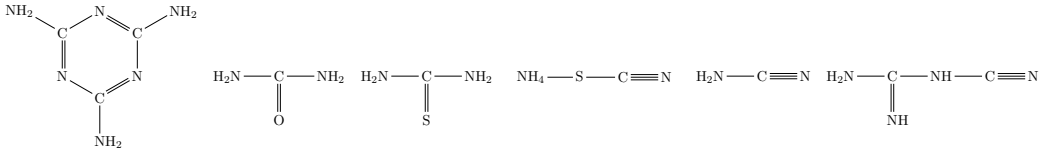

Chemical structures of the precursors

The bottles used in the experiment were labelled as follows: AT-gCN, CY-gCN, DC-gCN, MEL-gCN, TU-gCN, and U-gCN. Each label corresponds to a specific type of carbon nitride prepared from different precursors. The carbon nitride samples were prepared using the following precursors: ammonium thiocyanate (AT), cyanamide (CY), dicyandiamide (DC), melamine (MEL), thiourea (TU), and urea (U).

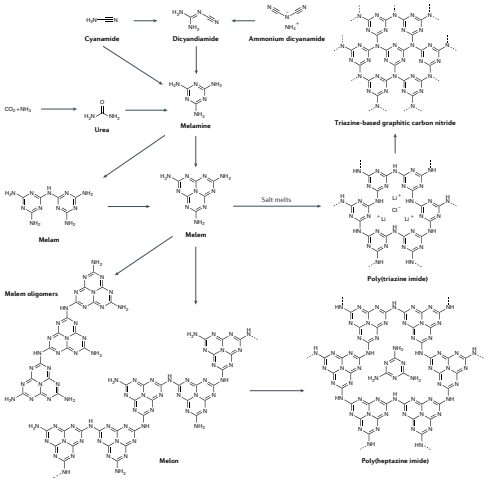

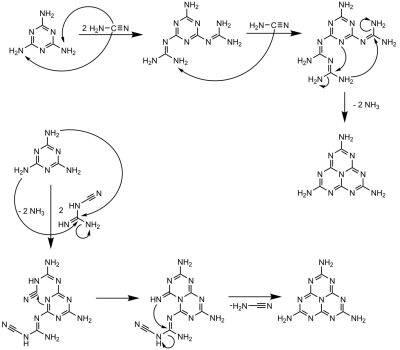

Z. Anorg. Allg. Chem. **2019**, 645: 857-862; *J. Appl. Chem.* **1959**, 9, 340-344;
J. Am. Chem. Soc. **1984**, 106, 2805-2811.

X-Ray Diffraction Analysis

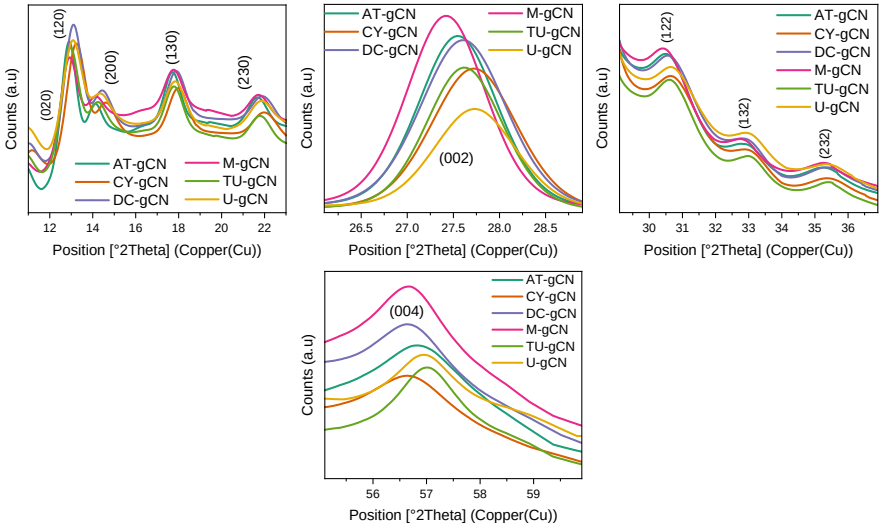

X-Ray Diffraction Analysis: LeBail Fits

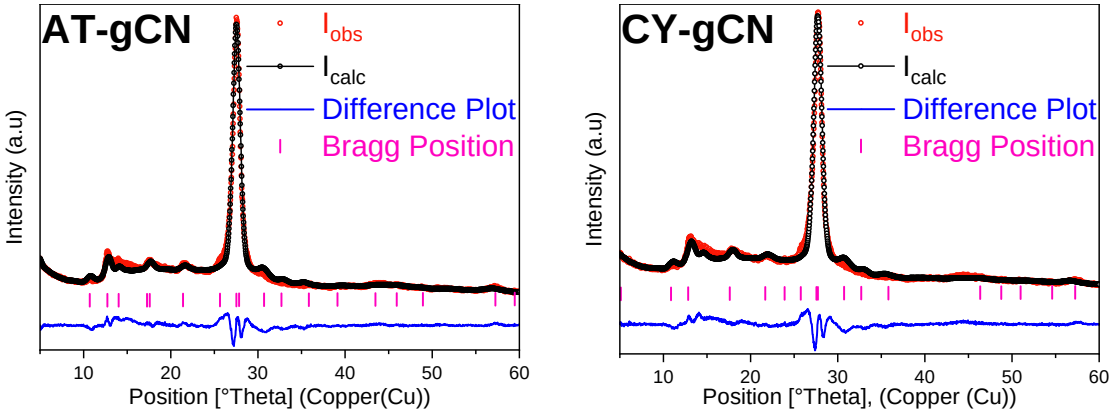

Proc. R. Soc. Lond. **1913**, A88428–438; *J. Appl. Cryst.* **1969**. 2, 65-71; *J. Appl. Cryst.* **1982**, 15, 361–374; *J. Appl. Cryst.* **1995**, 28, 738–744; *Nucl. Instrum.* **1958**, 3, 223; *J. Appl. Cryst.* **1992**, 25, 109–121; *Powder Diffr.* **2007b**, 22, 268–278; *Powder Diffr.* **2011**, 26, 88–93.

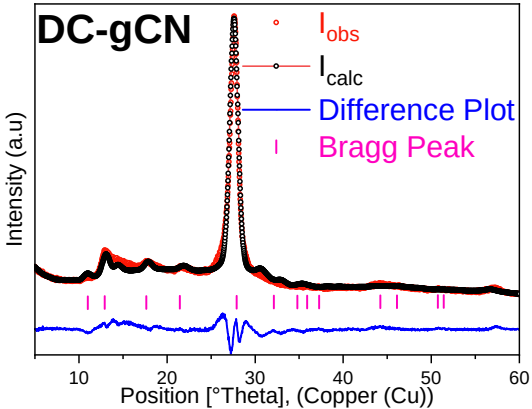
DC-gCN
I_{obs}
I_{calc}
Difference Plot
Bragg Peak
Intensity (a.u)
10
20
30
40
50
60
Position [°Theta], (Copper (Cu))

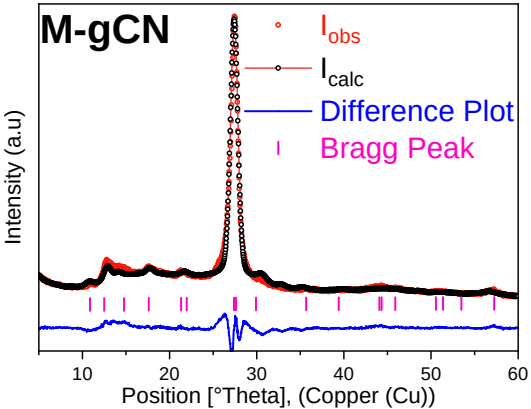
M-gCN
I_{obs}
I_{calc}
Difference Plot
Bragg Peak
Intensity (a.u)
10
20
30
40
50
60
Position [°Theta], (Copper (Cu))

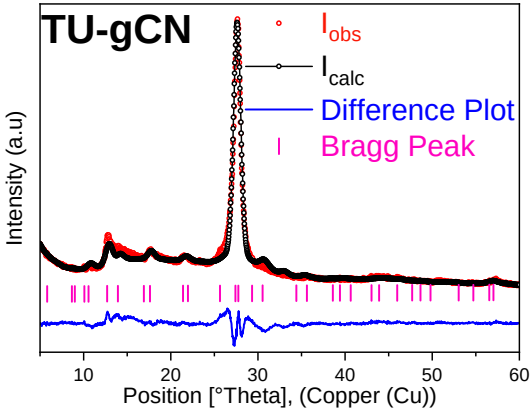
TU-gCN
I obs
I calc
Difference Plot
Bragg Peak
Intensity (a.u)
10
20
30
40
50
60
Position [°Theta], (Copper (Cu))

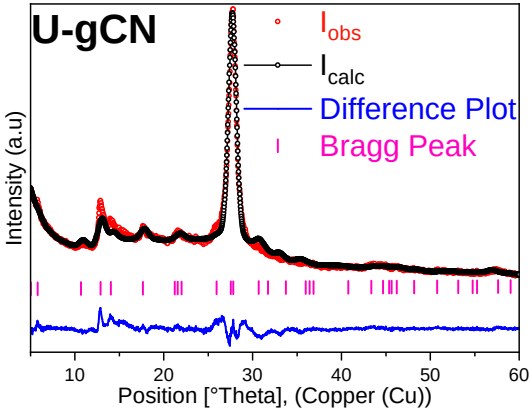
U-gCN
I obs
I calc
Difference Plot
Bragg Peak
Intensity (a.u)
10
20
30
40
50
60
Position [°Theta], (Copper (Cu))

XRD Analysis Table

	Peak Position		Peak Height		FWHM		d-spacing		Peak Area		Particle Size
(hkl) →	(120)	(002)	(120)	(002)	(120)	(002)	(120)	(002)	(120)	(002)	
AT-gCN	12.88	27.53	531.87	6714.82	0.83	1.02	6.87	3.24	482.61	8082.24	9.37
CY-gCN	13.21	27.70	474.89	5536.13	1.01	1.11	6.69	3.22	698.37	7211.91	8.02
DC-gCN	13.08	27.58	530.07	6577.41	0.97	1.11	6.76	3.23	564.33	8614.82	8.09
M-gCN	12.89	27.39	391.04	7456.07	0.92	1.01	6.86	3.25	394.88	8906.91	8.68
TU-gCN	12.97	27.59	229.07	5577.94	0.94	0.99	6.84	3.23	236.22	6540.69	8.77
U-gCN	13.08	27.71	214.25	3880.81	1.03	1.05	6.78	3.27	241.73	4832.18	8.14

Chem. Mater. **2015**, 27, 7, 2612–2618,*J. Phys.: Condens. Matter*, **2013**, 25, 395402, *Jpn. J. Appl. Phys.* **2011**, 50, 095503, *Jpn. J. Appl. Phys.* **2020**, 59, 080907

Pertinent Crystallographic Data Deduced

	AT-gCN	CY-gCN	DC-gCN	M-gCN	TU-gCN	U-gCN
Structure Type	Crystal	Crystal	Crystal	Crystal	Crystal	Crystal
Space Group:	P 21 21 2	P 21 21 2	P 21 21 2	P 21 21 2	P 21 21 2	P 21 21 2
Crystal System	Orthorhombic	Orthorhombic	Orthorhombic	Orthorhombic	Orthorhombic	Orthorhombic
a	12.5900	12.5600	12.5100	12.5200	12.4900	12.5900
b	16.3900	16.6300	16.5000	16.2500	16.3500	16.5400
c	6.4700	6.5400	6.5200	6.4800	6.4600	6.4910
Alpha	90	90	90	90	90	90
Beta	90	90	90	90	90	90
Gamma	90	90	90	90	90	90
Cell Volume	1335.085	1366.028	1345.826	1318.356	1319.206	1351.677
Asymmetric Unit	36 sites	36 sites	36 sites	36 sites	36 sites	36 sites
Unit Cell	144 sites/unit cell	144 sites/unit cell	144 sites/unit cell	144 sites/unit cell	144 sites/unit cell	144 sites/unit cell
Density	2.0017 g/cm^3	1.9564 g/cm^3	1.9858 g/cm^3	2.0271 g/cm^3	2.0258 g/cm^3	1.9772 g/cm^3
Rexp	3.22278	3.67344	3.49739	3.13598	3.35939	3.25745
Rp	6.6254	6.78451	6.88073	6.4663	6.56856	4.98192
Rwp	8.95199	8.95923	9.04364	8.66453	8.84663	6.85618
GOF	7.71573	5.94834	6.68649	7.63386	6.93481	4.43006

Z= number of molecules (or formula units) in the unit cell, Rexp= R Expected, Rp= R Profile, Rwp= R Weighted Profile, GOF= Goodness of Fit

Structure Elucidation: Layer, Packing and Asymmetric Structure of AT-gCN

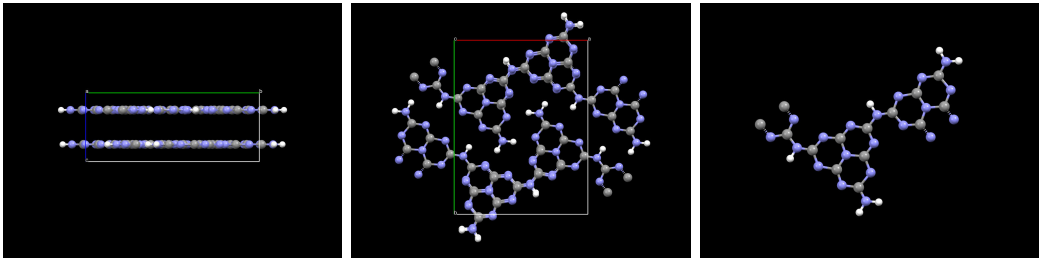

The B. E. T Surface Area

	S.A	C
AT-gCN	29.48	**-681.09**
CY-gCN	14.46	823.582
DC-gCN	14.1	**-585.807**
M-gCN	14.65	306.52
TU-gCN	15	**-239.13**
U-gCN	110.08	272.295

S.A= B.E.T surface area, C= B.E.T constant

Is the B.E.T equation applicable?

Charact. Porous Solids Vii - Proc. 7th Int. Symp. . Charact. Porous Solids **2006**, pp. 49-56; *Adv. Mater.* **2022**, 34, 2201502; https://github.com/fairen-group/betsi-gui; *Pure Appl. Chem.* **2015**, 9-10(87), 1051-1069, *J. Open Source Softw.* **2023**, 8, 86; *J. Phys. Chem. C* **2019**, 123, 33, 20195–20209; *J. Phys. Chem. Lett.* **2020**, 11, 14, 5412–5417

B.E.T Surface Identification (BETSI) Analysis

BETSI Method Overview

- The BETSI algorithm is a powerful tool for analyzing adsorption isotherms.
- It utilizes linear regressions, full B.E.T analyses, and matrix operations.
- Written in Python, leveraging the NumPy library.
- BETSI Outputs and Diagnostics: Six plots for result validation
  - Isotherm with optimal linear region and B.E.T fit.
  - Rouquerol representation: $N(1 - \frac{P}{P_0})$ vs. $\frac{P}{P_0}$.
  - Linearized plot with OLS regression and parameters.
  - Filtered percentage error vs. B.E.T areas with knee and optimal B.E.T area.
  - Filtered monolayer loadings plot.
  - Statistical distribution of permissible B.E.T areas (boxplot).

SESAMI (Script to Estimate the Surface Area of Materials from their Isotherms) performs Brunauer-Emmett-Teller (BET), BET+Excess Sorption Work (ESW), and Machine Learning (ML) methods for surface area estimation in nanoporous materials.

BET Surface Identification (BETSI) Analysis of AT-gCN

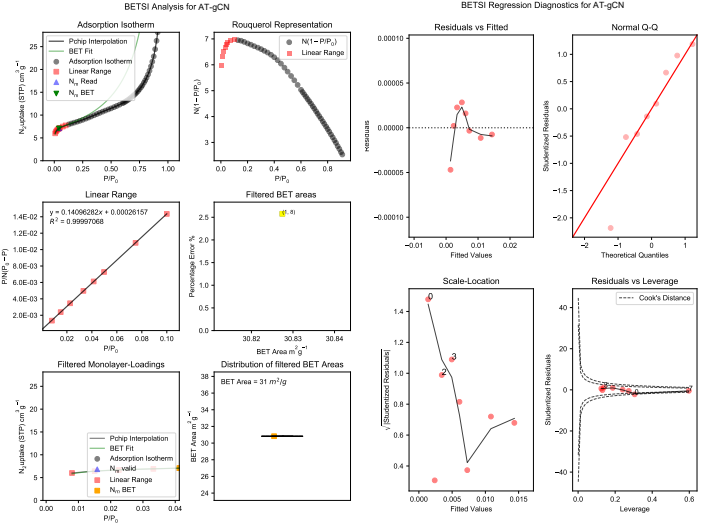

BET Surface Identification (BETSI) Analysis of CY-gCN

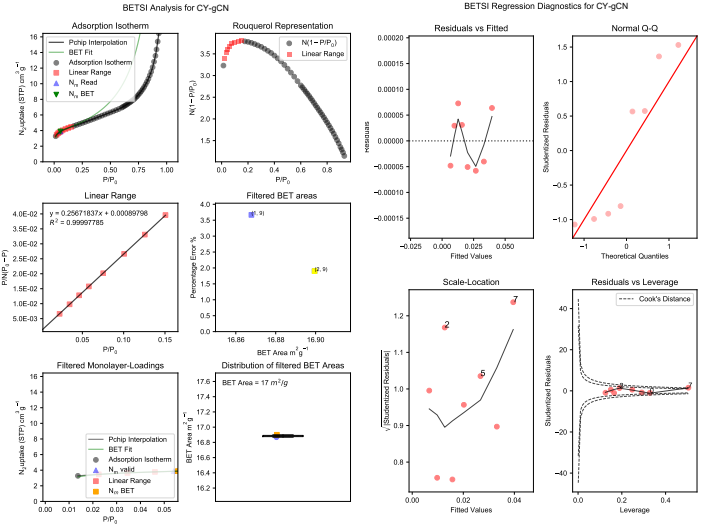

BET Surface Identification (BETSI) Analysis of DC-gCN

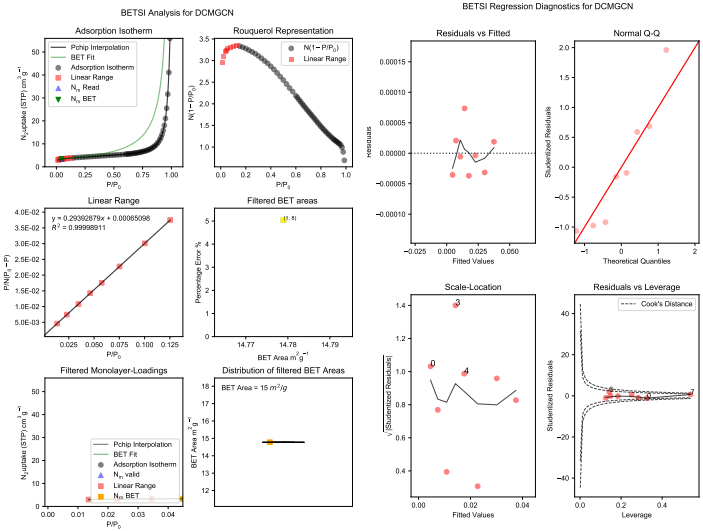

BET Surface Identification (BETSI) Analysis of M-gCN

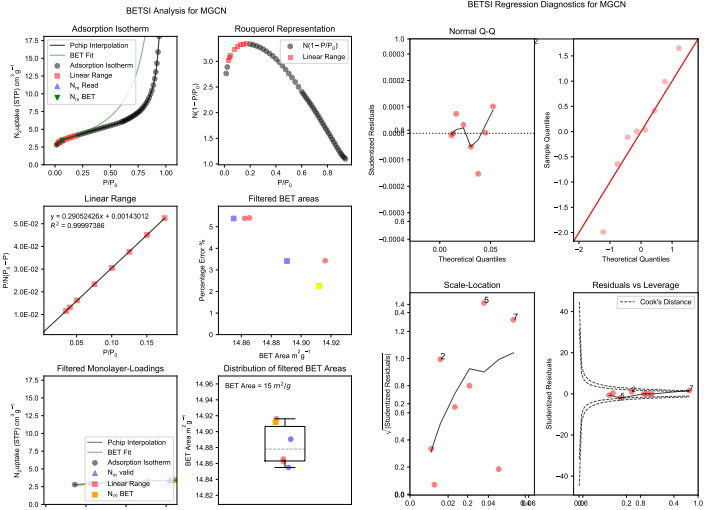

BET Surface Identification (BETSI) Analysis of TU-gCN

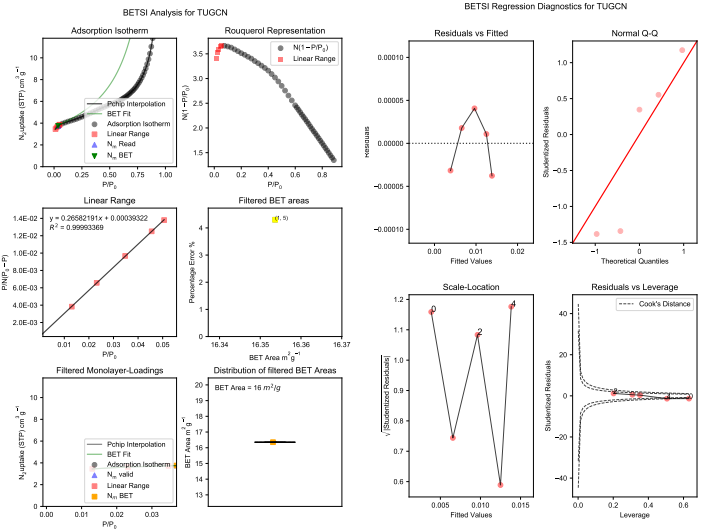

BET Surface Identification (BETSI) Analysis of U-gCN

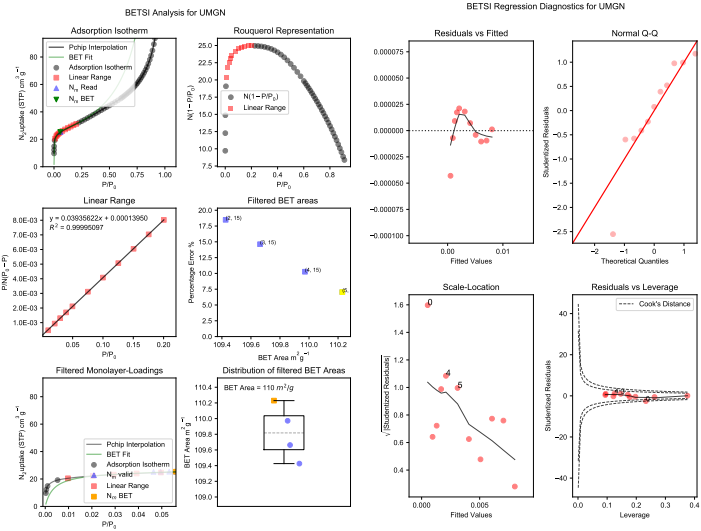

SESAMI Analysis

SESAMI (Script to Estimate the Surface Area of Materials from their Isotherms) performs Brunauer-Emmett-Teller (BET), BET+Excess Sorption Work (ESW), and Machine Learning (ML) methods for surface area estimation in nanoporous materials.

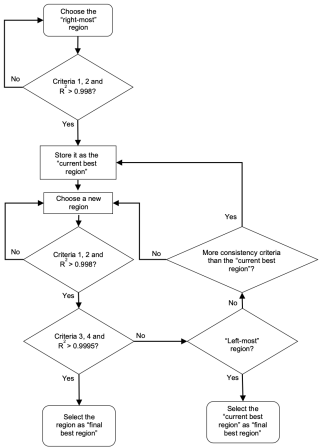

Figure S2: Flowchart of the algorithm implemented to determine the BET linear region.

SESAMI Analysis of AT-gCN

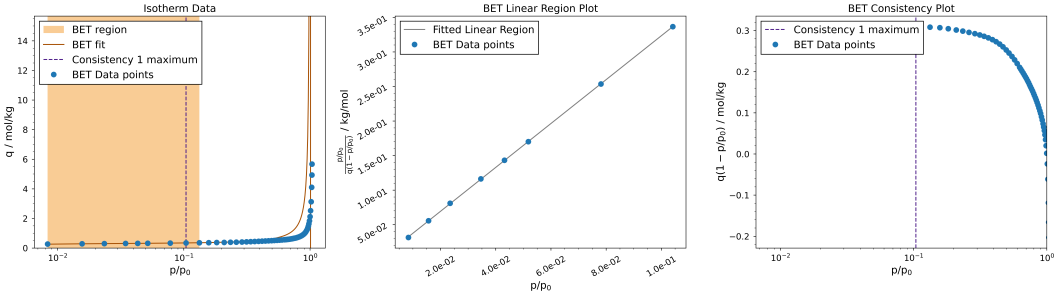

SESAMI Analysis of CY-gCN

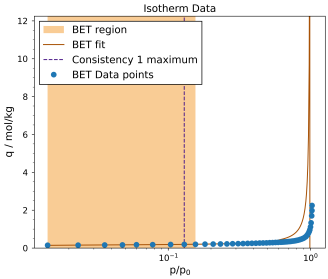

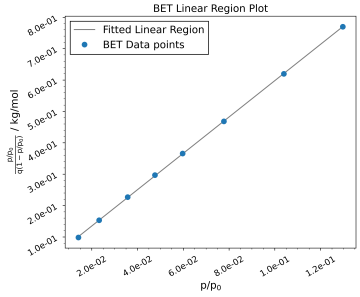

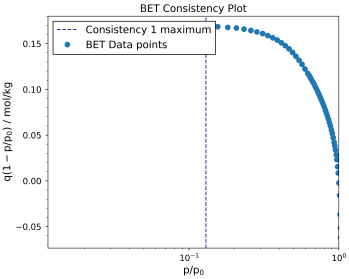

SESAMI Analysis of DC-gCN

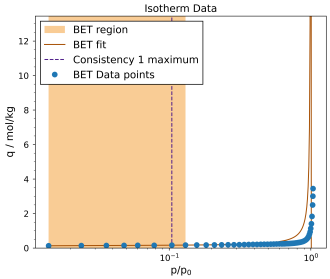

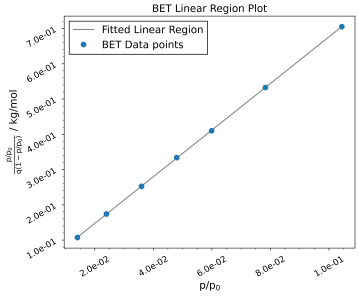

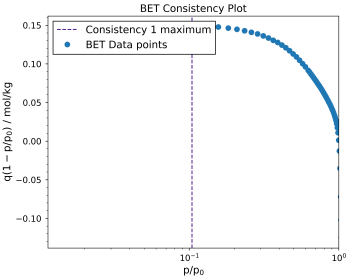

SESAMI Analysis of M-gCN

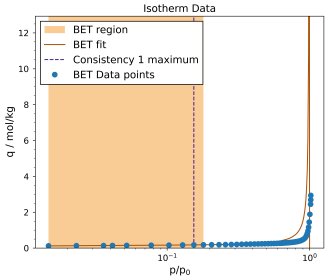

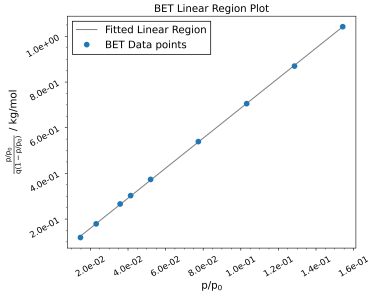

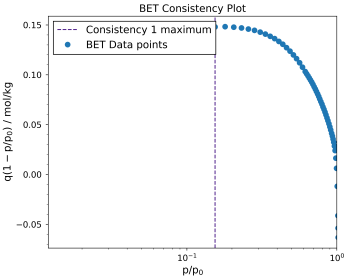

SESAMI Analysis of TU-gCN

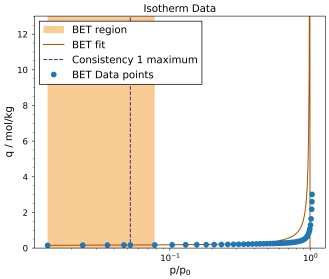

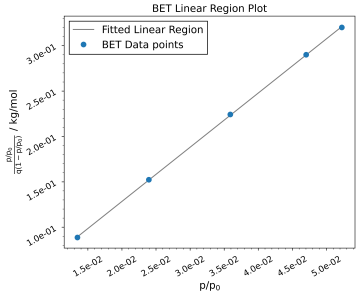

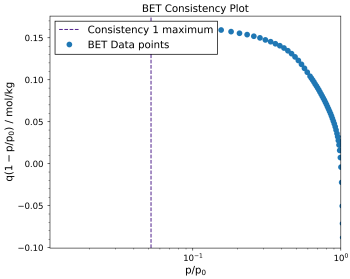

SESAMI Analysis of U-gCN

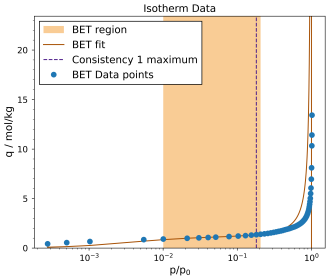

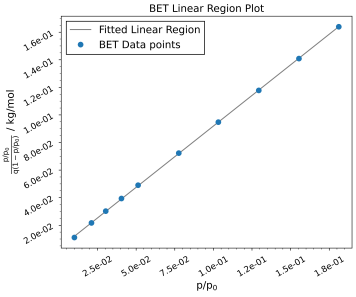

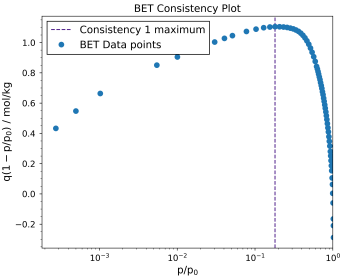

Surface Area Analysis: BETSI vs. SESAMI Method

	Surface Area, m^2/g							
	B.E.T	**BETSI**	**SESAMI**	**C, SESAMI**	**qm, mol/kg**	**Pore Size, nm**	**t-plot M.A**	**%micropore**
AT-gCN	29.48	31	30.7	547.6	0.31	26.67	10.41	33.92
CY-gCN	14.46	17	16.8	304.9	0.17	18.94	4.53	26.97
DC-gCN	14.1	15	14.7	452.3	0.15	33.89	5.54	37.67
M-gCN	14.65	15	14.8	231.3	0.15	27.79	3.29	22.29
TU-gCN	15	16	16.3	670.4	0.17	27.83	6.61	40.56
U-gCN	110.08	110	109.5	292.4	1.12	16.91	16.77	15.31

Physical Adsorption Characterization

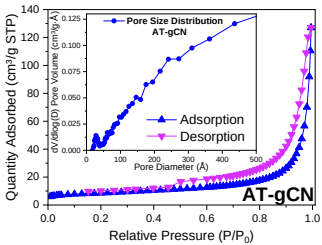

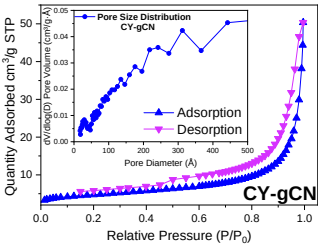

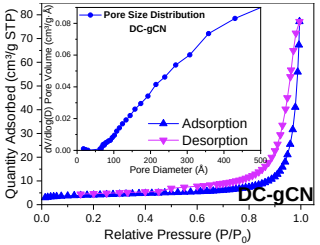

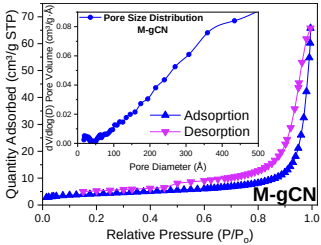

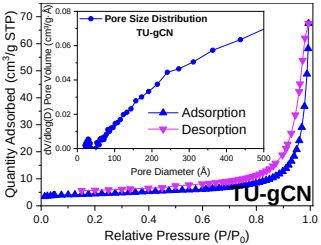

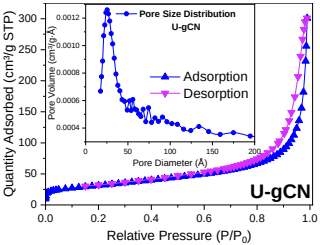

CO_2 Conversion Yield w.r.t Surface Area

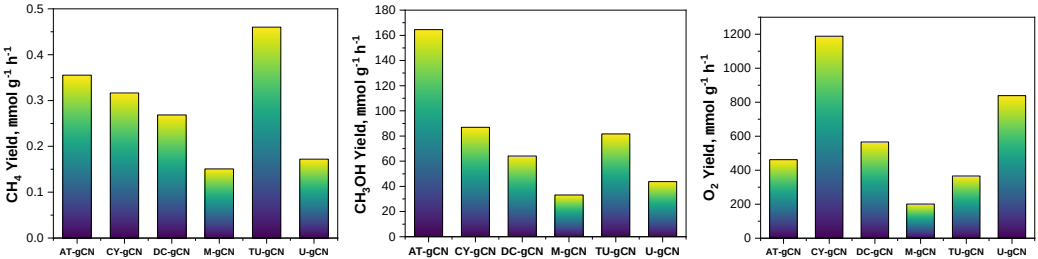

- Conventional reporting of the CO_2 conversion.
- w.r.t surface area

CO_2 Conversion Yield in Unit Surface Area

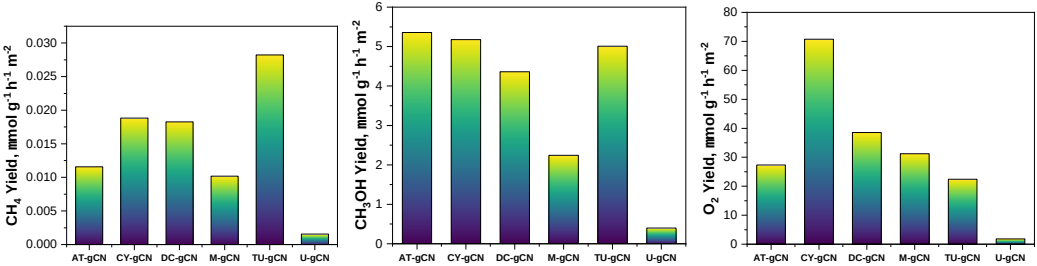

Isotherm Summation

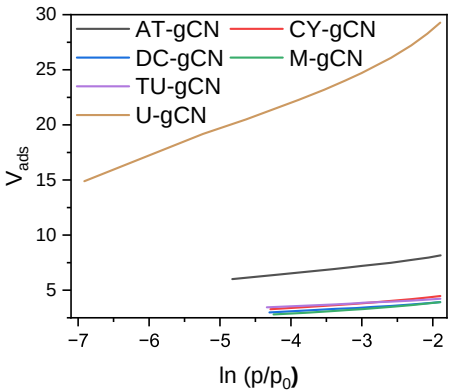

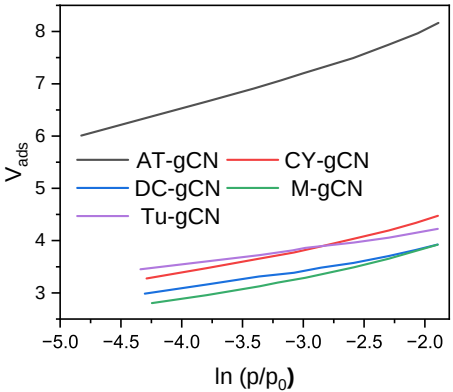

First Derivative Isotherm Summation

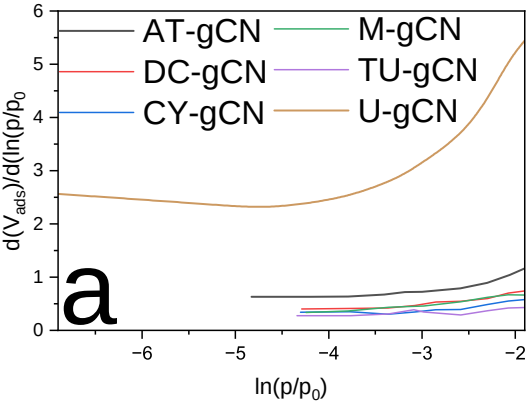

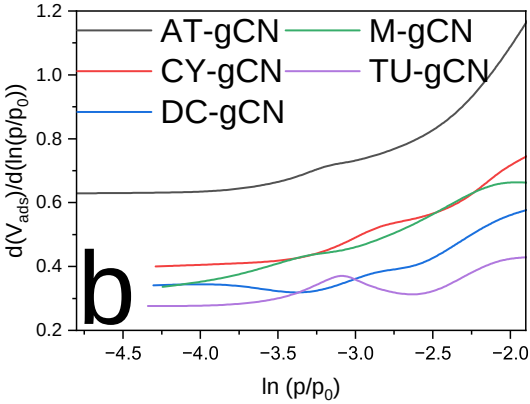

Second Derivative Isotherm Summation

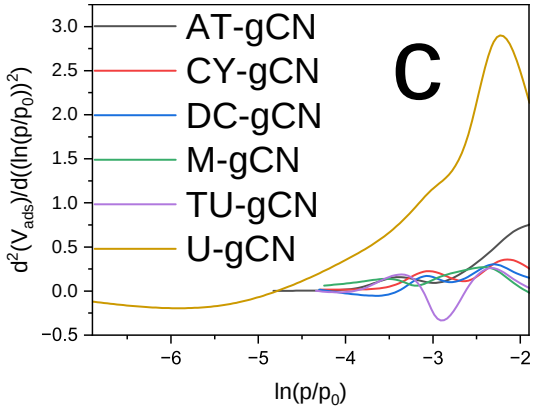

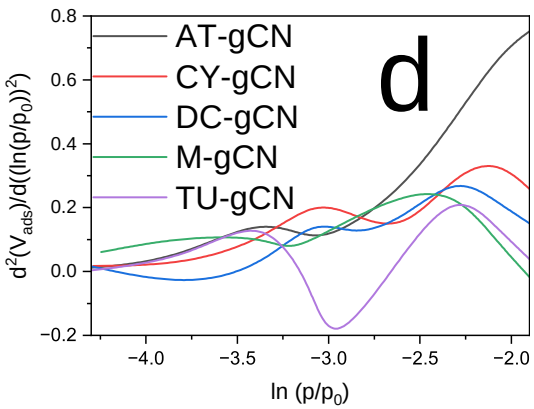

Field Emission Scanning Electron Microscopy (FESEM)

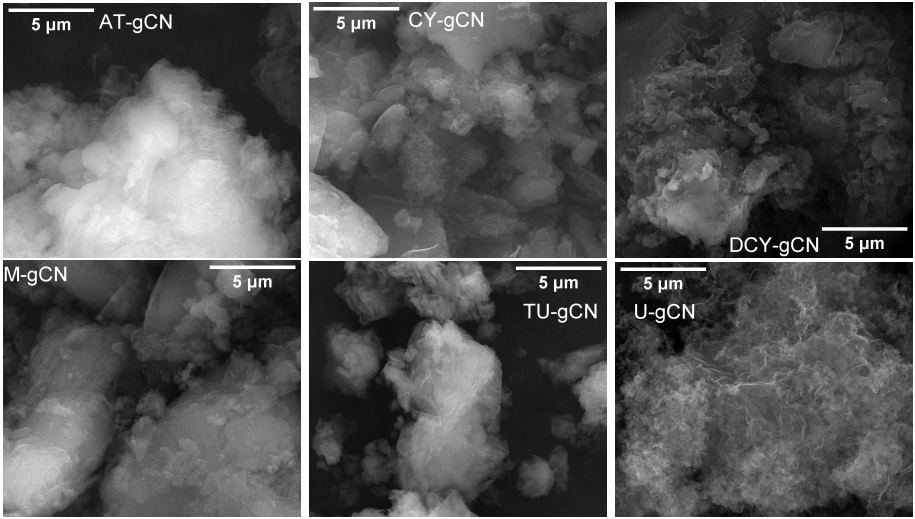

Energy-Dispersive X-ray Analysis (EDAX)

	Element	Weight %	MDL	Atomic %	Net Int.	Error %
AT-gCN	C K	42.8	0.38	46.8	727.6	10.7
	N K	54.3	1.02	50.8	264.1	12.2
	O K	2.9	0.46	2.4	23.2	19.2
CY-gCN	C K	49.3	0.70	53.2	387.1	11.1
	N K	50.0	2.20	46.2	94.9	13.6
	O K	0.7	0.89	0.6	2.6	85.7
DY-gCN	C K	41.6	0.54	45.5	461.2	11.0
	N K	56.2	1.43	52.7	183.4	12.5
	O K	2.1	0.65	1.7	10.9	25.2
M-gCN	C K	48.9	1.13	52.8	247.9	11.4
	N K	50.5	3.51	46.8	62.5	15.0
	O K	0.6	1.43	0.5	1.3	100.0
TU-gCN	C K	52.4	0.24	56.5	1054.3	9.6
	N K	44.3	0.90	40.9	192.9	12.5
	O K	3.3	0.41	2.7	29.4	18.9
	S K	0.0	0.00	0.0	2.1	68.6
U-gCN	C K	60.1	0.53	63.9	646.3	10.7
	N K	37.9	2.02	34.5	78.2	14.3
	O K	2.1	0.94	1.7	10.1	30.6

Solid UV-Visible Spectroscopy

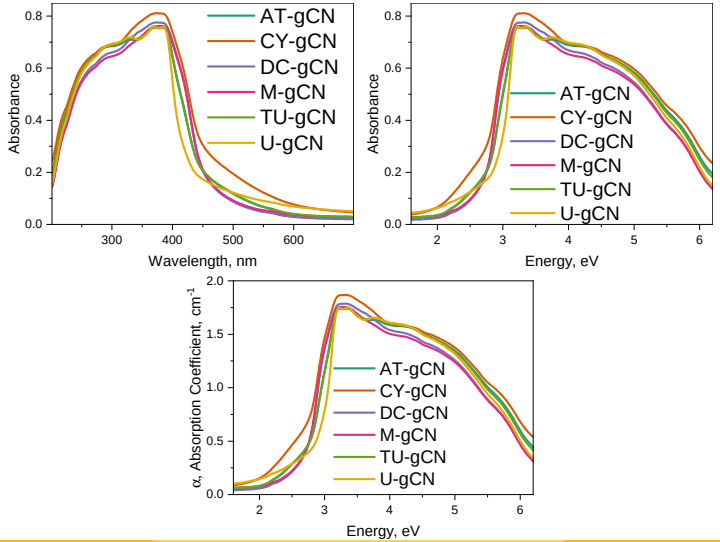

Tauc Plot

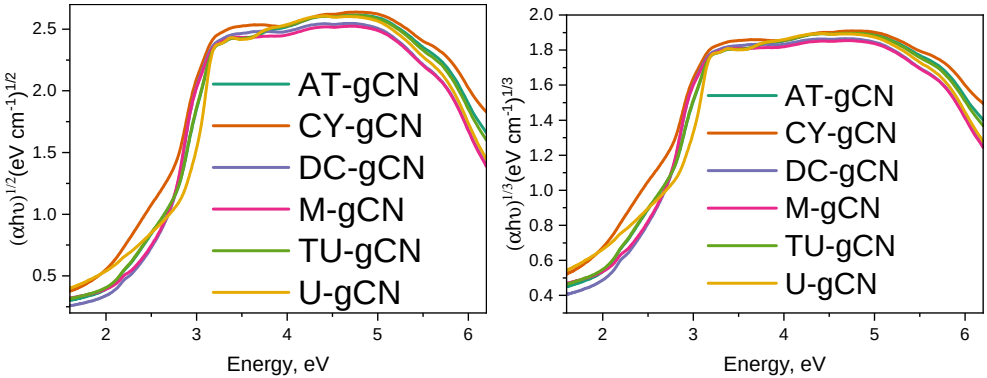
(αhυ)^1/2(eV cm^-1)^1/2
Energy, eV
AT-gCN
CY-gCN
DC-gCN
M-gCN
TU-gCN
U-gCN
(αhυ)^1/3(eV cm^-1)^1/3
Energy, eV
AT-gCN
CY-gCN
DC-gCN
M-gCN
TU-gCN
U-gCN

Tauc Plot

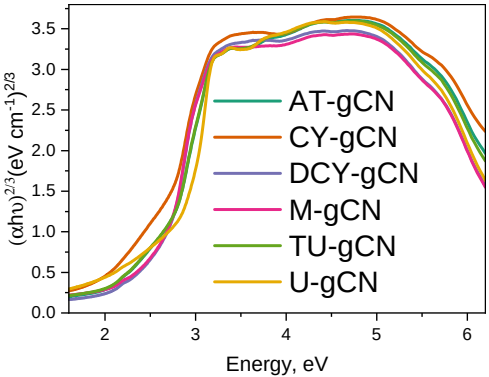
(αhυ)^2/3(eV cm^-1)^2/3
Energy, eV
AT-gCN
CY-gCN
DCY-gCN
M-gCN
TU-gCN
U-gCN

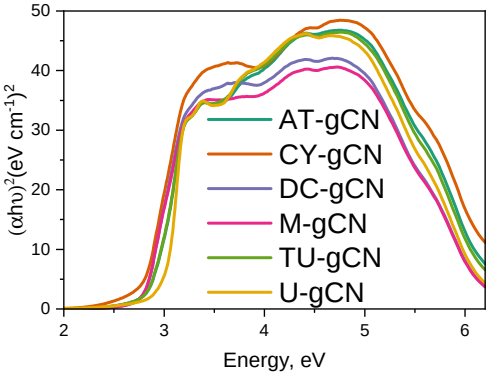
(αhυ)^2(eV cm^-1)^2
Energy, eV
AT-gCN
CY-gCN
DC-gCN
M-gCN
TU-gCN
U-gCN

Derivative Tauc Plot

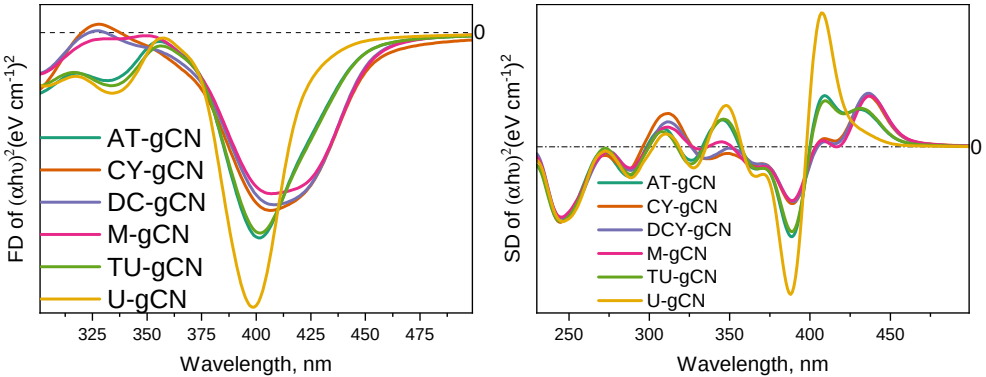

Derivative Tauc Plot Analysis

	Min	Intensity	Max	Intensity	D Parameter	S.A	Slope	D.P / S.A
AT-gCN	389	-0.03786	409	0.02158	0.05944	30.7	547.6	0.001936156
CY-gCN	389	-0.02394	436	0.02157	0.04551	16.8	304.9	0.002708929
DC-gCN	389	-0.02306	436	0.02258	0.04564	14.7	452.3	0.003104762
M-gCN	389	-0.02269	437	0.02145	0.04414	14.8	231.3	0.002982432
TU-gCN	389	-0.03576	409	0.01941	0.05517	16.3	670.4	0.003384663
U-gCN	389	-0.06124	407	0.05642	0.11766	109.5	292.4	0.001074521

Note: D.P = D parameter, difference between the maxima and minima, S.A= surface area, slope= B.E.T Slope from SESAMI Analysis

Urbach Energy Plot

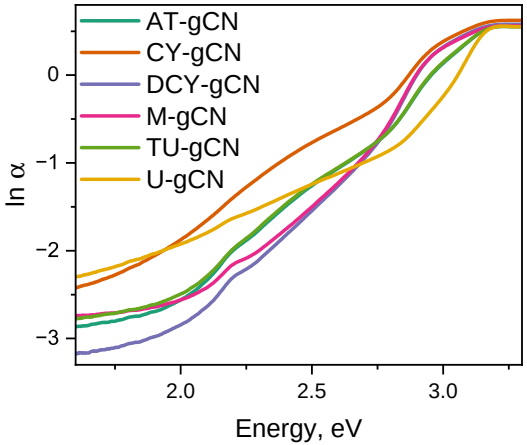

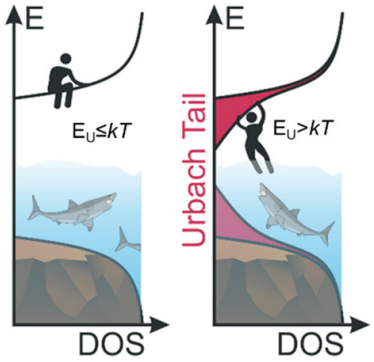

J. Phys. Chem. Lett. **2022**, 13, 33, 7702–7711

UV-Visible Diffuse Reflectance Spectroscopy

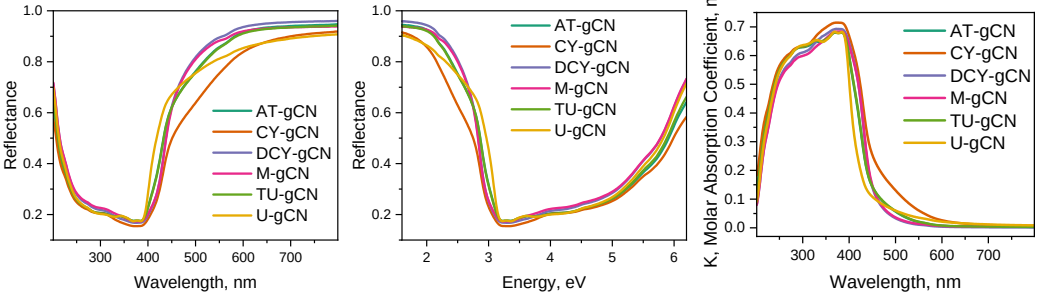

UV-Visible Diffuse Reflectance Spectroscopy

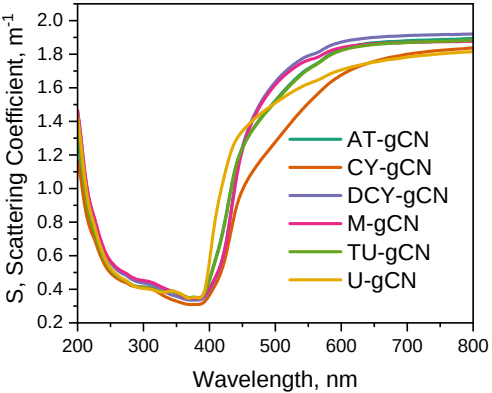

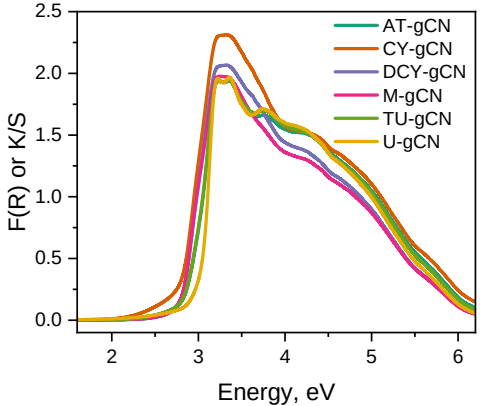

UV-Visible Diffuse Reflectance Spectroscopy

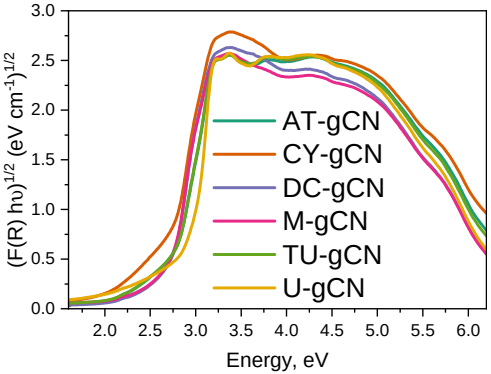

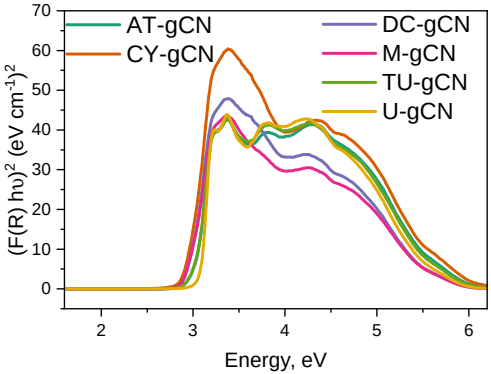

Derivative UV-Visible Diffuse Reflectance Spectroscopy

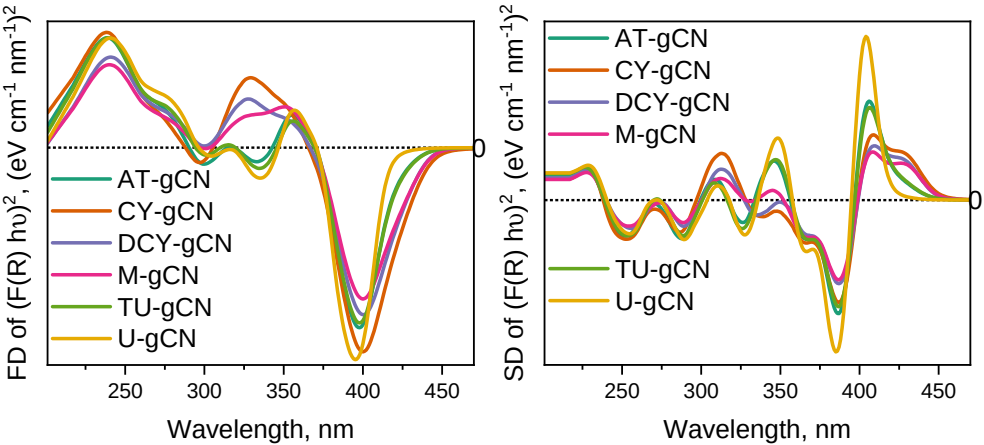

UV-Visible Diffuse Spectroscopy Analysis

Sample	Band Gap, eV						Urbach Energy, meV
	Tauc Plot			K-M Plot			
	L.R	F.D	S.D	L.R	F.D	S.D	L.R
AT-gCN	2.89	3.08	3.03	3.02	3.12	3.05	380
CY-gCN	2.76	3.04	2.84	2.95	3.10	3.03	430
DC-gCN	2.78	3.03	2.84	2.95	3.10	3.03	360
M-gCN	2.79	3.04	2.83	2.95	3.10	3.04	430
TU-gCN	2.84	3.08	3.03	3.02	3.12	3.05	390
U-gCN	2.99	3.11	3.05	3.08	3.14	3.07	750

L.R = Linear Regression; F.D = First Derivative; S.D = Second Derivative

J. Phys. Chem. Lett. **2018**, 9, 23, 6814–6817; *Rev. Sci. Instrum.* **2009**, 80, 046107; *J. Vac. Sci. Technol. B* **2016**, 34, 04J105; *J. Appl. Phys.* **2017**, 121, 234304; *J. Appl. Phys.* **2015** 117, 125701

Optical Conductivity

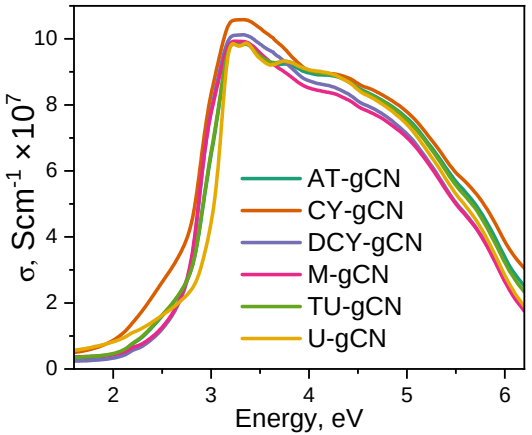

$$\sigma = \frac{\alpha n_0 C}{4\pi}$$

$\sigma =$ Optical conductivity

$\alpha =$ Absorption coefficient

$n_0 =$ Refractive index

$C =$ Speed of light

Derivative Diffuse Reflectance Spectroscopic Analysis

	Min	Intensity	Max	Intensity	D Parameter	S.A	C	D.P /S.A
AT-gCN	387	-0.08256	406	0.07196	0.15452	30.7	547.6	0.005033225
CY-gCN	387	-0.0745	409	0.04745	0.12195	16.8	304.9	0.007258929
DC-gCN	387	-0.06089	409	0.03946	0.10035	14.7	452.3	0.006826531
M-gCN	387	-0.05803	408	0.03494	0.09297	14.8	231.3	0.006281757
TU-gCN	387	-0.07766	406	0.06733	0.14499	16.3	670.4	0.008895092
U-gCN	385	-0.11053	404	0.11909	0.22962	109.5	292.4	0.002096986

Note: D.P = D parameter, difference between the maxima and minima, S.A= surface area, C= B.E.T constant from SESAMI Analysis

Photoluminescence Spectroscopy

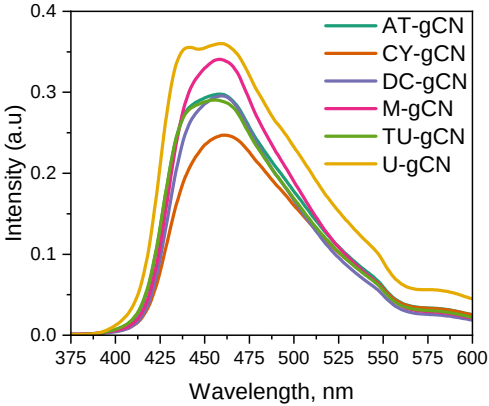

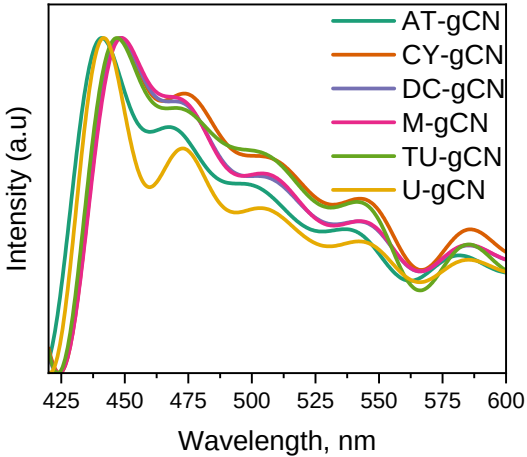

^{13}C Solid State NMR Studies

The convolution of ^{13}C spectra has been performed using the Pseudo Voigt (PsdVoigt1) function. Other functions such as PsdVoigt2 and Voigt did not provide satisfactory convolution within the NMR dataset.

$$y = y_0 + A\left[m_u \frac{2}{\pi}\frac{w}{4(x-x_c)^2 + w^2} + (1-m_u)\frac{\sqrt{4\ln 2}}{\sqrt{\pi}w} e^{-\frac{4\ln 2}{w^2}(x-x_c)^2}\right]$$

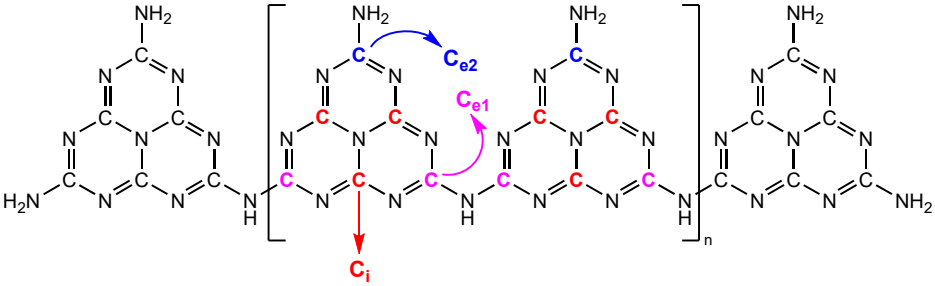

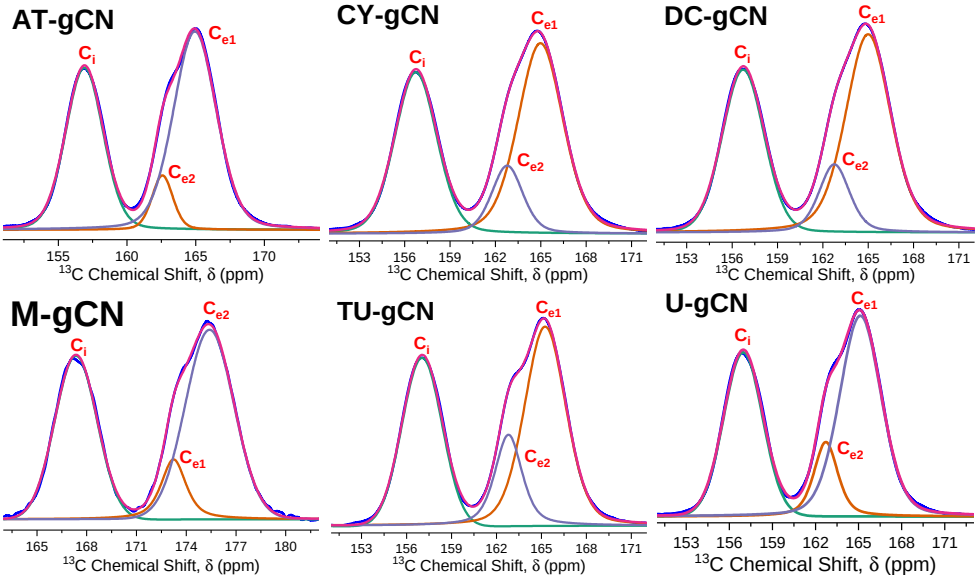
AT-gCN
C_i
C_{e1}
C_{e2}
155 160 165 170
^{13}C Chemical Shift, δ (ppm)
CY-gCN
C_i
C_{e1}
C_{e2}
153 156 159 162 165 168 171
^{13}C Chemical Shift, δ (ppm)
DC-gCN
C_i
C_{e1}
C_{e2}
153 156 159 162 165 168 171
^{13}C Chemical Shift, δ (ppm)
M-gCN
C_i
C_{e2}
C_{e1}
165 168 171 174 177 180
^{13}C Chemical Shift, δ (ppm)
TU-gCN
C_i
C_{e1}
C_{e2}
153 156 159 162 165 168 171
^{13}C Chemical Shift, δ (ppm)
U-gCN
C_i
C_{e1}
C_{e2}
153 156 159 162 165 168 171
^{13}C Chemical Shift, δ (ppm)

^{13}C NMR Analysis

	13C NMR Intensity			13C NMR Area			13C FWHM		
	Ce2	Ce1	Ci	Ce2	Ce1	Ci	Ce2	Ce1	Ci
AT-gCN	60387.43323	22317.50452	50169.58319	222274.083	53336.47047	173011.8831	3.45788	2.24516	3.23969
CY-gCN	77620.28368	16321.01998	63342.252	318145.449	41965.3368	225643.6627	3.85051	2.41552	3.34655
DC-gCN	72084.60796	14561.73235	57579.35451	295793.134	34792.51503	201786.7846	3.8549	2.24461	3.29226
M-gCN	72475.40193	19294.90928	61334.31367	268995.7949	35763.71358	194541.3502	3.48676	1.74128	2.97973
TU-gCN	59485.56841	24291.39018	49952.2479	212974.344	55227.12404	167261.7225	3.36344	2.13584	3.14564
U-gCN	109619.0349	40877.38273	90018.80342	396537.6737	92378.32054	305711.466	3.39834	2.12302	3.19041

^{15}N Solid State NMR Studies

The convolution of ^{15}N spectra has been performed using the Pseudo Voigt (PsdVoigt1) function. Other functions such as Guass, Lorentz, PsdVoigt2 and Voigt did not provide satisfactory convolution.

$$y = y_0 + A\left[m_u \frac{2}{\pi}\frac{w}{4(x-x_c)^2 + w^2} + (1-m_u)\frac{\sqrt{4\ln 2}}{\sqrt{\pi}w} e^{-\frac{4\ln 2}{w^2}(x-x_c)^2}\right]$$

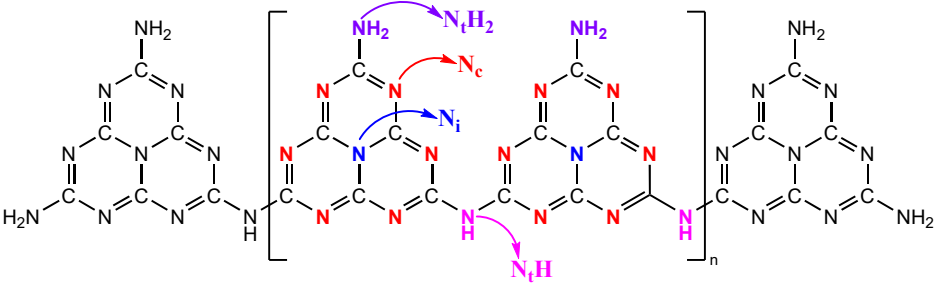

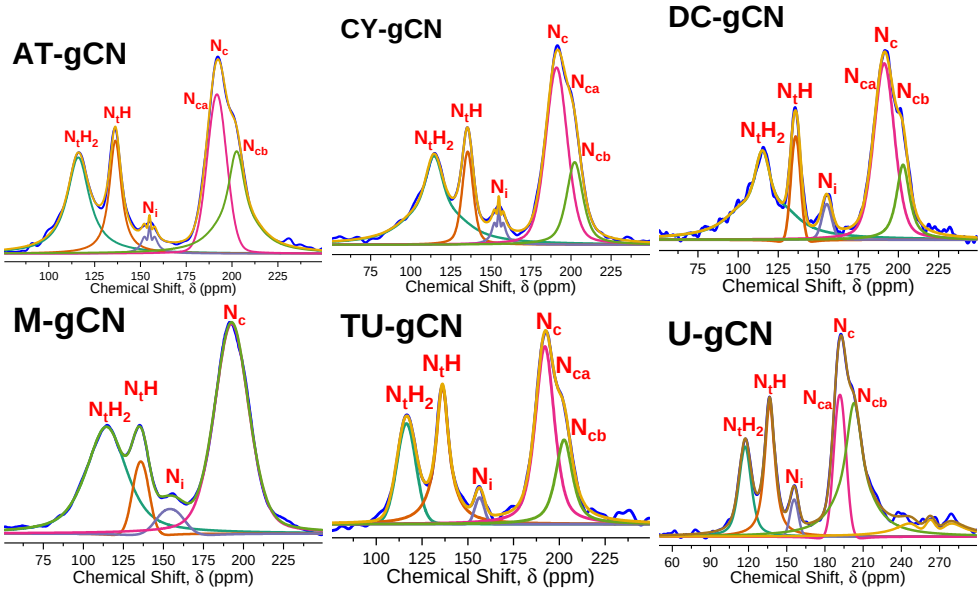
AT-gCN
N_tH_2
N_tH
N_i
N_{ca}
N_c
N_{cb}
100 125 150 175 200 225
Chemical Shift, δ (ppm)
CY-gCN
N_tH_2
N_tH
N_i
N_c
N_{ca}
N_{cb}
75 100 125 150 175 200 225
Chemical Shift, δ (ppm)
DC-gCN
N_tH_2
N_tH
N_i
N_c
N_{ca}
N_{cb}
75 100 125 150 175 200 225
Chemical Shift, δ (ppm)
M-gCN
N_tH_2
N_tH
N_i
N_c
75 100 125 150 175 200 225
Chemical Shift, δ (ppm)
TU-gCN
N_tH_2
N_tH
N_i
N_c
N_{ca}
N_{cb}
100 125 150 175 200 225
Chemical Shift, δ (ppm)
U-gCN
N_tH_2
N_tH
N_i
N_{ca}
N_c
N_{cb}
60 90 120 150 180 210 240 270
Chemical Shift, δ (ppm)

XPS Analysis

Peak Shape and Background Method

- Peak analysis using CasaXPS v2.3.26rev 1.1P
- Three-parameter Tougaard (U3) background
- Shirley-type background possible (terminate after largest N1s peak)
- Lorentzian asymmetric (LA) Voigt line shapes (LA(α, β, m))
- Fitting parameters: LA(1.3, 243) for all peaks (except C(1s) and N(1s))
- LA(1.03, 1.24, 243) used for C(1s) and N(1s) peaks

Quantitation Method

- CasaXPS V2.3.24 rev 1.1Z
- Three-parameter Tougaard (U3) background
- Utilizing Scofield sensitivity factors
- Kinetic energy dependence of -0.6

Appl. Surf. Sci. Adv. **2021**, 5, 100112; *Surf. Sci. Spectra* **2023**, 30, 014004; *Surf. Sci. Spectra* **2021**, 28, 014007

XPS Analysis

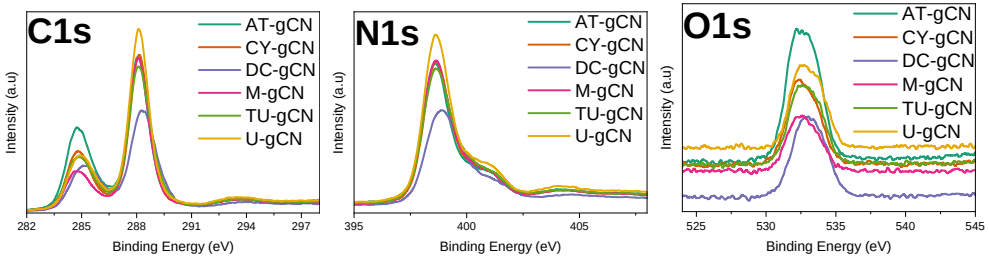

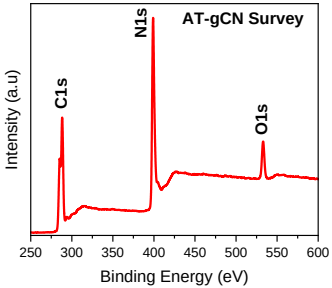
AT-gCN Survey
C1s
N1s
O1s
Intensity (a.u)
250 300 350 400 450 500 550 600
Binding Energy (eV)

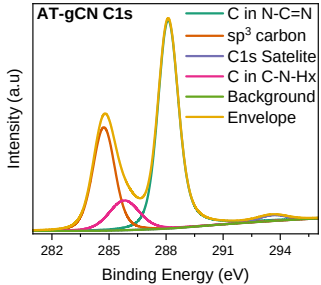
AT-gCN C1s
C in N-C=N
sp3 carbon
C1s Satelite
C in C-N-Hx
Background
Envelope
Intensity (a.u)
282 285 288 291 294
Binding Energy (eV)

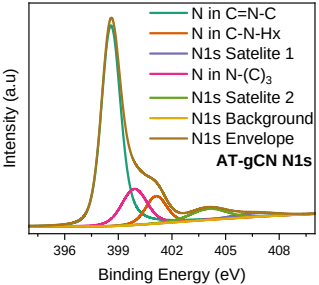
N in C=N-C
N in C-N-Hx
N1s Satelite 1
N in N-(C)3
N1s Satelite 2
N1s Background
N1s Envelope
AT-gCN N1s
Intensity (a.u)
396 399 402 405 408
Binding Energy (eV)

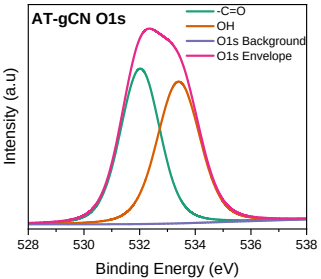
AT-gCN O1s
-C=O
OH
O1s Background
O1s Envelope
Intensity (a.u)
528 530 532 534 536 538
Binding Energy (eV)

Peak Assignment	Pos.	FWHM	L. Sh	Area	At%	Total%	SD
sp^3 carbon	284.72	1.35	LA(1.3,243)	48332.41	15.09		1.279
C in C−N−Hx	285.78	1.78	LA(1.3,243)	19553.36	6.11	31	
C in N−C=N	288.09	1.28	LA(1.03,1.24,243)	99290.94	31		
C1s Satelite	293.05	2.45	LA(1.3,243)	5872.15	1.83		
N in C=N−C	398.56	1.23	LA(1.03,1.24,243)	152273.87	26.41	41.29	1.249
N in $N-(C)_3$	399.84	1.6	LA(1.3,243)	33386.93	5.79		
N in C−N−Hx	401.08	1.45	LA(1.3,243)	26118.53	4.53		
N1s Satelite 1	404.03	2.45	LA(1.3,243)	18059.51	3.13		
N1s Satelite 2	406.57	2.84	LA(1.3,243)	8219.32	1.43		
OH	531.97	1.61	LA(1.3,243)	19800.37	2.11	4.67	0.9518
O1s	533.33	1.91	LA(1.3,243)	24058.04	2.56		

Spectral Features Table of AT-gCN

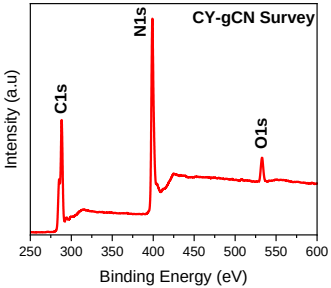
CY-gCN Survey
N1s
C1s
O1s
Intensity (a.u)
250 300 350 400 450 500 550 600
Binding Energy (eV)

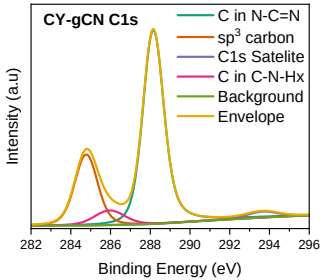
CY-gCN C1s
C in N-C=N
sp3 carbon
C1s Satelite
C in C-N-Hx
Background
Envelope
Intensity (a.u)
282 284 286 288 290 292 294 296
Binding Energy (eV)

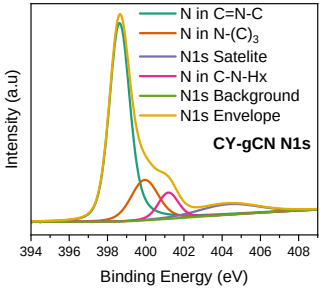
N in C=N-C
N in N-(C)3
N1s Satelite
N in C-N-Hx
N1s Background
N1s Envelope
CY-gCN N1s
Intensity (a.u)
394 396 398 400 402 404 406 408
Binding Energy (eV)

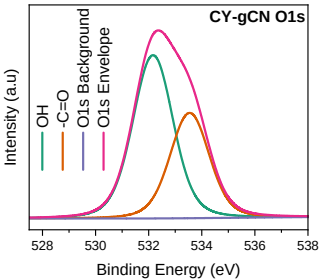
CY-gCN O1s
OH
-C=O
O1s Background
O1s Envelope
Intensity (a.u)
528 530 532 534 536 538
Binding Energy (eV)

Peak Assignment	Pos.	FWHM	Area	L.Sh.	At%	Total%	SD
sp^3 carbon	284.77	1.32	35783.41	LA(1.3,243)	12.12		
C in C−N−Hx	285.89	1.66	10232.31	LA(1.3,243)	3.47	33.47	1.295
C in N−C=N	288.13	1.25	98820.41	LA(1.03, 1.24,243)	33.47		
C1s Satelite	293.6	2.25	5795.45	LA(1.3,243)	1.96		
N in C=N−C	398.6	1.23	154079.63	LA(1.03, 1.24,243)	28.99		
N in chN-(C)3	399.75	1.5	33378.31	LA(1.3,243)	6.28	45.91	1.267
N in C−N−Hx	401.05	1.56	32673.34	LA(1.3,243)	6.15		
N1s Satelite 1	403.9	2.22	14087.94	LA(1.3,243)	2.65		
N1s Satelite 2	405.8	2.86	9784.91	LA(1.3,243)	1.84		
OH	532.17	1.77	16192.96	LA(1.3,243)	1.87	3.06	0.9514
O1s	533.54	1.76	10281.52	LA(1.3,243)	1.19		

Spectral Features Table of CY-gCN

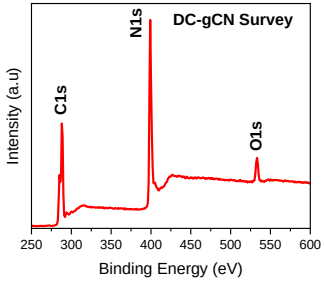
DC-gCN Survey
C1s
N1s
O1s
Intensity (a.u)
250 300 350 400 450 500 550 600
Binding Energy (eV)

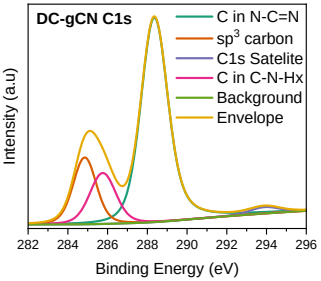
DC-gCN C1s
C in N-C=N
sp3 carbon
C1s Satelite
C in C-N-Hx
Background
Envelope
Intensity (a.u)
282 284 286 288 290 292 294 296
Binding Energy (eV)

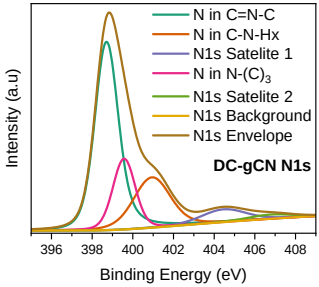
N in C=N-C
N in C-N-Hx
N1s Satelite 1
N in N-(C)3
N1s Satelite 2
N1s Background
N1s Envelope
DC-gCN N1s
Intensity (a.u)
396 398 400 402 404 406 408
Binding Energy (eV)

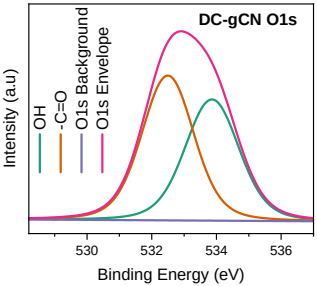
DC-gCN O1s
OH
-C=O
O1s Background
O1s Envelope
Intensity (a.u)
530 532 534 536
Binding Energy (eV)

Peak Assignment	Pos.	FWHM	Area	L. Sh.	At%	Total %	SD
sp^3 carbon	284.8	1.3	19002.36	LA(1.3,243)	7.81		
C in C−N−Hx	285.7	1.5	20252.58	LA(1.3,243)	8.32	33.94	1.575
C in N−C=N	288.32	1.61	82626.08	LA(1.03, 1.24, 243)	33.94		
C1s Satelite	293.85	2.06	3992.94	LA(1.3,243)	1.52		
N in C=N−C	398.67	1.33	98181.33	LA(1.03, 1.24, 243)	22.41		
N in $N-(C)_3$	399.57	1.37	39315.97	LA(1.3,243)	8.97	44.68	1.23
N in C−N−Hx	401.03	2.05	38243.54	LA(1.3,243)	8.73		
N1s Satelite 1	404.41	2.74	15139.02	LA(1.3,243)	3.46		
N1s Satelite 2	406.75	2.45	4860.19	LA(1.3,243)	1.11		
OH	532.55	1.94	15555.74	LA(1.3,243)	2.18	2.18	0.8745
O1s	533.91	1.9	11082.75	LA(1.3,243)	1.55		

Spectral Features Table of DC-gCN

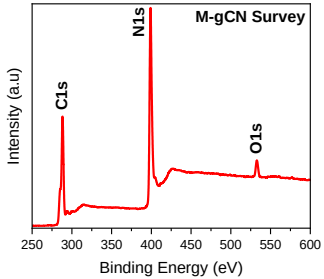
M-gCN Survey
C1s
N1s
O1s
Intensity (a.u)
250 300 350 400 450 500 550 600
Binding Energy (eV)

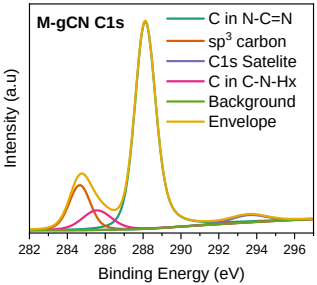
M-gCN C1s
C in N-C=N
sp3 carbon
C1s Satelite
C in C-N-Hx
Background
Envelope
Intensity (a.u)
282 284 286 288 290 292 294 296
Binding Energy (eV)

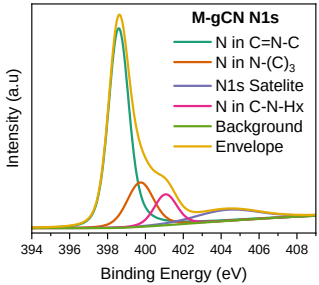
M-gCN N1s
N in C=N-C
N in N-(C)3
N1s Satelite
N in C-N-Hx
Background
Envelope
Intensity (a.u)
394 396 398 400 402 404 406 408
Binding Energy (eV)

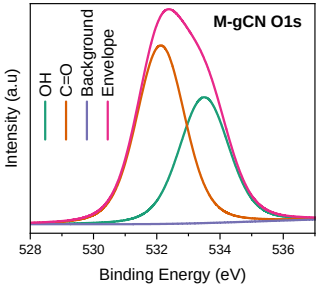
M-gCN O1s
OH
C=O
Background
Envelope
Intensity (a.u)
528 530 532 534 536
Binding Energy (eV)

Peak Assignment	Pos.	FWHM	Area	L. Sh.	At%	Total %	SD
sp^3 carbon	284.65	1.31	21483.55	LA(1.3, 243)	7.38		
C in C−N−Hx	285.61	1.69	11742.23	LA(1.3, 243)	4.03	34.73	1.054
C in N−C=N	288.09	1.31	101131.04	LA(1.03,1.24,243)	34.73		
C1s Satelite	293.53	2.82	8404	LA(1.3, 243)	2.89		
N in C=N−C	398.55	1.24	153593.59	LA(1.03,1.24,243)	29.30		
N in N	399.56	1.44	34724.23	LA(1.3, 243)	6.62	48.92	1.455
N in C−N−Hx	400.93	1.76	40948.11	LA(1.3, 243)	7.81		
N1s Satelite 1	403.98	2.33	15983.99	LA(1.3, 243)	3.05		
N1s Satelite 2	406.03	3.15	11190.98	LA(1.3, 243)	2.14		
OH	532.17	2.33	10707.88	LA(1.3, 243)	1.26	1.26	0.9108
O1s	533.57	1.81	6760.98	LA(1.3, 243)	0.79		

Spectral Features Table of M-gCN

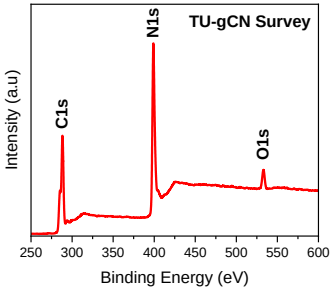
TU-gCN Survey
C1s
N1s
O1s
Intensity (a.u)
250 300 350 400 450 500 550 600
Binding Energy (eV)

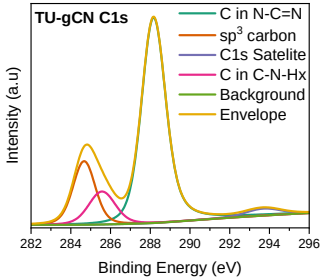
TU-gCN C1s
C in N-C=N
sp3 carbon
C1s Satelite
C in C-N-Hx
Background
Envelope
Intensity (a.u)
282 284 286 288 290 292 294 296
Binding Energy (eV)

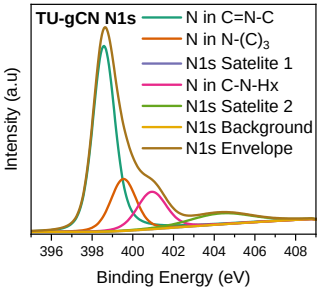
TU-gCN N1s
N in C=N-C
N in N-(C)3
N1s Satelite 1
N in C-N-Hx
N1s Satelite 2
N1s Background
N1s Envelope
Intensity (a.u)
396 398 400 402 404 406 408
Binding Energy (eV)

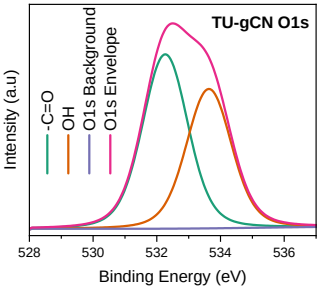
TU-gCN O1s
-C=O
OH
O1s Background
O1s Envelope
Intensity (a.u)
528 530 532 534 536
Binding Energy (eV)

Peak Assignment	Pos.	FWHM	Area	L. Sh.	At%	Total %	SD
sp^3 carbon	284.69	1.33	29181.02	LA(1.3,243)	9.64		
C in C−N−Hx	285.62	1.49	15504.08	LA(1.3,243)	5.12	34.76	1.057
C in N−C=N	288.14	1.44	105197.29	LA(1.03,1.24,243)	34.76		
C1s Satelite	293.63	2.7	7493.6	LA(1.3,243)	2.48		
N in C=N−C	398.54	1.23	136673.05	LA(1.03,1.24,243)	25.09		
N in $N-(C)_3$	399.45	1.41	43079.29	LA(1.3,243)	7.91		1.435
N in C−N−Hx	400.88	1.9	45234.2	LA(1.3,243)	8.30	45.29	
N1s Satelite 1	403.97	2.25	14767.21	LA(1.3,243)	2.71		
N1s Satelite 2	405.81	2.49	6955.82	LA(1.3,243)	1.28		
OH	532.26	1.6	13026.95	LA(1.3,243)	1.47	1.47	0.8656
O1s	533.62	1.65	11061.02	LA(1.3,243)	1.25		

Spectral Features Table of TU-gCN

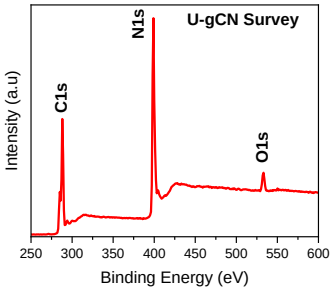
U-gCN Survey
C1s
N1s
O1s
Intensity (a.u)
250 300 350 400 450 500 550 600
Binding Energy (eV)

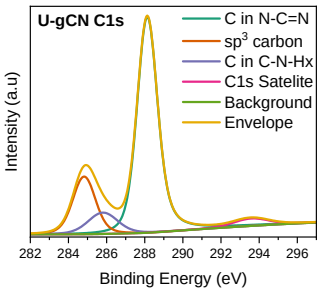
U-gCN C1s
C in N-C=N
sp3 carbon
C in C-N-Hx
C1s Satelite
Background
Envelope
Intensity (a.u)
282 284 286 288 290 292 294 296
Binding Energy (eV)

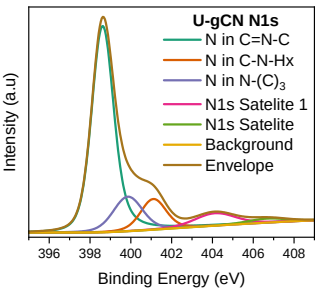
U-gCN N1s
N in C=N-C
N in C-N-Hx
N in N-(C)3
N1s Satelite 1
N1s Satelite
Background
Envelope
Intensity (a.u)
396 398 400 402 404 406 408
Binding Energy (eV)

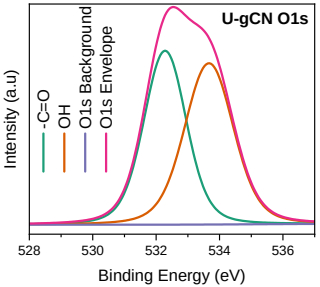
U-gCN O1s
-C=O
OH
O1s Background
O1s Envelope
Intensity (a.u)
528 530 532 534 536
Binding Energy (eV)

Peak Assignment	Pos.	FWHM	Area	L. Sh.	At%	Total%	SD
sp^3-carbon	284.81	1.38	32179.20	LA(1.3,243)	9.40		1.013
C in C−N−Hx	285.81	1.68	14954.77	LA(1.3,243)	4.37	34.02	
C in N−C=N	288.11	1.27	116500.17	LA(1.03, 1.24, 243)	34.02		
C1s Satellite	293.53	3.02	10329.09	LA(1.3,243)	3.02		
N in C=N−C	398.6	1.25	188066.63	LA(1.03, 1.24, 243)	30.51		
N in $N-(C)_3$	399.89	1.52	34707.54	LA(1.3,243)	5.63	46.53	1.557
N in C−N−Hx	401.11	1.47	33458.95	LA(1.3,243)	5.43		
N1s Satellite 1	404.12	2.52	23747.67	LA(1.3,243)	3.85		
N1s Satellite 2	406.71	2.07	6864.9	LA(1.3,243)	1.11		
OH	532.28	1.55	12623.51	LA(1.3,243)	1.26	1.26	0.8665
O1s	533.66	1.84	14052.99	LA(1.3,243)	1.4		

Spectral Features Table of U-gCN

Valence Band XPS Analysis

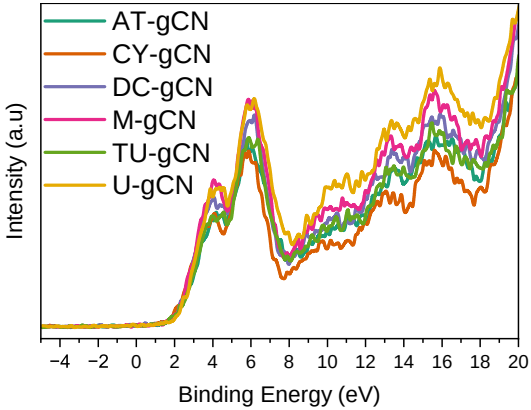

Valence Band XPS

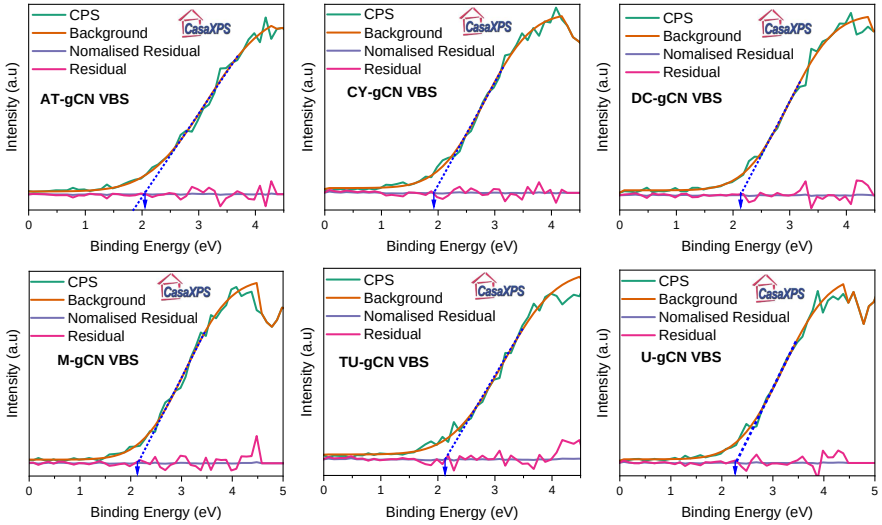

Derivative Valence Band XPS

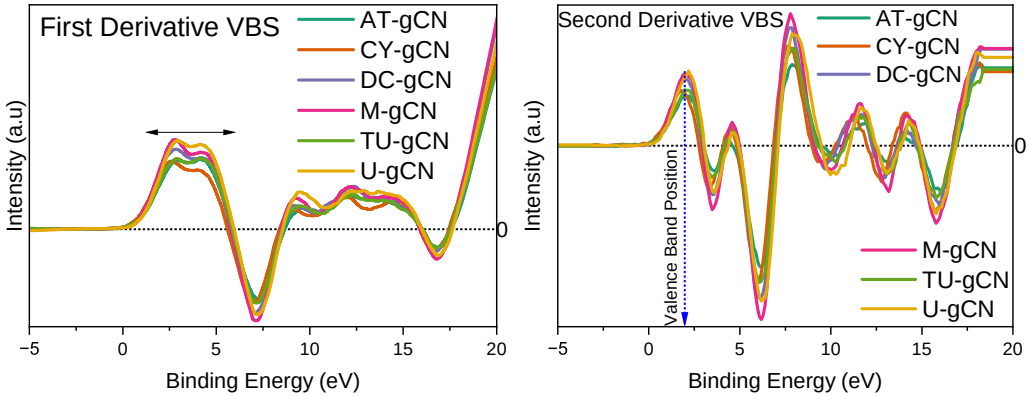

Valence Band XPS Analysis

	Highest Occupied Molecular Orbital (HOMO), eV				
Sample	**Second Derivative**	**Curve Fitting**			
		Position	**Original Value**	**FWHM**	**STD**
AT-gCN	2.18	2	1.9957	1.91	1.302
CY-gCN	1.78	1.91	1.9138	1.52	1.224
DC-gCN	1.98	2.11	2.1113	1.47	1.157
M-gCN	1.98	2.11	2.1115	1.62	1.317
TU-gCN	1.98	2.12	2.1201	1.71	1.515
U-gCN	2.18	2.22	2.2199	1.64	1.305

Energy Band Diagram Elucidation

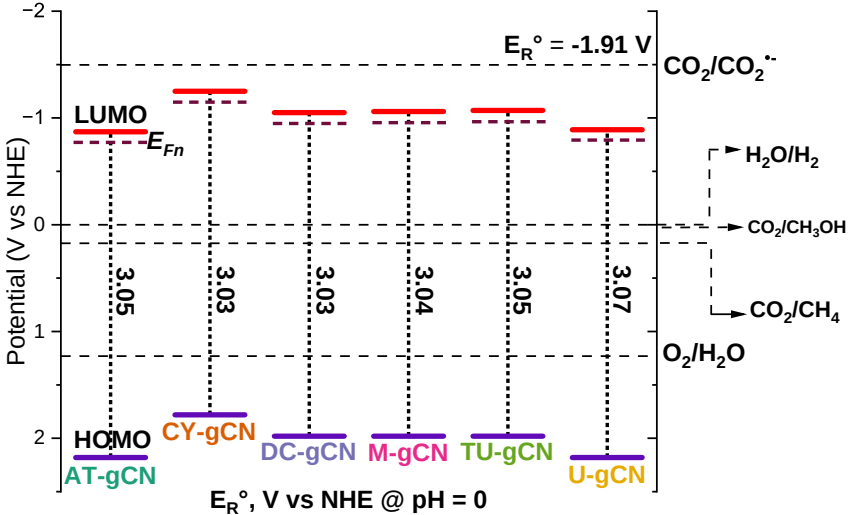

Energy Band Diagram Elucidation: pH Correction

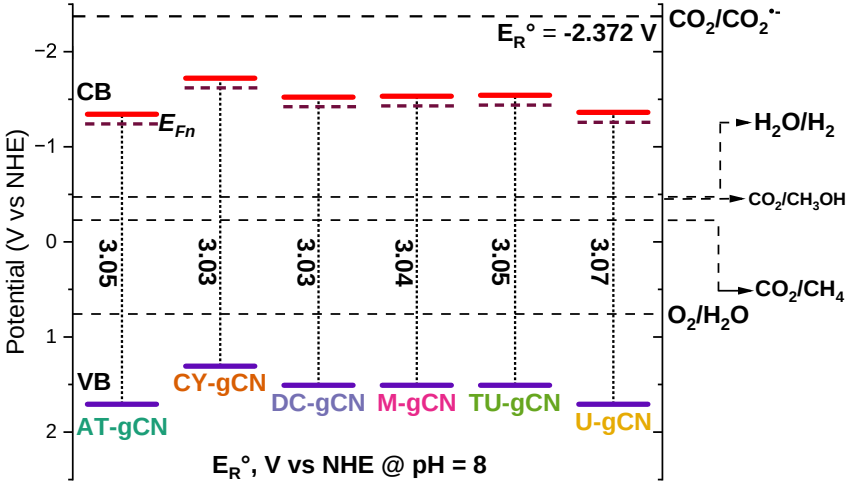

Band Position, Ionization Potential, and Electron Affinity

Sample	Bandgap	HOMO	LUMO	I.E	E.A	C	N	C/N
AT-gCN	3.05 eV	2.18 V	−0.87 V	6.62 eV	3.57 eV	31	41.29	0.7507
CY-gCN	3.03 eV	1.78 V	−1.25 V	6.22 eV	3.19 eV	33.47	45.91	0.7290
DC-gCN	3.03 eV	1.98 V	−1.05 V	6.42 eV	3.39 eV	33.94	44.68	0.7596
M-gCN	3.04 eV	1.98 V	−1.06 V	6.42 eV	3.38 eV	34.73	48.92	0.7099
TU-gCN	3.05 eV	1.98 V	−1.07 V	6.42 eV	3.37 eV	34.76	45.29	0.7674
U-gCN	3.07 eV	2.18 V	−0.89 V	6.62 eV	3.54 eV	34.02	46.53	0.7311

Table of Contents

Context

Crucibles used for material synthesis

(a) Alumina

(b) Silica

(c) Graphite

(d) Platinum

(e) Nickel

(f) Zirconia

(g) Quartz

Synthesis

1. General preparation method for graphitic carbon nitride:
   1. Recrytalization of melamine with acetone
   2. Grinding of precursors in a mortar.
   3. Transfer of ground precursors into different crucibles: alumina, silica, platinum, graphite, nickel, zirconia, and quartz with lid.
2. Heating process:
   1. Placement of the alumina crucible in a SIGMA Laboratory Muffle Furnace.
   2. Heating for 4 h with a ramping rate of 2 °C min.
   3. Removal of samples once the oven reaches room temperature.
3. Post-heating process:
   1. Transfer of the resultant hard yellow block of graphitic carbon nitride into a mortar.
   2. Grinding of the block using a pestle.
   3. Transfer of the delicate yellow powder into a 25 mL storage amber glass vial.

X-ray Diffraction: LeBail Fits

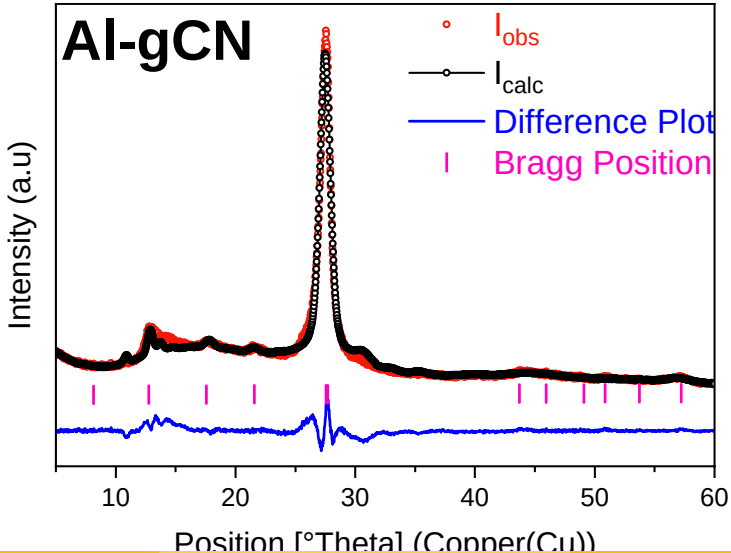

X-ray Diffraction: LeBail Fits

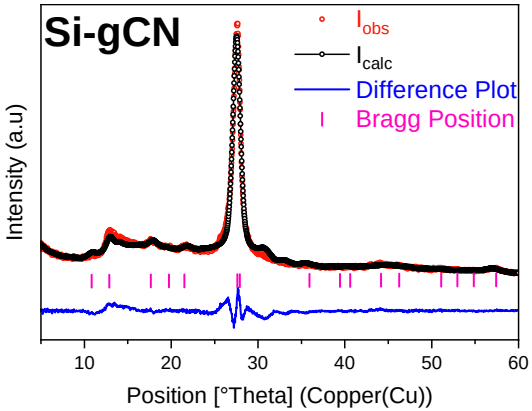

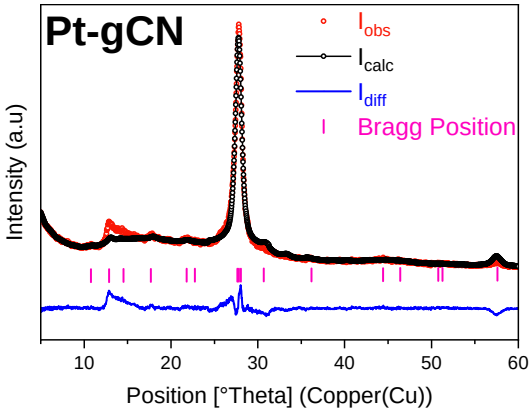

X-ray Diffraction: LeBail Fits

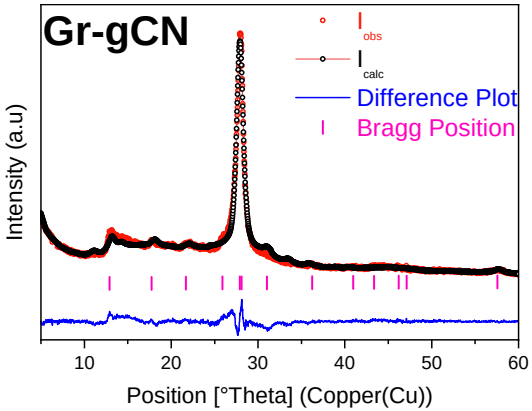

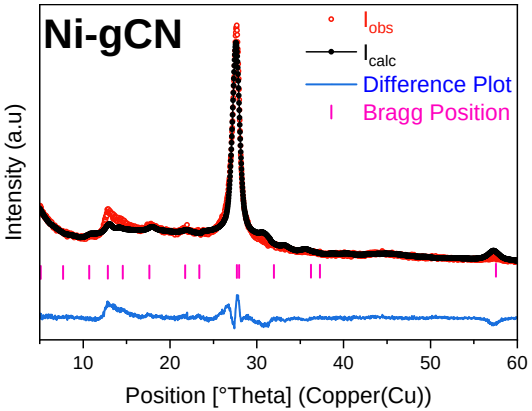

X-ray Diffraction: LeBail Fits

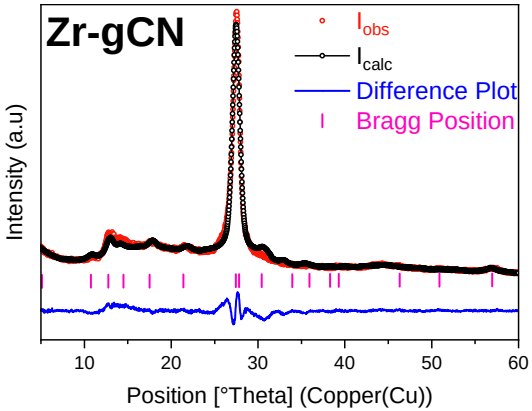

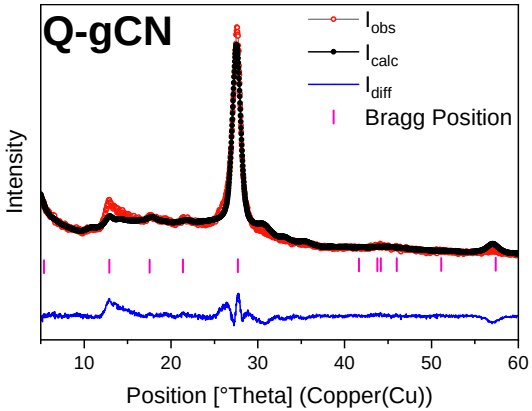

X-ray Diffraction Analysis

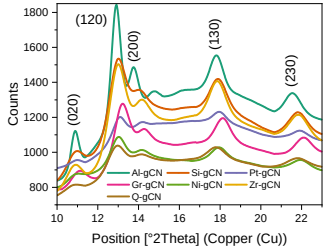

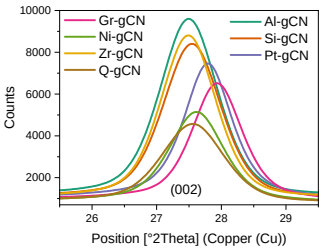

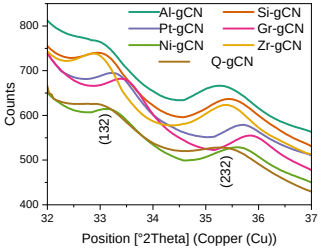

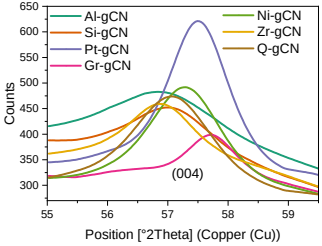

The B.E.T Surface Area

	B.E.T SA	C
Al-gCN	11.86	-52.35
Si-gCN	15.21	-34.41
Pt-gCN	63.77	-242.77
Gr-gCN	70.25	-959.38
Ni-gCN	18.76	-37.09
Zr-gCN	14.39	-46.23
Q-gCN	46.04	-145.22

Surface Area Analysis: BETSI vs. SESAMI Method

	Surface Area, m^2/g						
	B.E.T	**BETSI**	**SESAMI**	**C, SESAMI**	**q_m, mol/kg**	**Pore Size, nm**	**t-plot M.A**
Al-gCN	11.86	15	15.2	1093	0.16	37.53	12.43
Si-gCN	15.21	21	20.8	948.6	0.21	39.74	14.69
Pt-gCN	63.77	67	67	423.7	0.69	22.97	18.74
Gr-gCN	70.25	73	72.2	335.4	0.74	22.08	15.86
Ni-gCN	18.76	34	34	515.9	0.35	27.98	35.88
Zr-gCN	14.39	13	12.6	512.3	0.13	22.93	18.09
Q-gCN	46.04	50	49.4	530.7	0.51	30.88	16.89

Physical Adsorption Characterization

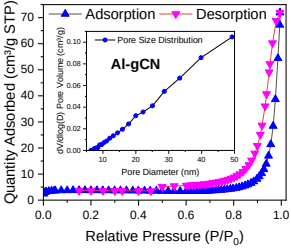

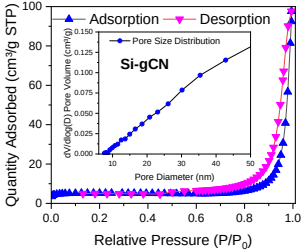

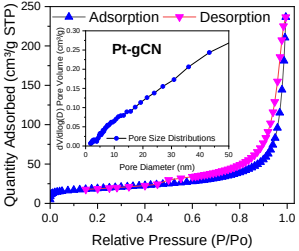

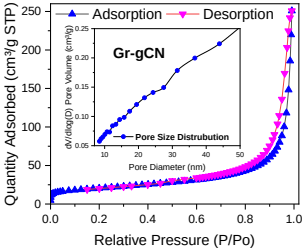

Physical Adsorption Characterization

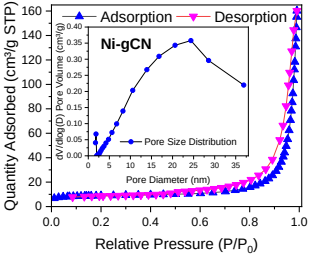

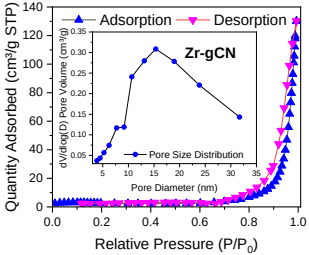

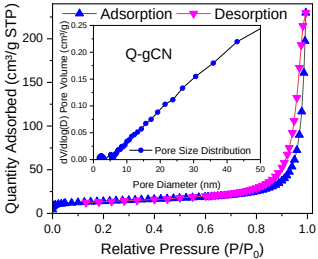

Surface Areas versus CH_4 Yield

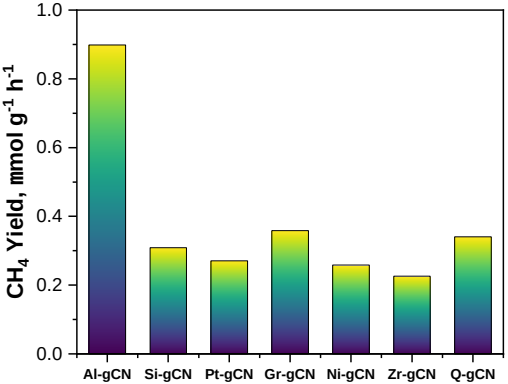

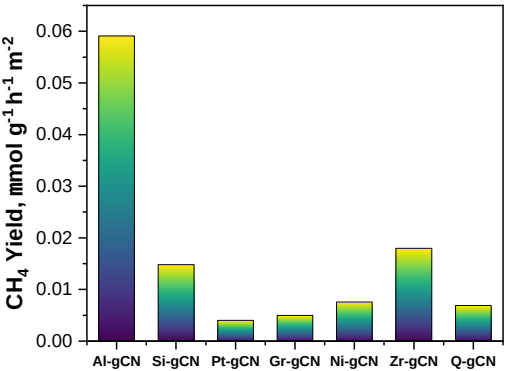

Surface Areas versus CH_3OH Yield

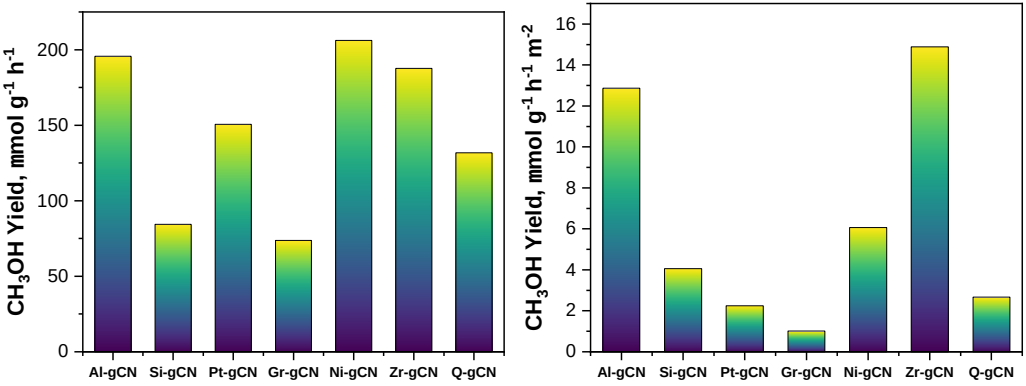

Surface Areas versus O_2 Yield

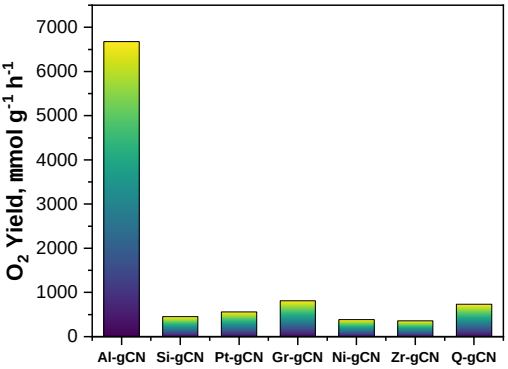

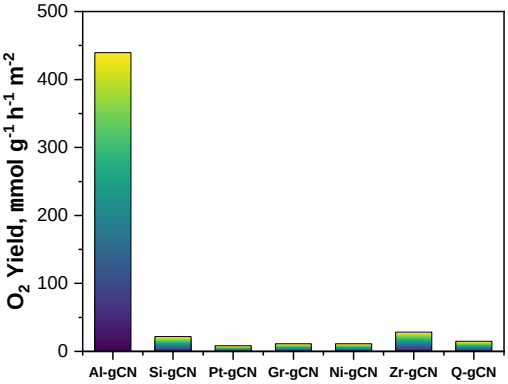

Isotherm Summation

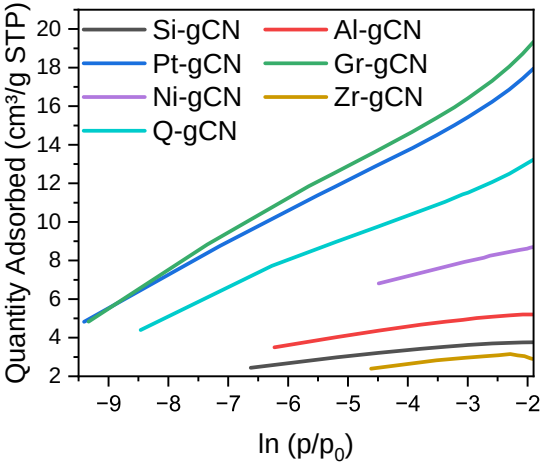

First Derivative Isotherm Summation

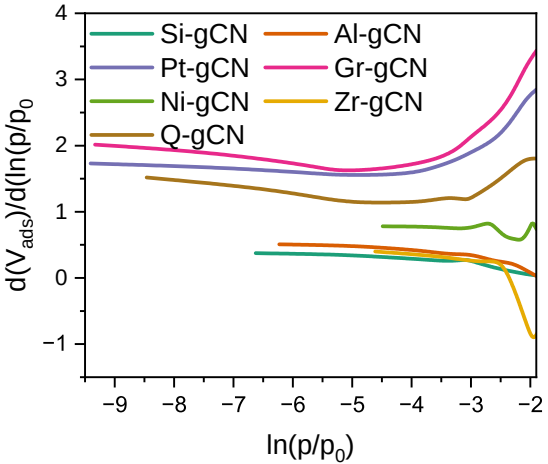

Second Derivative Isotherm Summation

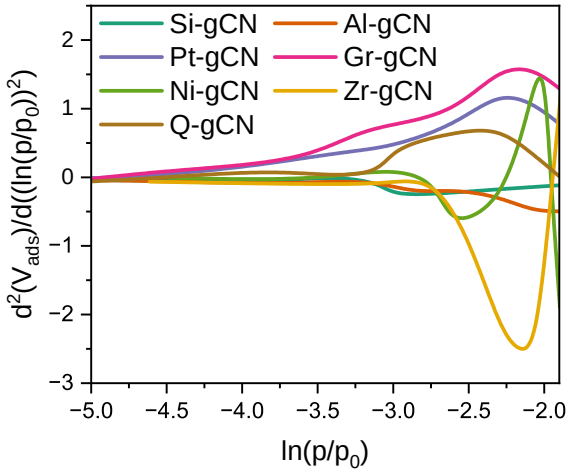

Field Emission Scanning Electron Microscopy (FESEM) 5 µm

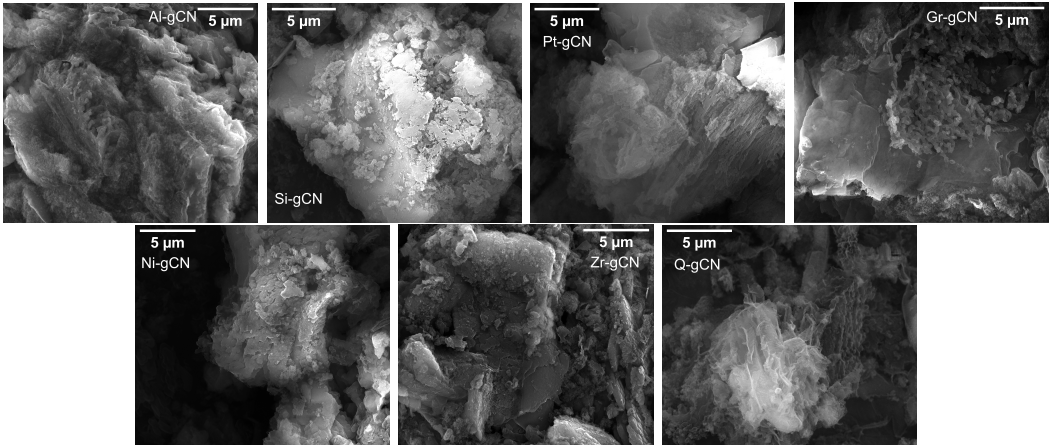

Field Emission Scanning Electron Microscopy (FESEM) 1 µm

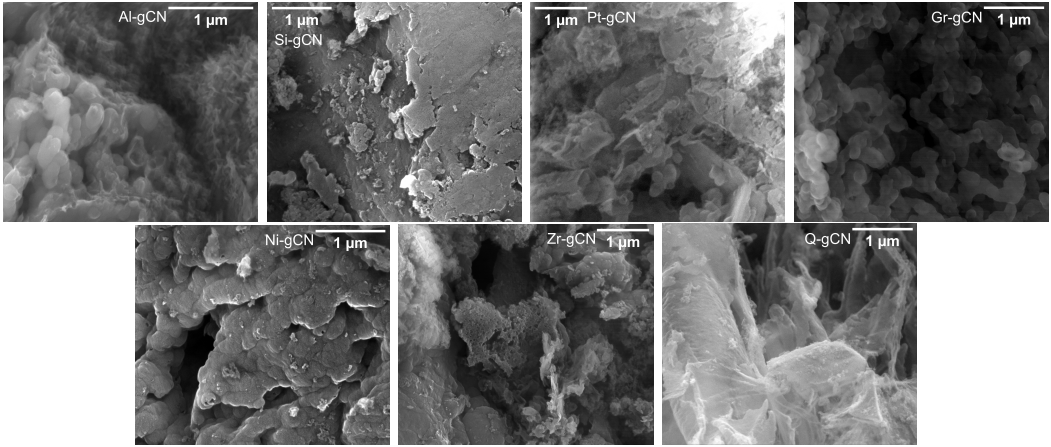

Energy-Dispersive X-ray Analysis (EDAX)

	Element	Weight %	MDL	Atomic %	Net Int.	Error %
Al-gCN	C K	43.6	0.10	47.5	1758.3	9.2
	N K	54.9	0.30	51.3	593.9	11.1
	O K	1.5	0.20	1.2	25.8	19.3
	Al K	0.1	0.01	0.0	29.4	12.8
Si-gCN	C K	51.0	0.19	54.9	1152.6	9.3
	N K	48.8	0.75	45.0	243.5	11.8
	O K	0.1	0.35	0.1	0.8	100.0
	Si K	0.1	0.03	0.0	18.3	23.7
Pt-gCN	C K	51.0	0.19	54.9	1152.6	9.3
	N K	48.8	0.75	45.0	243.5	11.8
	O K	0.1	0.35	0.1	0.8	100.0
	Si K	0.1	0.03	0.0	18.3	23.7
Gr-gCN	C K	46.7	0.14	50.6	1451.7	9.2
	N K	53.0	0.47	49.2	403.2	11.3
	O K	0.2	0.25	0.2	3.1	89.7

Energy-Dispersive X-ray Analysis (EDAX)

	Element	Weight %	MDL	Atomic %	Net Int.	Error %
Ni-gCN	C K	52.2	0.19	56.1	1163.1	9.3
	N K	47.7	0.78	43.9	227.3	11.8
	O K	0.1	0.36	0.1	0.6	100.0
	Ni K	0.1	0.08	0.0	3.8	59.9
Zr-gCN	C K	52.2	0.19	56.1	1163.1	9.3
	N K	47.7	0.78	43.9	227.3	11.8
	O K	0.1	0.36	0.1	0.6	100.0
	Ni K	0.1	0.08	0.0	3.8	59.9
Q-gCN	C K	54.9	0.06	59.0	4154.1	9.0
	N K	41.6	0.28	38.3	646.8	11.5
	O K	3.4	0.14	2.7	114.8	15.0
	Si K	0.0	0.01	0.0	44.1	8.5

Solid UV-Visible Spectroscopy

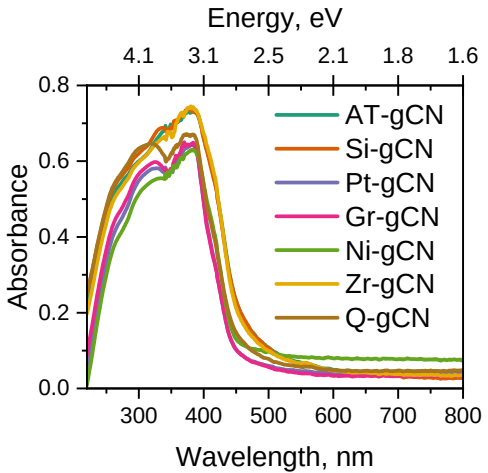

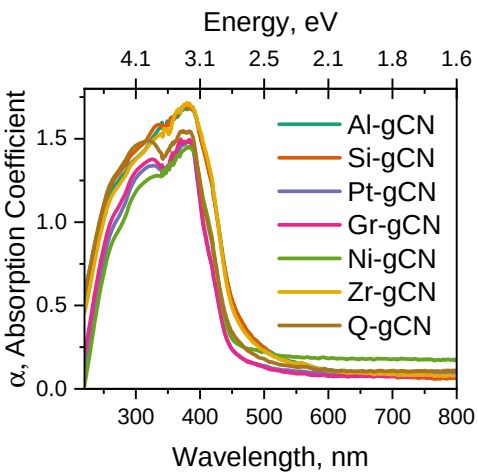

Tauc Plot Validation

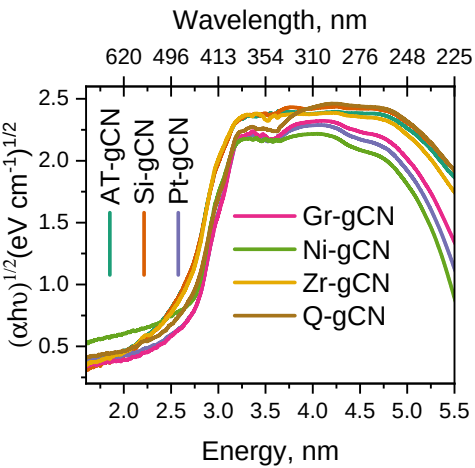

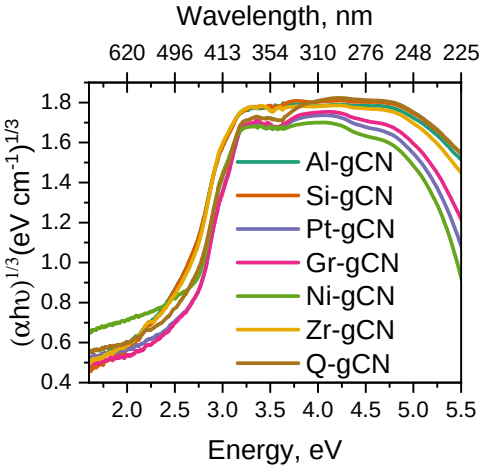

Tauc Plot Validation

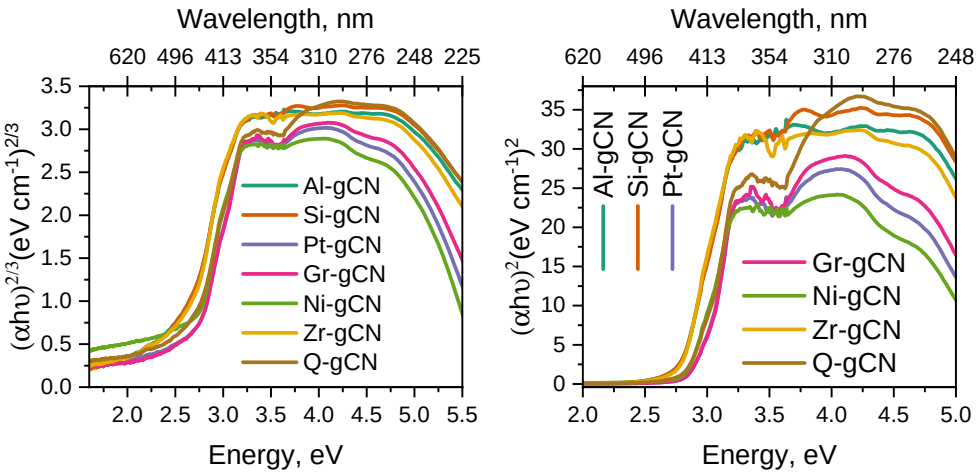

Derivative Tauc Plot

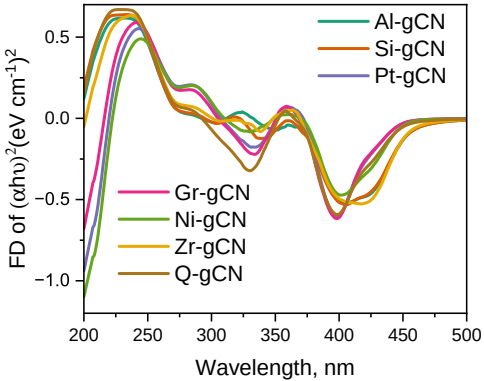

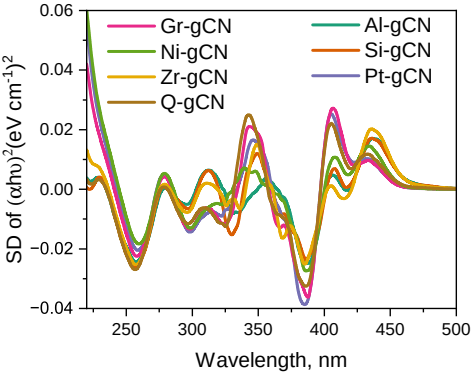

Derivative Tauc Plot Analysis

	Min	Intensity	Max	Intensity	D Parameter	S.A	Slope	D.P / S.A
Al-gCN	386	-0.02504	437	0.01708	0.04212	15.2	1093	0.002771053
Si-gCN	386	-0.02366	436	0.01717	0.04083	20.8	948.6	0.001962981
Pt-gCN	385	-0.03872	405	0.02542	0.06414	67	423.7	0.000957313
Gr-gCN	388	-0.03636	407	0.02731	0.06367	72.2	335.4	0.000881856
Ni-gCN	386	-0.02748	434	0.01462	0.0421	34	515.9	0.001238235
Zr-gCN	385	-0.02521	436	0.02031	0.04552	12.6	512.3	0.003612698
Q-gCN	386	-0.03256	405	0.02216	0.05472	49.4	530.7	0.001107692

Note: D.P = D parameter, difference between the maxima and minima, S.A= surface area, slope= B.E.T Slope from SESAMI Analysis

Urbach Plot

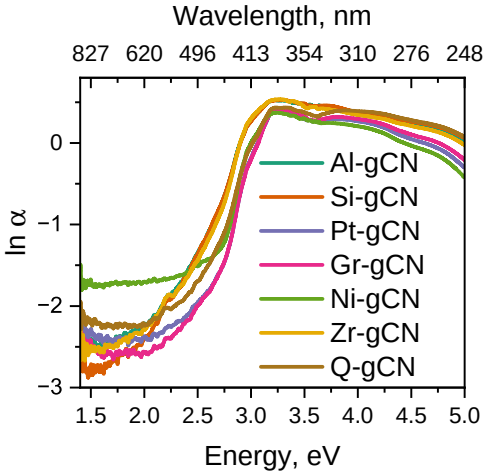
Wavelength, nm
827 620 496 413 354 310 276 248
ln α
0
−1
−2
−3
1.5 2.0 2.5 3.0 3.5 4.0 4.5 5.0
Energy, eV
Al-gCN
Si-gCN
Pt-gCN
Gr-gCN
Ni-gCN
Zr-gCN
Q-gCN

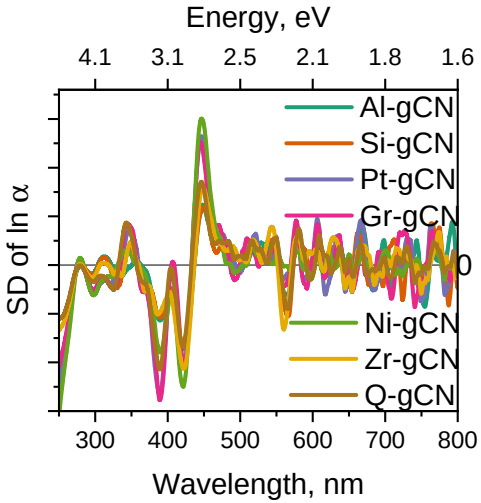
Energy, eV
4.1 3.1 2.5 2.1 1.8 1.6
SD of ln α
0
300 400 500 600 700 800
Wavelength, nm
Al-gCN
Si-gCN
Pt-gCN
Gr-gCN
Ni-gCN
Zr-gCN
Q-gCN

Diffuse Reflectance Spectroscopy

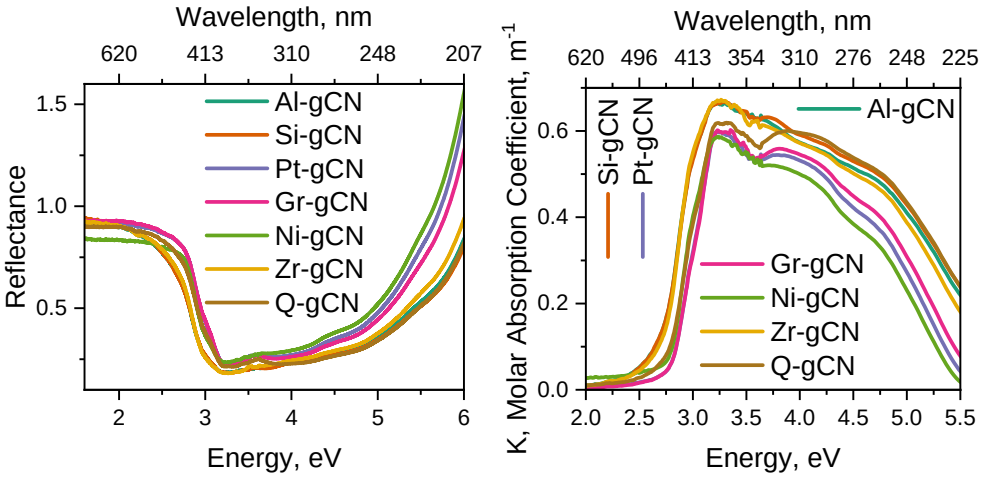

Diffuse Reflectance Spectroscopy

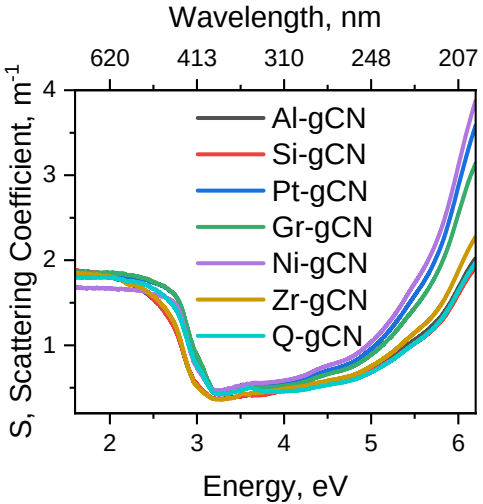

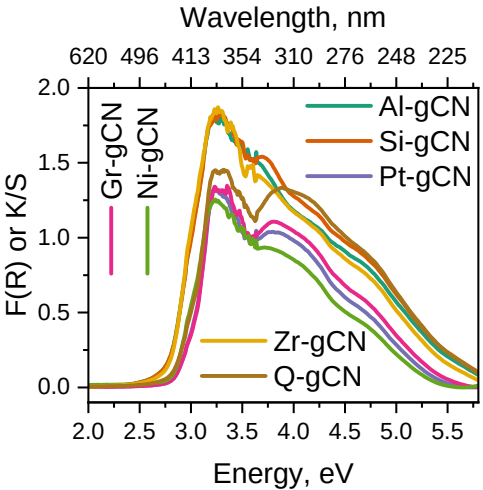

Kubelka-Monk Plot

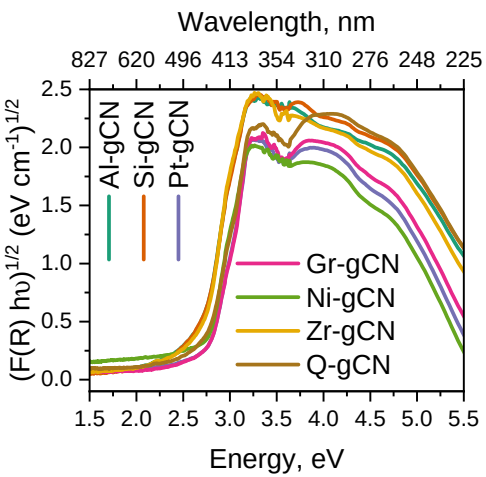

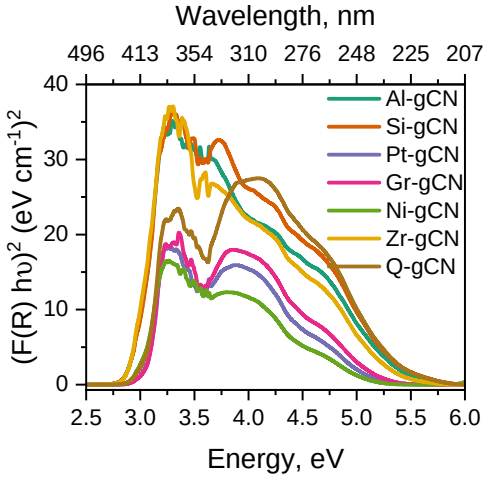

Derivative Diffuse Reflectance Spectroscopy

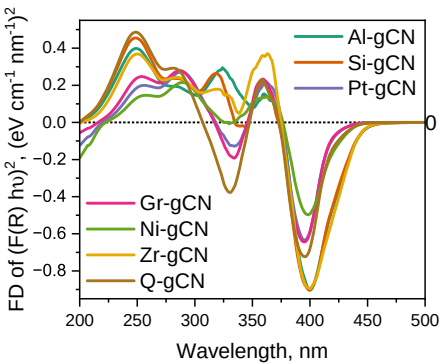

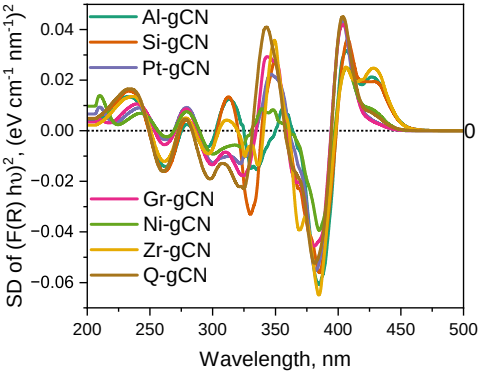

UV-Visible Diffuse Spectroscopy Analysis

Sample	Band Gap, eV						U.E meV	R.I
	Tauc Plot			K-M Plot				
	L.R	F.D	S.D	L.R	F.D	S.D	L.R	
Al-gCN	2.77	3.06	2.84	2.76	3.1	3.05	409	2.3655
Si-gCN	2.78	3.06	2.84	2.77	3.12	3.04	365	2.3691
Pt-gCN	2.94	3.12	3.06	2.95	3.14	3.08	163	2.3555
Gr-gCN	2.94	3.12	3.05	2.95	3.14	3.07	163	2.3589
Ni-gCN	2.83	3.08	2.86	2.84	3.12	3.05	165	2.3657
Zr-gCN	2.78	2.97	2.84	2.77	3.1	3.05	198	2.3657
Q-gCN	2.91	3.11	3.06	2.90	3.13	3.07	208	2.3589

L.R = Linear Regression; F.D = First Derivative; S.D = Second Derivative;
U.E= Urbach Energy; R.I= Refractive Index

Optical Conductivity

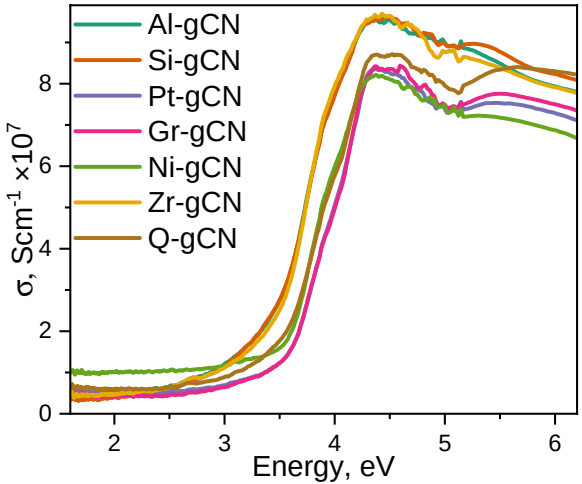

Derivative Diffuse Reflectance Spectroscopic Analysis

	Min	Intensity	Max	Intensity	D Parameter	S.A	Slope	D.P / S.A
Al-gCN	385	-0.06109	407	0.03189	0.09298	15.2	1093	0.006117105
Si-gCN	385	-0.05629	408	0.03621	0.0925	20.8	948.6	0.004447115
Pt-gCN	382	-0.05562	403	0.04362	0.09924	67	423.7	0.001481194
Gr-gCN	381	-0.04569	404	0.04213	0.08782	72.2	335.4	0.001216343
Ni-gCN	385	-0.03963	407	0.02506	0.06469	34	515.9	0.001902647
Zr-gCN	385	-0.06508	406	0.02561	0.09069	12.6	512.3	0.007197619
Q-gCN	381	-0.0526	403	0.04524	0.09784	49.4	530.7	0.001980567

Note: D.P = D parameter, difference between the maxima and minima, S.A= surface area, slope= B.E.T Slope from SESAMI Analysis

Photoluminescence Spectroscopy

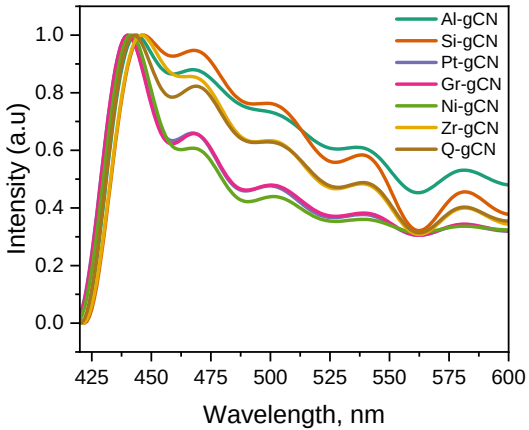

^{13}C Solid State NMR Studies

The convolution of ^{13}C spectra has been performed using the Pseudo Voigt (PsdVoigt1) function. Other functions such as Guass, Lorentz, PsdVoigt2 and Voigt did not provide satisfactory convolution.

$$y = y_0 + A\left[m_u \frac{2}{\pi}\frac{w}{4(x-x_c)^2 + w^2} + (1-m_u)\frac{\sqrt{4\ln 2}}{\sqrt{\pi}w} e^{-\frac{4\ln 2}{w^2}(x-x_c)^2}\right]$$

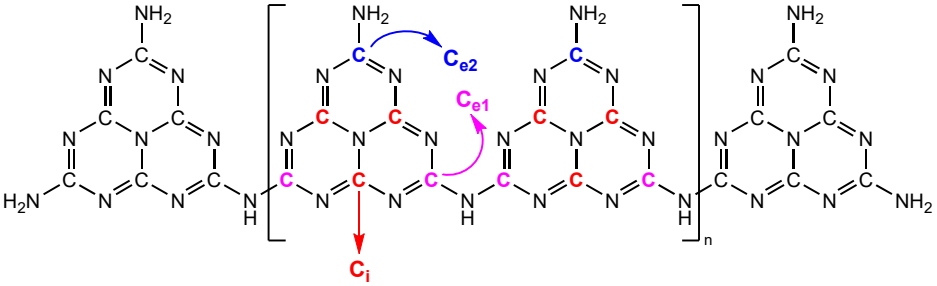

^{13}C NMR

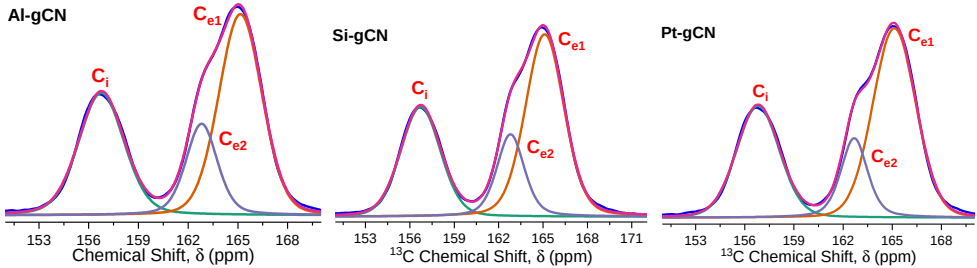
Al-gCN
C_{e1}
C_i
C_{e2}
153 156 159 162 165 168
Chemical Shift, δ (ppm)
Si-gCN
C_{e1}
C_i
C_{e2}
153 156 159 162 165 168 171
^{13}C Chemical Shift, δ (ppm)
Pt-gCN
C_{e1}
C_i
C_{e2}
153 156 159 162 165 168
^{13}C Chemical Shift, δ (ppm)

^{13}C NMR: The Surprise!

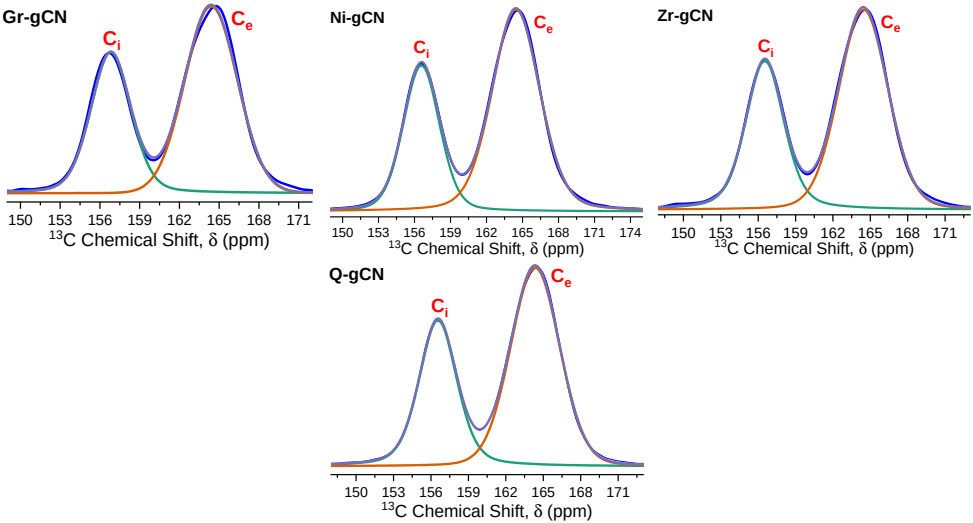

^{13}C NMR: The Surprise!

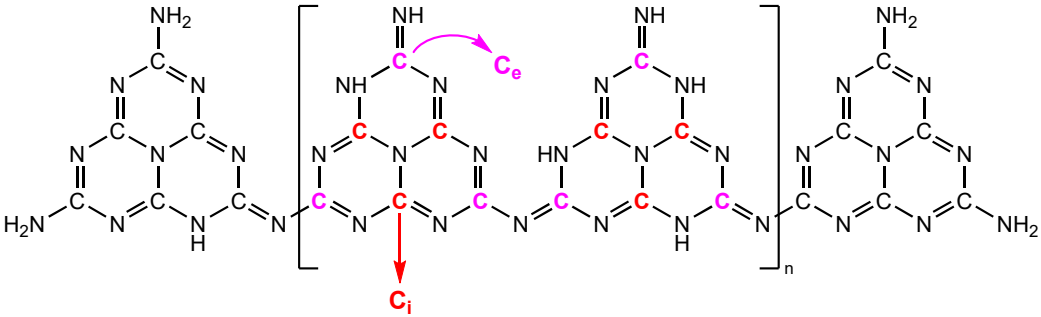

^{15}N Solid State NMR Studies

$$y = y_0 + \frac{A}{w\sqrt{\pi/2}} e^{-2\frac{(x-x_c)^2}{w^2}}$$

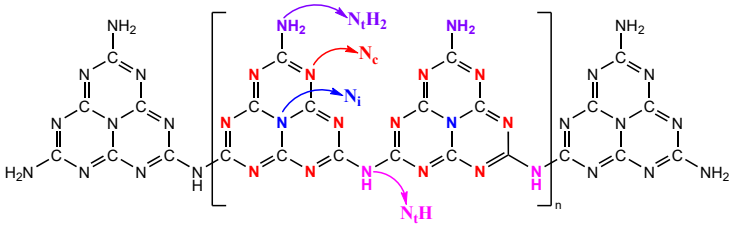

Excessive line broadening was observed in the case of porous materials, which led us to exclude the ^{15}N spectra from any quantitative analysis. To address this, we performed the convolution of the ^{15}N spectra using the Gauss function. However, alternative functions such as Lorentz, PsdVoigt1, PsdVoigt2, and Voigt did not yield satisfactory convolution results.

^{15}N NMR

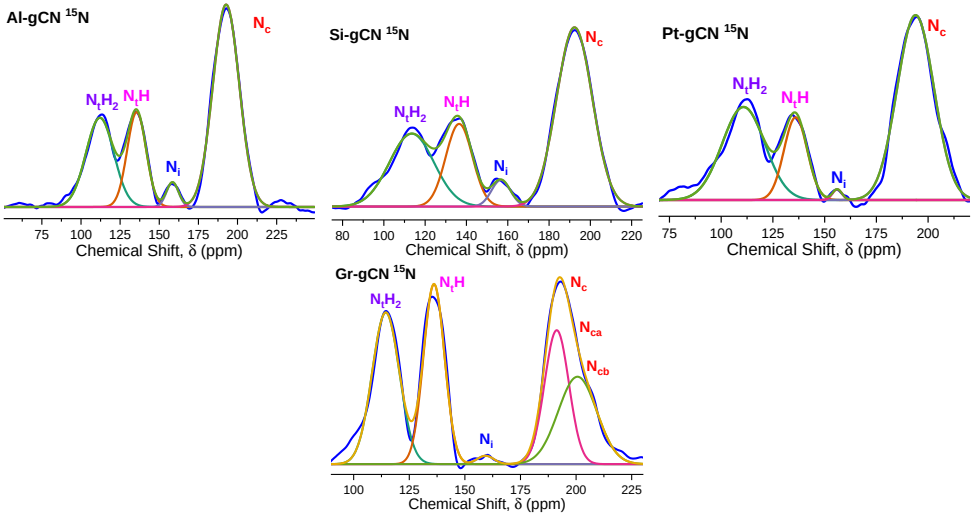
Al-gCN 15N
Nc
NtH2
NtH
Ni
75 100 125 150 175 200 225
Chemical Shift, δ (ppm)
Si-gCN 15N
Nc
NtH2
NtH
Ni
80 100 120 140 160 180 200 220
Chemical Shift, δ (ppm)
Pt-gCN 15N
Nc
NtH2
NtH
Ni
75 100 125 150 175 200
Chemical Shift, δ (ppm)
Gr-gCN 15N
NtH2
NtH
Nc
Nca
Ncb
Ni
100 125 150 175 200 225
Chemical Shift, δ (ppm)

^{15}N NMR

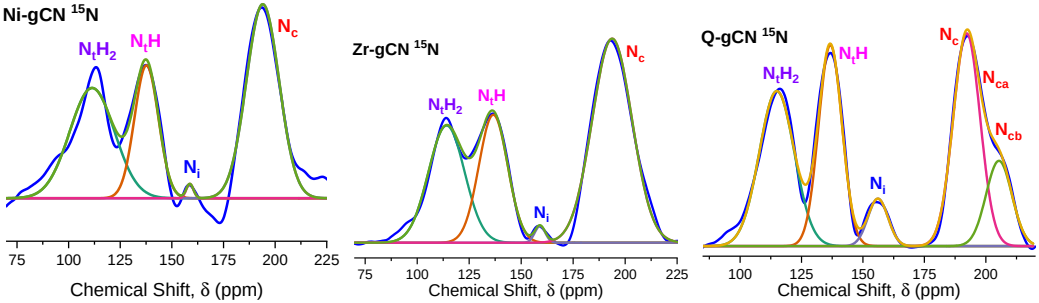
Ni-gCN 15N
NtH2
NtH
Nc
Ni
75 100 125 150 175 200 225
Chemical Shift, δ (ppm)
Zr-gCN 15N
NtH2
NtH
Nc
Ni
75 100 125 150 175 200 225
Chemical Shift, δ (ppm)
Q-gCN 15N
NtH2
NtH
Nc
Nca
Ncb
Ni
100 125 150 175 200
Chemical Shift, δ (ppm)

Survey Spectrum

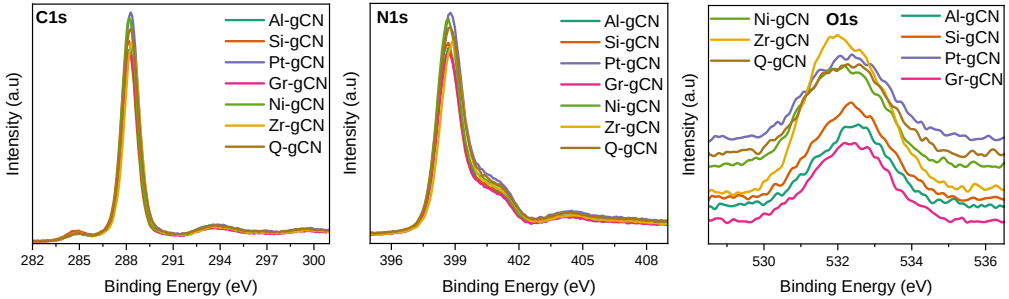

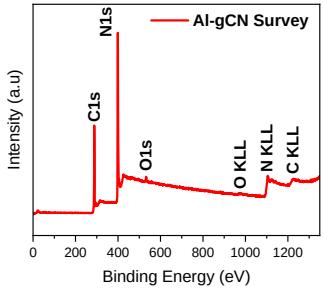
Al-gCN Survey
N1s
C1s
O1s
O KLL
N KLL
C KLL
Intensity (a.u)
0
200
400
600
800
1000
1200
Binding Energy (eV)

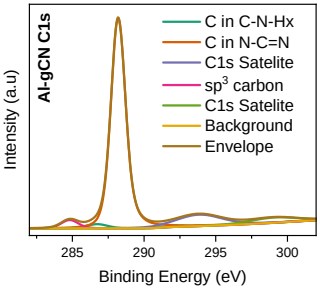
Al-gCN C1s
C in C-N-Hx
C in N-C=N
C1s Satelite
sp3 carbon
C1s Satelite
Background
Envelope
Intensity (a.u)
285
290
295
300
Binding Energy (eV)

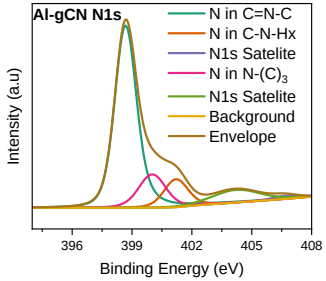
Al-gCN N1s
N in C=N-C
N in C-N-Hx
N1s Satelite
N in N-(C)3
N1s Satelite
Background
Envelope
Intensity (a.u)
396
399
402
405
408
Binding Energy (eV)

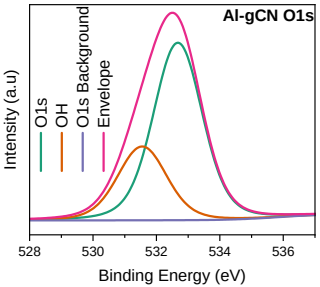
Al-gCN O1s
O1s
OH
O1s Background
Envelope
Intensity (a.u)
528
530
532
534
536
Binding Energy (eV)

Peak Assignment	Pos.	FWHM	L.Sh	Area	At%	Total%	STD
sp^3	284.81	1.4	LA(1.3, 243)	5627.59	1.55		
C in C−N−Hx	286.73	1.72	LA(1.3, 243)	3468.8	0.95	35.31	1.074
C in N−C=N	288.17	1.19	LA(1.03, 1.24, 243)	128413.69	35.31		
C1s Satellite 1	293.83	3.76	LA(1.3, 243)	20580.71	5.66		
C1s Satellite 2	299.1	3.93	LA(1.3, 243)	9818.59	2.7		
N in C=N−C	398.65	1.26	LA(1.03, 1.24, 243)	225747.71	34.48	47.42	1.149
N in N−(C_3)	400.02	1.6	LA(1.3, 243)	48595	7.42		
N in C−N−Hx	401.2	1.42	LA(1.3, 243)	36139.46	5.52		
N1s Satellite 1	404.21	2.79	LA(1.3, 243)	32238.59	4.92		
N1s Satellite 2	406.66	1.43	LA(1.3, 243)	4115.82	0.63		
O1s	532.68	1.81	LA(1.3, 243)	6404.64	0.6		
OH	351.55	1.82	LA(1.3, 243)	2671.83	0.25	0.25	0.8523

Table 1: Spectral Features of Al-gCN

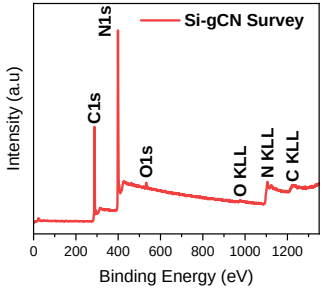
Si-gCN Survey
N1s
C1s
O1s
O KLL
N KLL
C KLL
Intensity (a.u)
0 200 400 600 800 1000 1200
Binding Energy (eV)

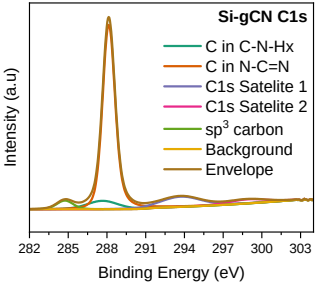
Si-gCN C1s
C in C-N-Hx
C in N-C=N
C1s Satelite 1
C1s Satelite 2
sp3 carbon
Background
Envelope
Intensity (a.u)
282 285 288 291 294 297 300 303
Binding Energy (eV)

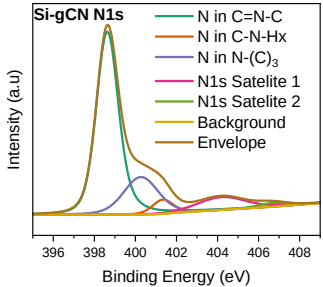
Si-gCN N1s
N in C=N-C
N in C-N-Hx
N in N-(C)3
N1s Satelite 1
N1s Satelite 2
Background
Envelope
Intensity (a.u)
396 398 400 402 404 406 408
Binding Energy (eV)

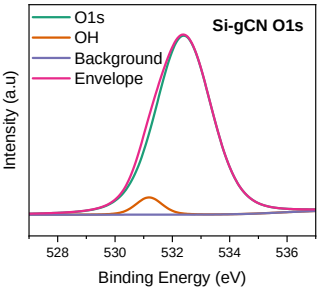
Si-gCN O1s
O1s
OH
Background
Envelope
Intensity (a.u)
528 530 532 534 536
Binding Energy (eV)

Peak Assignment	Pos.	FWHM	L.Sh	Area	At%	Total%	STD
sp^3	284.75	1.49	LA(1.3, 243)	7127.04	1.93		
C in C−N−Hx	287.65	2.78	LA(1.3, 243)	12847.86	3.48	32.85	1.03
C in N−C=N	288.12	1.12	LA(1.03, 1.24, 243)	121240.61	32.85		
C1s Satelite 1	293.88	3.65	LA(1.3, 243)	20422.54	5.53		
C1s Satelite 2	298.88	3.4	LA(1.3, 243)	7592.12	2.06		
N in C=N−C	398.6	1.24	LA(1.03, 1.24, 243)	228709.48	34.42	47.26	1.223
N in N−(C_3)	400.27	1.98	LA(1.3, 243)	69572.14	10.47		
N in C−N−Hx	401.33	1.19	LA(1.3, 243)	15752.26	2.37		
N1s Satelite 1	404.19	2.73	LA(1.3, 243)	32850.53	4.94		
N1s Satelite 2	406.67	1.69	LA(1.3, 243)	5830.68	0.88		
OH	531.19	1.08	LA(1.3, 243)	505.32	0.05	0.05	0.7975
O1s	532.4	2.26	LA(1.3, 243)	11008.28	1.02		

Table 2: Spectral Features of Si-gCN

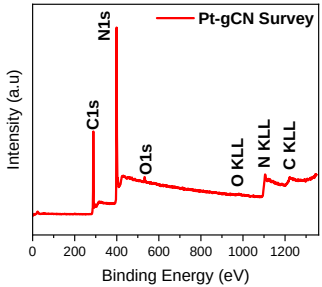
Pt-gCN Survey
N1s
C1s
O1s
O KLL
N KLL
C KLL
Intensity (a.u)
0 200 400 600 800 1000 1200
Binding Energy (eV)

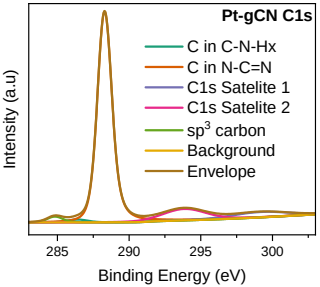
Pt-gCN C1s
C in C-N-Hx
C in N-C=N
C1s Satelite 1
C1s Satelite 2
sp3 carbon
Background
Envelope
Intensity (a.u)
285 290 295 300
Binding Energy (eV)

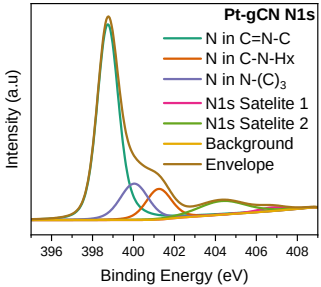
Pt-gCN N1s
N in C=N-C
N in C-N-Hx
N in N-(C)3
N1s Satelite 1
N1s Satelite 2
Background
Envelope
Intensity (a.u)
396 398 400 402 404 406 408
Binding Energy (eV)

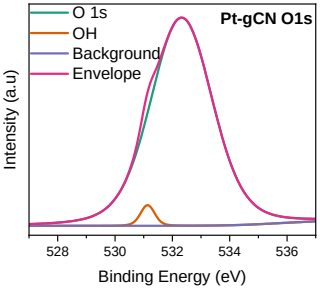
Pt-gCN O1s
O 1s
OH
Background
Envelope
Intensity (a.u)
528 530 532 534 536
Binding Energy (eV)

Peak Assignment	Pos.	FWHM	L.Sh	Area	At%	Total%	STD
sp^3	284.83	1.27	LA(1.3, 243)	4198.2	0.99		
C in C−N−Hx	286.41	1.65	LA(1.3, 243)	2642.2	0.62		
C in N−C=N	288.27	1.17	LA(1.03, 1.24, 243)	150671.56	35.5	35.5	1.071
C1s Satelite 1	293.85	3.53	LA(1.3, 243)	22959.31	5.41		
C1s Satelite 2	299.17	4.64	LA(1.3, 243)	14290.23	3.37		
N in C=N−C	398.72	1.21	LA(1.03, 1.24, 243)	257519.28	33.71	47.43	1.216
N in N−(C_3)	400.04	1.62	LA(1.3, 243)	59633.64	7.81		
N in C−N−Hx	401.24	1.45	LA(1.3, 243)	45182.26	5.91		
N1s Satelite 1	404.32	2.74	LA(1.3, 243)	38094.54	4.99		
N1s Satelite 2	406.75	1.56	LA(1.3, 243)	5596.46	0.73		
OH	531.14	0.58	LA(1.3, 243)	267.99	0.02		
O1s	532.32	2.53	LA(1.3, 243)	11759.7	0.95	0.95	0.8612

Table 3: Spectral Features of Pt-gCN

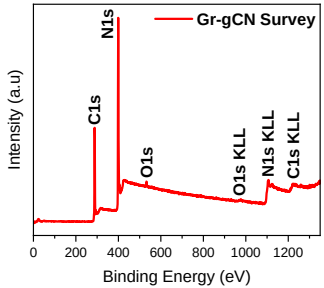
Gr-gCN Survey
N1s
C1s
O1s
O1s KLL
N1s KLL
C1s KLL
Intensity (a.u)
0
200
400
600
800
1000
1200
Binding Energy (eV)

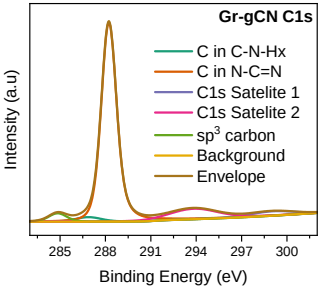
Gr-gCN C1s
C in C-N-Hx
C in N-C=N
C1s Satelite 1
C1s Satelite 2
sp3 carbon
Background
Envelope
Intensity (a.u)
285
288
291
294
297
300
Binding Energy (eV)

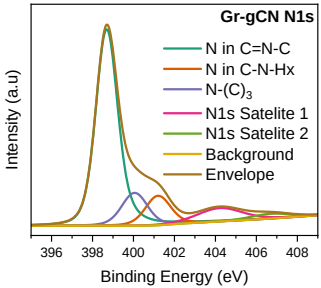
Gr-gCN N1s
N in C=N-C
N in C-N-Hx
N-(C)3
N1s Satelite 1
N1s Satelite 2
Background
Envelope
Intensity (a.u)
396
398
400
402
404
406
408
Binding Energy (eV)

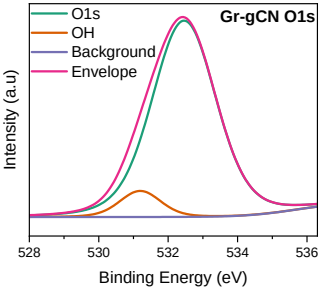
Gr-gCN O1s
O1s
OH
Background
Envelope
Intensity (a.u)
528
530
532
534
536
Binding Energy (eV)

Peak Assignment	Pos.	FWHM	L.Sh	Area	At%	Total%	STD
sp^3	284.84	1.39	LA(1.3, 243)	5745.44	1.65		
C in C−N−Hx	286.88	1.99	LA(1.3, 243)	4433	1.27		
C in N−C=N	288.2	1.17	LA(1.03, 1.24, 243)	122826.81	35.21	35.21	1.072
C1s Satelite 1	293.83	3.74	LA(1.3, 243)	19335.27	5.54		
C1s Satelite 2	299.07	3.36	LA(1.3, 243)	7306.16	2.09		
N in C=N−C	398.67	1.24	LA(1.03, 1.24, 243)	219392.84	34.94	47.15	1.357
N in N−(C_3)	400.06	1.48	LA(1.3, 243)	40844.67	6.5		
N in C−N−Hx	401.2	1.45	LA(1.3, 243)	35843.11	5.71		
N1s Satelite 1	404.21	2.59	LA(1.3, 243)	29127.17	4.64		
N1s Satelite 2	406.69	2.31	LA(1.3, 243)	9202.73	1.47		
O1s	531.19	1.39	LA(1.3, 243)	788.03	0.08		
OH	532.46	2.17	LA(1.3, 243)	9225.01	0.9	0.9	0.8307

Table 4: Spectral Features of Gr-gCN

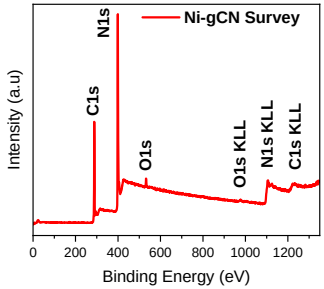
Ni-gCN Survey
N1s
C1s
O1s
O1s KLL
N1s KLL
C1s KLL
Intensity (a.u)
0
200
400
600
800
1000
1200
Binding Energy (eV)

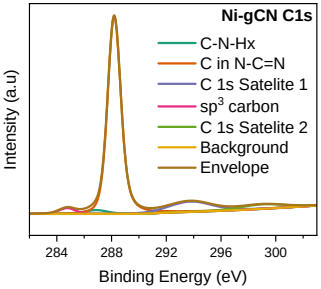
Ni-gCN C1s
C-N-Hx
C in N-C=N
C 1s Satelite 1
sp3 carbon
C 1s Satelite 2
Background
Envelope
Intensity (a.u)
284
288
292
296
300
Binding Energy (eV)

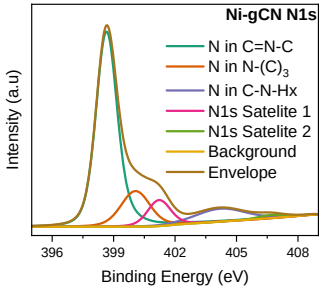
Ni-gCN N1s
N in C=N-C
N in N-(C)3
N in C-N-Hx
N1s Satelite 1
N1s Satelite 2
Background
Envelope
Intensity (a.u)
396
399
402
405
408
Binding Energy (eV)

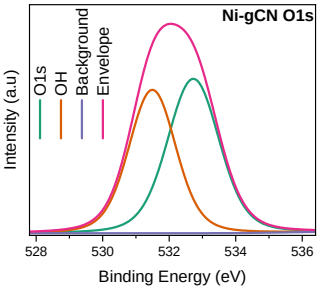
Ni-gCN O1s
O1s
OH
Background
Envelope
Intensity (a.u)
528
530
532
534
536
Binding Energy (eV)

Peak Assignment	Pos.	FWHM	L.Sh	Area	At%	Total%	STD
sp^3	284.76	1.42	LA(1.3, 243)	4901.74	1.23		
C in C−N−Hx	286.87	1.94	LA(1.3, 243)	4384.29	1.1		
C in N−C=N	288.17	1.11	LA(1.03, 1.24, 243)	139622.69	35.08	35.08	1.052
C1s Satelite 1	293.77	3.67	LA(1.3, 243)	22359.24	5.62		
C1s Satelite 2	299.04	3.86	LA(1.3, 243)	10180.4	2.56		
N in C=N−C	398.63	1.2	LA(1.03, 1.24, 243)	247920.94	34.6	47.53	1.213
N in N−(C_3)	400.07	1.67	LA(1.3, 243)	58823.2	8.21		
N in C−N−Hx	401.22	1.31	LA(1.3, 243)	33819.38	4.72		
N1s Satelite 1	404.21	2.85	LA(1.3, 243)	36603.86	5.11		
N1s Satelite 2	406.69	1.51	LA(1.3, 243)	4771.17	0.67		
OH	531.49	1.66	LA(1.3, 243)	5922.36	0.51	0.51	0.8392
O1s	532.73	1.83	LA(1.3, 243)	7018.92	0.6		

Table 5: Spectral Features of Ni-gCN

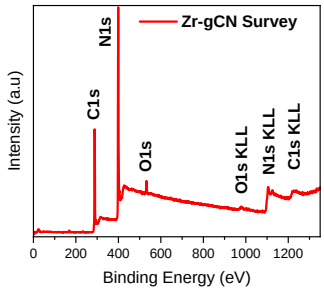
Zr-gCN Survey
N1s
C1s
O1s
O1s KLL
N1s KLL
C1s KLL
Intensity (a.u)
0
200
400
600
800
1000
1200
Binding Energy (eV)

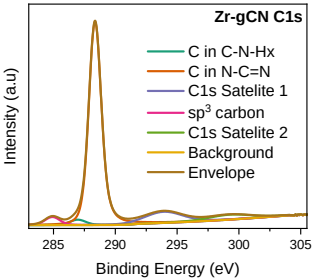
Zr-gCN C1s
C in C-N-Hx
C in N-C=N
C1s Satelite 1
sp3 carbon
C1s Satelite 2
Background
Envelope
Intensity (a.u)
285
290
295
300
305
Binding Energy (eV)

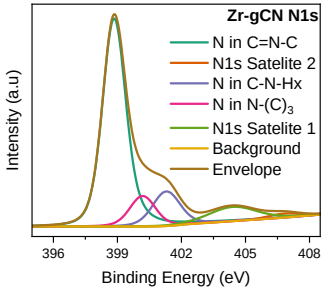
Zr-gCN N1s
N in C=N-C
N1s Satelite 2
N in C-N-Hx
N in N-(C)3
N1s Satelite 1
Background
Envelope
Intensity (a.u)
396
399
402
405
408
Binding Energy (eV)

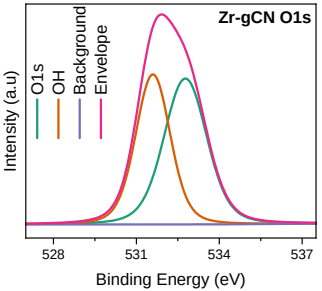
Zr-gCN O1s
O1s
OH
Background
Envelope
Intensity (a.u)
528
531
534
537
Binding Energy (eV)

Peak Assignment	Pos.	FWHM	L.Sh	Area	At%	Total%	STD
sp^3	284.91	1.43	LA(1.3, 243)	5879.86	1.57		
C in C−N−Hx	286.97	1.5	LA(1.3, 243)	4131.01	1.1		
C in N−C=N	288.34	1.16	LA(1.03, 1.24, 243)	130331.12	34.82	34.82	1.093
C1s Satelite 1	293.93	3.59	LA(1.3, 243)	20410.1	5.45		
C1s Satelite 2	299.25	4.07	LA(1.3, 243)	10241.21	2.74		
N in C=N−C	398.82	1.27	LA(1.03, 1.24, 243)	236880.8	35.16	47.05	1.361
N in N−(C_3)	400.18	1.42	LA(1.3, 243)	36200.44	5.37		
N in C−N−Hx	401.29	1.52	LA(1.3, 243)	43930.24	6.52		
N1s Satelite 1	404.4	2.63	LA(1.3, 243)	31457.64	4.67		
N1s Satelite 2	406.82	1.73	LA(1.3, 243)	5773.05	0.86		
OH	531.6	1.47	LA(1.3, 243)	8631.56	0.79	0.79	0.8421
O1s	532.77	1.82	LA(1.3, 243)	10410.36	0.95		

Table 6: Spectral Features of Zr-gCN

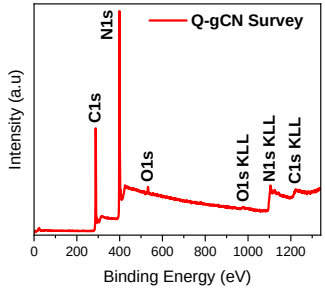
Q-gCN Survey
N1s
C1s
O1s
O1s KLL
N1s KLL
C1s KLL
Intensity (a.u)
0
200
400
600
800
1000
1200
Binding Energy (eV)

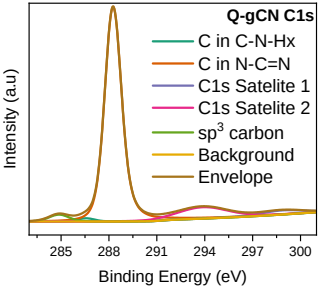
Q-gCN C1s
C in C-N-Hx
C in N-C=N
C1s Satelite 1
C1s Satelite 2
sp3 carbon
Background
Envelope
Intensity (a.u)
285
288
291
294
297
300
Binding Energy (eV)

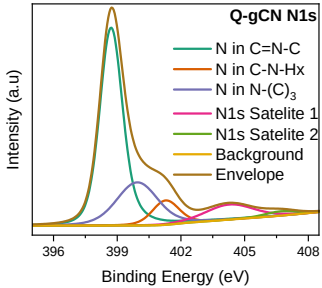
Q-gCN N1s
N in C=N-C
N in C-N-Hx
N in N-(C)3
N1s Satelite 1
N1s Satelite 2
Background
Envelope
Intensity (a.u)
396
399
402
405
408
Binding Energy (eV)

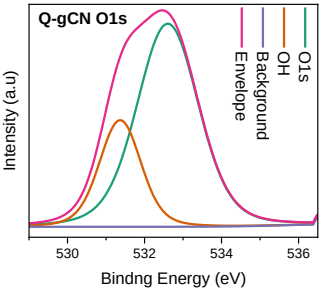
Q-gCN O1s
Envelope
Background
OH
O1s
Intensity (a.u)
530
532
534
536
Bindng Energy (eV)

Peak Assignment	Pos.	FWHM	L.Sh	Area	At%	Total%	STD
sp^3	284.87	1.48	LA(1.3, 243)	5303.14	1.3		
C in C−N−Hx	286.56	1.28	LA(1.3, 243)	2181.78	0.54		
C in N−C=N	288.23	1.22	LA(1.03, 1.24, 243)	145867.7	35.89	35.89	1.143
C1s Satelite 1	293.88	3.71	LA(1.3, 243)	21888.45	5.39		
C1s Satelite 2	298.88	3.1	LA(1.3, 243)	6649.06	1.64		
N in C=N−C	398.69	1.24	LA(1.03, 1.24, 243)	235029.6	32.12	48.49	1.048
N in N−(C_3)	399.95	2.28	LA(1.3, 243)	87696.32	11.99		
N in C−N−Hx	401.28	1.47	LA(1.3, 243)	32011.48	4.38		
N1s Satelite 1	404.28	2.66	LA(1.3, 243)	35814.5	4.9		
N1s Satelite 2	406.7	1.79	LA(1.3, 243)	6791.29	0.93		
OH	531.37	1.27	LA(1.3, 243)	2933.32	0.25	0.25	0.8676
O1s	532.6	1.88	LA(1.3, 243)	8256.52	0.69		

Table 7: Spectral Features of Q-gCN

Valence Band XPS Analysis

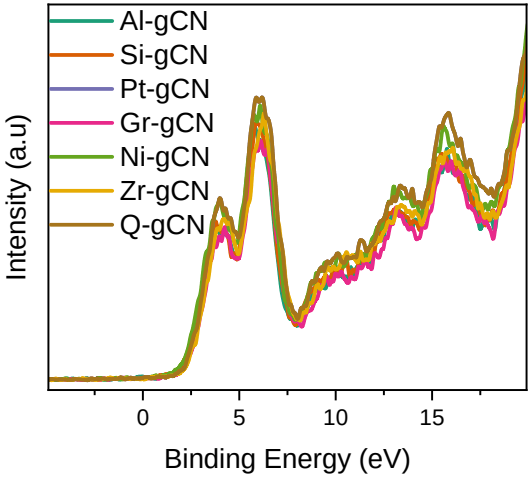

Valence Band XPS Analysis

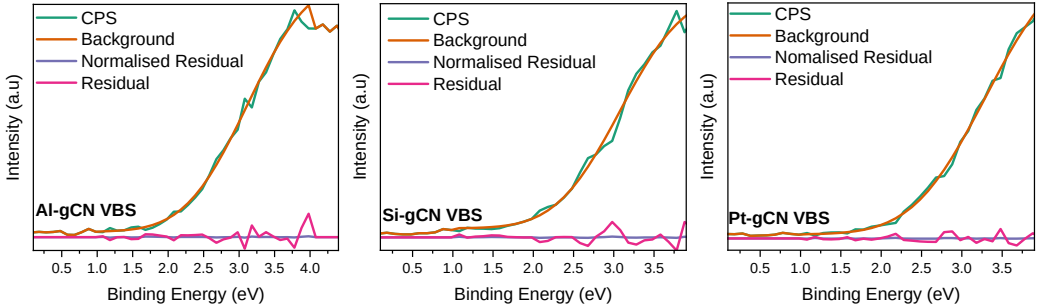

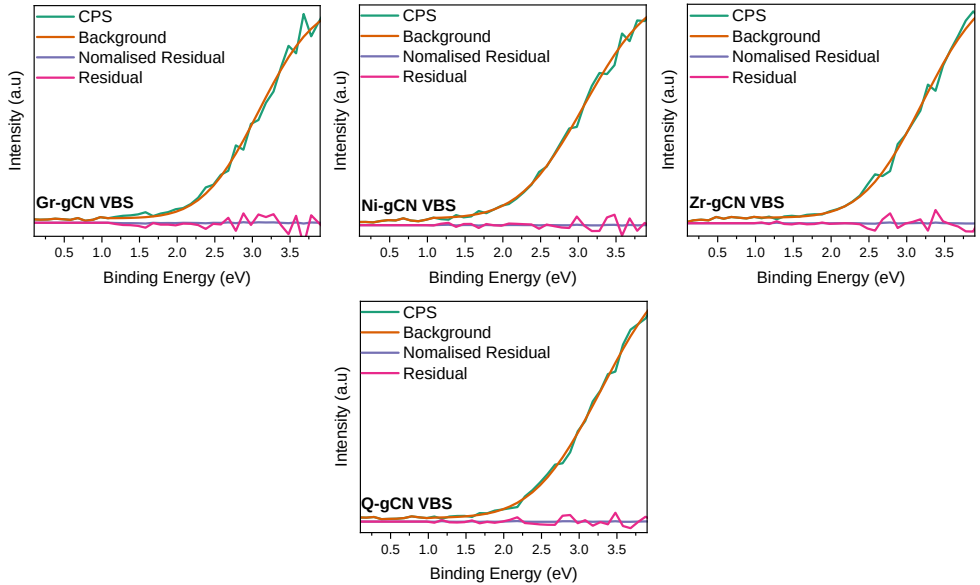
CPS
Background
Nomalised Residual
Residual
Intensity (a.u)
Gr-gCN VBS
Ni-gCN VBS
Zr-gCN VBS
Q-gCN VBS
0.5 1.0 1.5 2.0 2.5 3.0 3.5
Binding Energy (eV)

Derivative Valence Band XPS

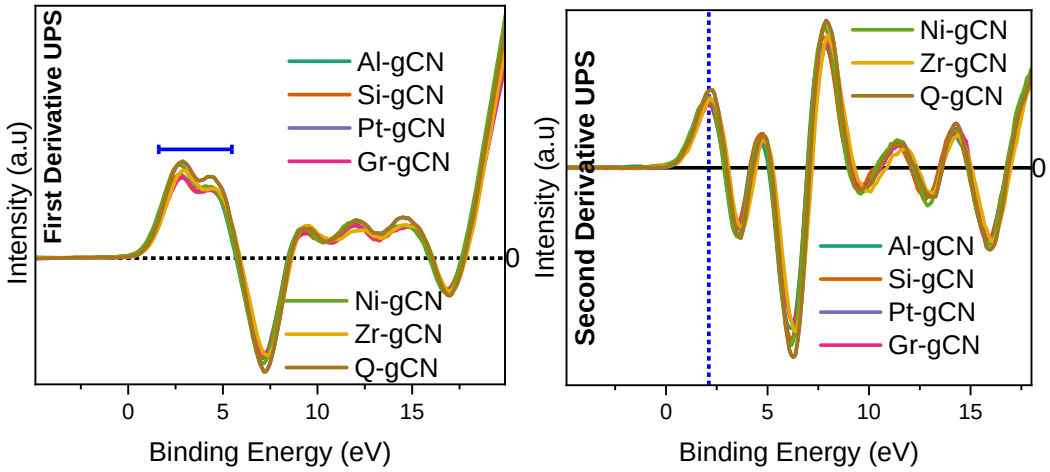

Valence Band XPS Analysis

	Highest Occupied Molecular Orbital (HOMO), eV				
Sample	**Second Derivative**	**Curve Fitting**			
		Position	**Original Value**	**FWHM**	**STD**
Al-gCN	2.08	2.14	2.1398	1.62	1.208
Si-gCN	2.08	2.19	2.1930	1.47	1.237
Pt-gCN	2.28	2.29	2.2870	1.67	1.1
Gr-gCN	1.98	2.26	2.2562	1.38	1.436
Ni-gCN	2.08	2.12	2.1207	1.6	1.023
Zr-gCN	2.18	2.33	2.33	1.46	1.078
Q-gCN	2.28	2.29	2.2870	1.67	1.034

Energy Band Diagram Elucidation

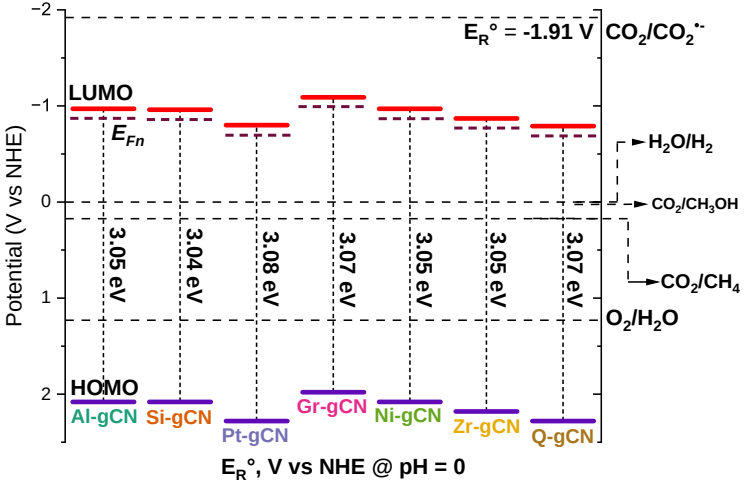

Energy Band Diagram Elucidation: pH Correction

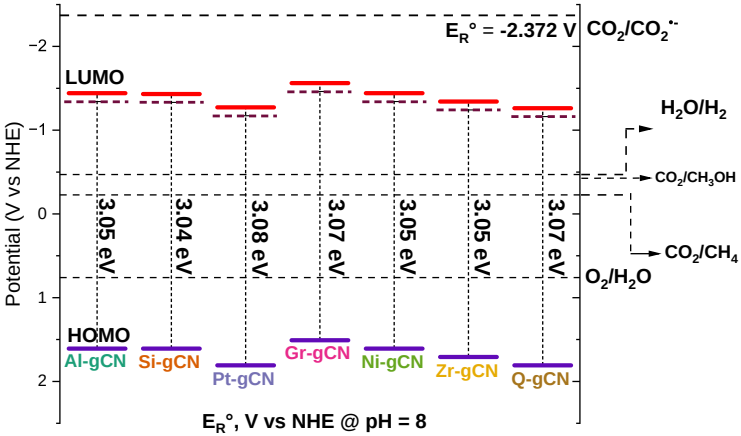

Band Position, Ionization Potential, and Electron Affinity

Sample	Bandgap	HOMO	LUMO	I.E	E.A	C	N	C/N
Al-gCN	3.05 eV	2.08 V	−0.97 V	6.52 eV	3.47 eV	35.31	47.42	0.7446
Si-gCN	3.04 eV	2.08 V	−0.96 V	6.52 eV	3.48 eV	32.38	47.26	0.6851
Pt-gCN	3.08 eV	2.28 V	−0.8 V	6.72 eV	3.64 eV	35.5	47.43	0.7485
Gr-gCN	3.07 eV	1.98 V	−1.09 V	6.42 eV	3.35 eV	35.21	47.15	0.7468
Ni-gCN	3.05 eV	2.08 V	−0.97 V	6.52 eV	3.47 eV	35.08	47.53	0.7381
Zr-gCN	3.05 eV	2.18 V	−0.87 V	6.62 eV	3.57 eV	34.82	47.05	0.7401
Q-gCN	3.07 eV	2.28 V	−0.79 V	6.72 eV	3.65 eV	35.89	48.49	0.7402

Table of Contents

Context

Synthesis of Li-PTI-AIR & Li-PTI-N_2

1. In a glove box under an inert atmosphere:
   1. Thorough grinding of 2 g (15.58 mmol) of melamine ($C_3H_6N_6$) recrystallized from acetone with lithium chloride 10 g.
   2. Transfer of the resulting mixture into a flat round bottom cylindrical alumina crucible with a lid.
2. Heating process:
   1. Placement of the crucible with the reaction mixture in a muffle furnace.
   2. Heating at a ramping rate of 2 °C min until reaching a terminal temperature of 550 °C.
   3. Duration of heating: 4 h.
3. Salt removal and drying process:
   1. Removal of the salt block from the reaction mixture through boiling distilled water washing.
   2. Centrifugation at 10 000 rpm for 15 min.
   3. Drying of the obtained material in a vacuum oven at 110 °C overnight under a 10^{-5} torr pressure.
4. Post-processing

X-ray Diffraction: Reitveld Refinement

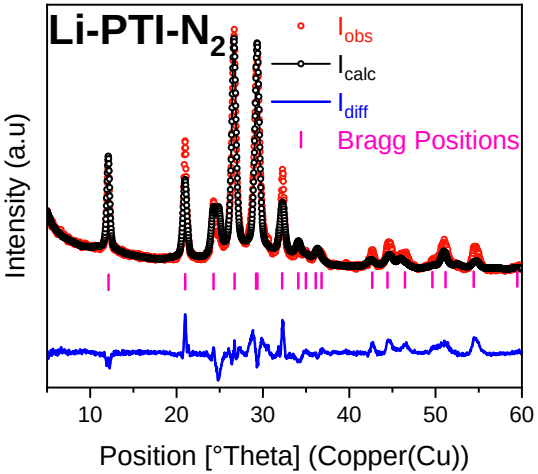

X-ray Diffraction Analysis

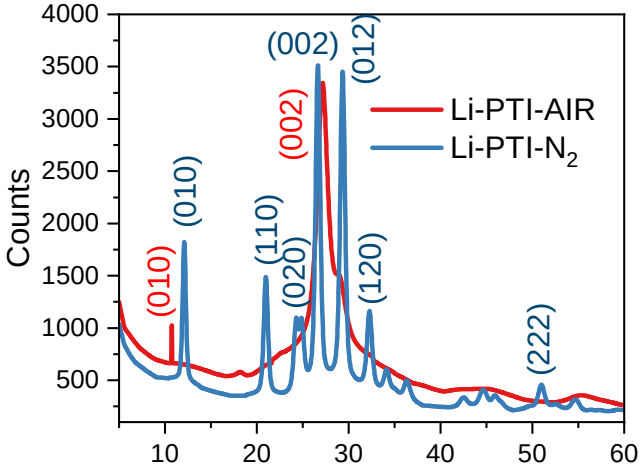

Structure Elucidation: Li-PTI-AIR

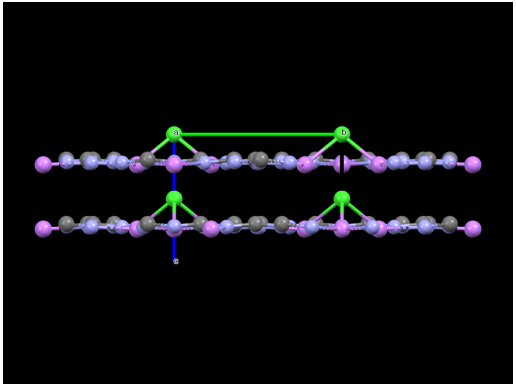

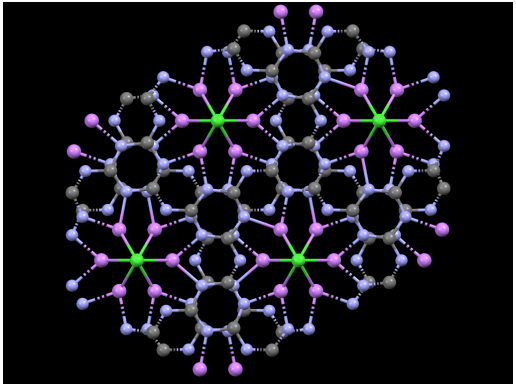

Structure Elucidation: Li-PTI-N_2

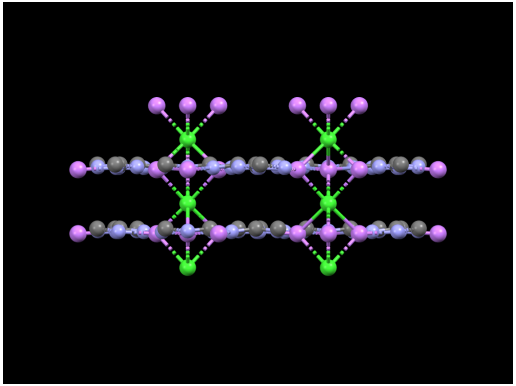

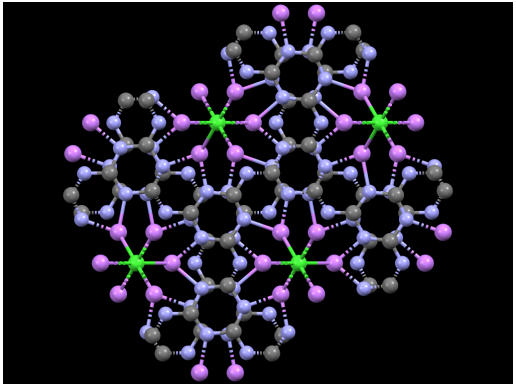

The B.E.T Surface Area

	B.E.T Surface Area	**C**
Li-PTI-AIR	148.94	-158.36
Li-PTI-N_2	74.67	-640.71

Surface Area Analysis: BETSI vs. SESAMI Method

	Surface Area, m^2/g						
	B.E.T	**BETSI**	**SESAMI**	**C, SESAMI**	**qm, mol/kg**	**Pore Size, nm**	**t-plot M.A**
Li-PTI-AIR	148.94	160	159.1	421.1	1.63	5.07	51.36
Li-PTI-N_2	74.67	77	77.1	298.2	0.79	20.16	17.32

Physical Adsorption Characterization

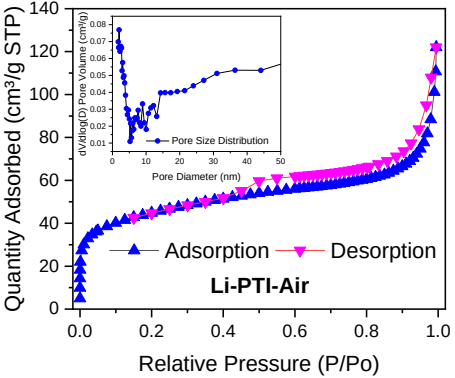

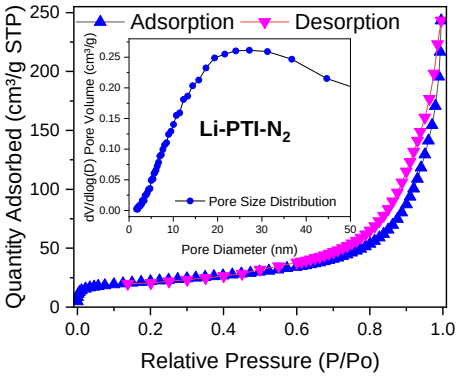

Surface Areas versus CH_4 Yield

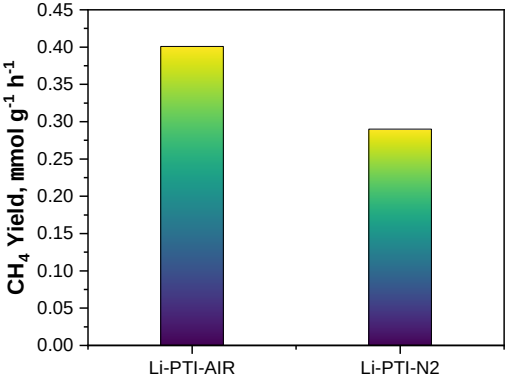

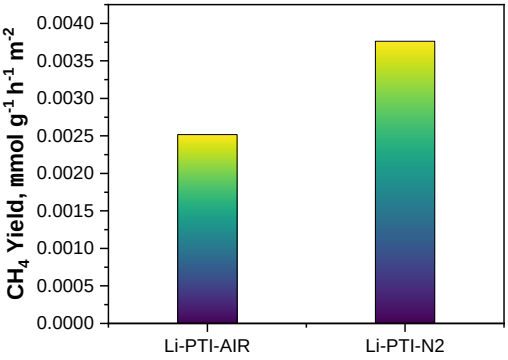

Surface Areas versus CH_3OH Yield

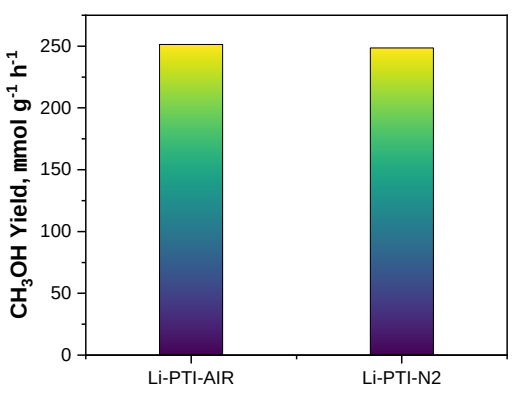

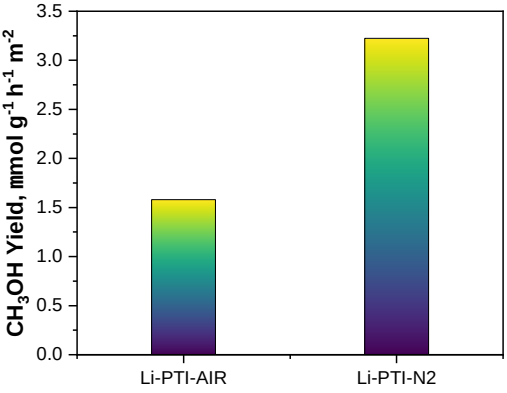

Surface Areas versus O_2 Yield

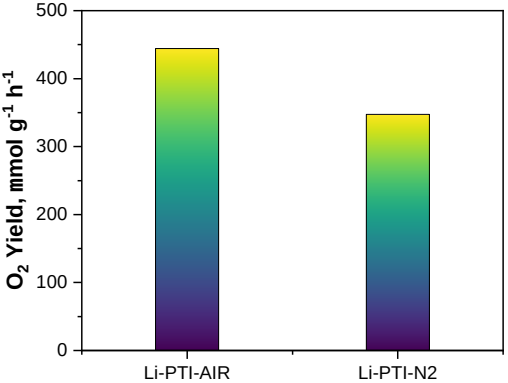

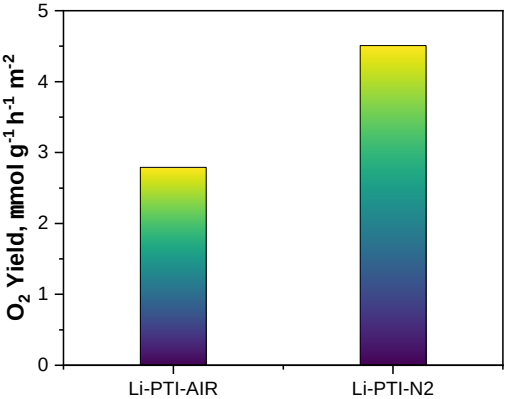

Derivative Isotherm Summation

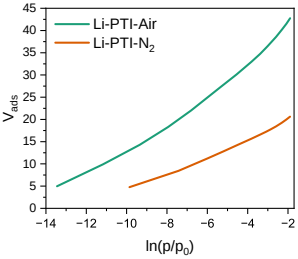

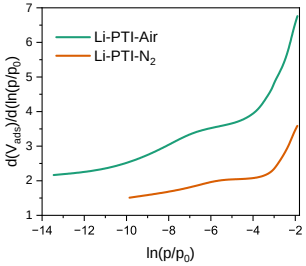

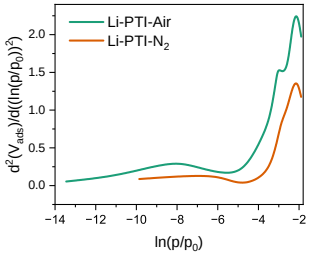

Derivative Isotherm Summation

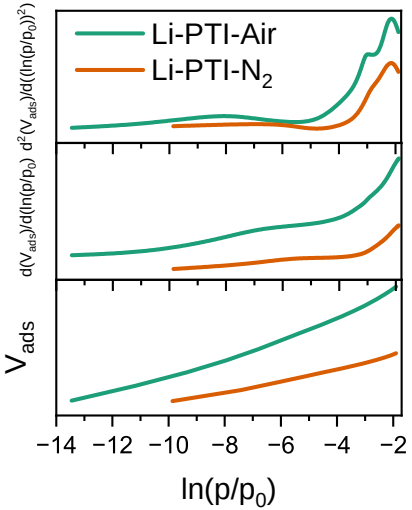

Field Emission Scanning Electron Microscopy (FESEM) 5 µm

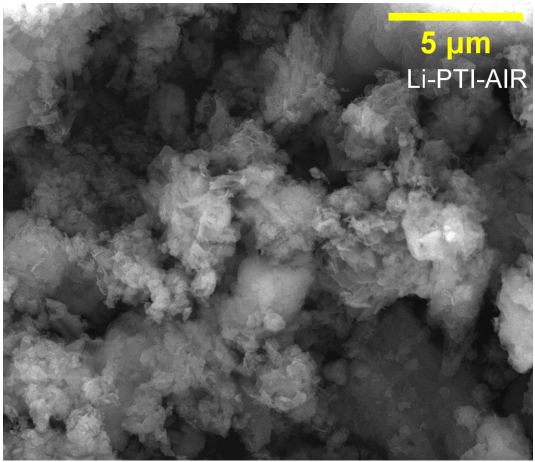

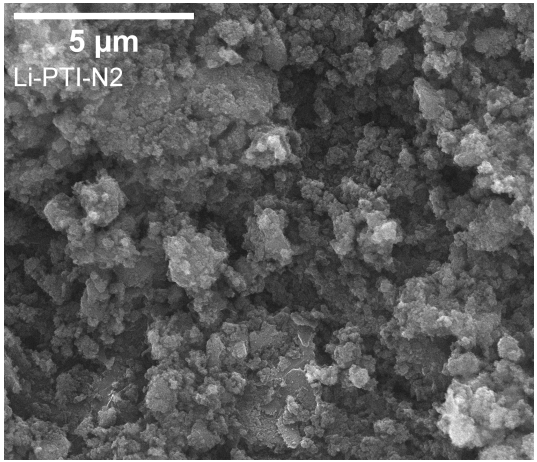

Field Emission Scanning Electron Microscopy (FESEM) 1 µm

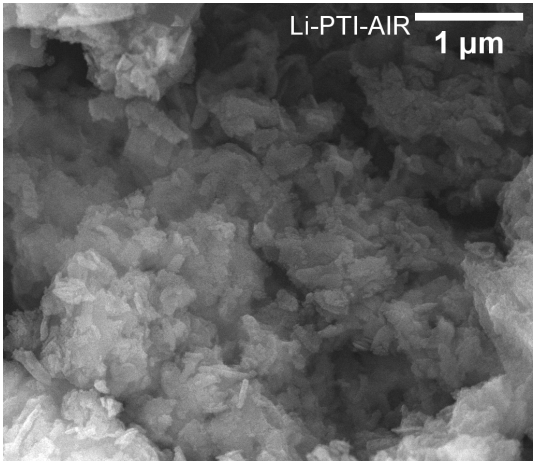

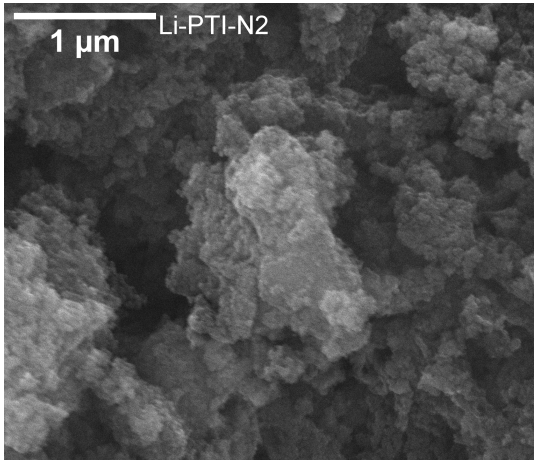

Energy-Dispersive X-ray Analysis (EDAX)

	Element	Weight %	MDL	Atomic %	Net Int.	Error %
Li-PTI-Air	C K	57.1	0.35	61.6	488.5	9.9
	N K	34.7	1.34	32.1	64.7	13.8
	O K	7.6	0.52	6.1	34.6	14.8
	Cl K	0.7	0.05	0.2	66.7	8.4
Li-PTI-N_2	C	56.6	1.06	61.2	-	11.6
	N	34.4	3.20	31.9	-	16.3
	O	8.1	1.10	6.6	-	18.3
	C l	0.9	0.07	0.3	-	7.8

UV-Visible Spectroscopy

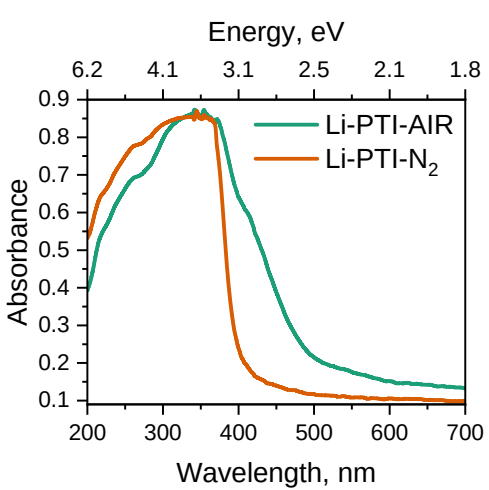

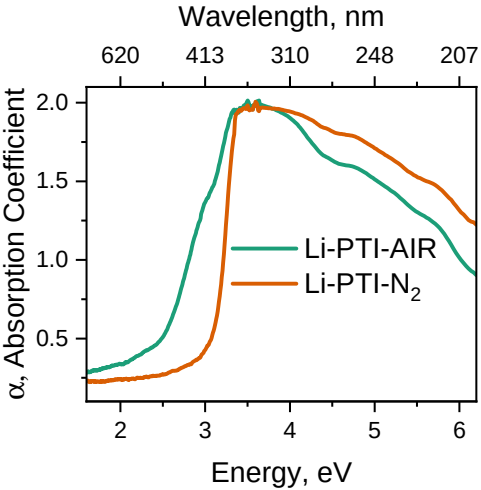

Tauc Plot Validation

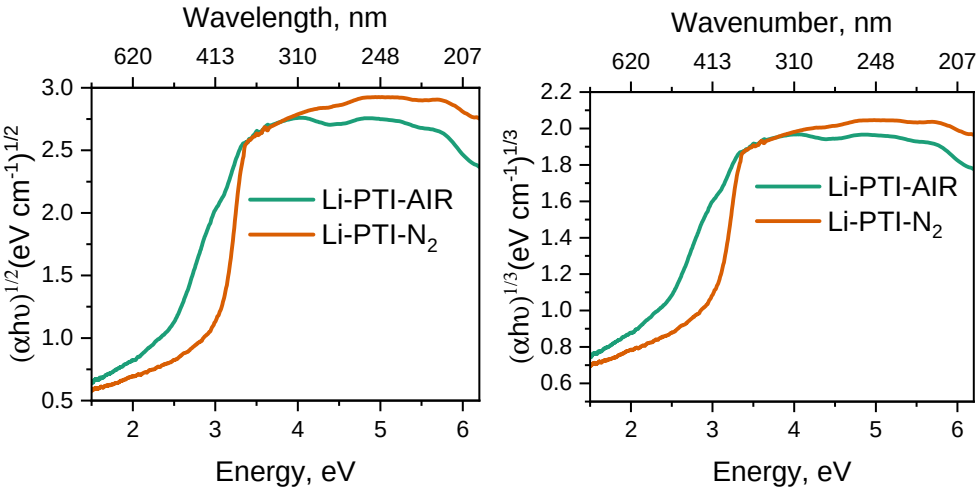

Tauc Plot Validation

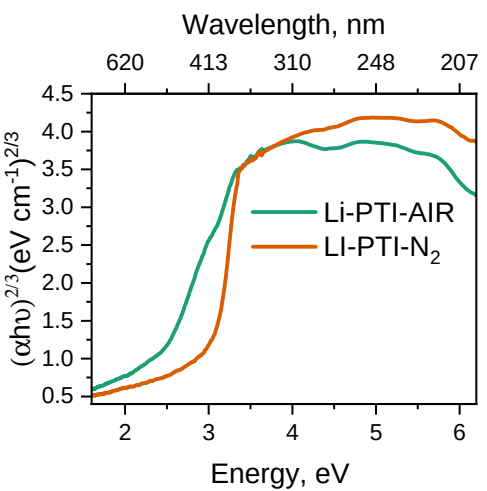

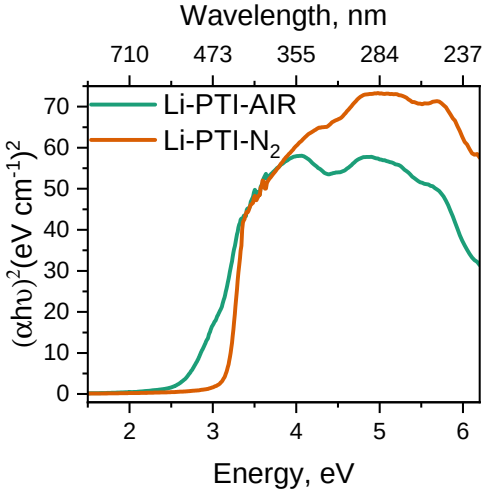

Derivative Tauc Plot

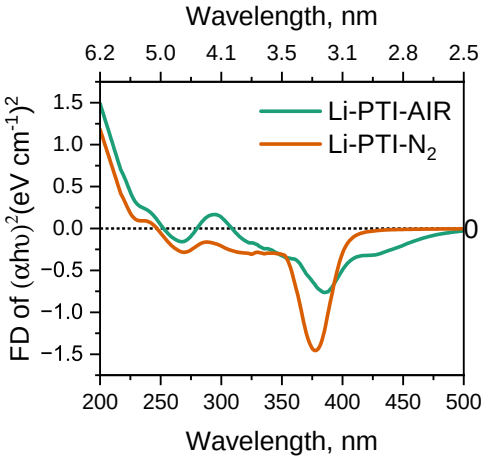

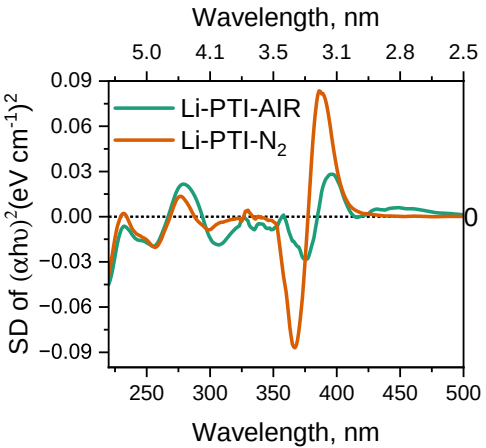

Derivative Tauc Plot Analysis

	Min	Intensity	Max	Intensity	D Parameter	S.A	Slope	D.P / S. A
Li-PTI-AIR	375	-0.02835	396	0.02812	0.05647	159.1	421.1	0.000354934
Li-PTI-N_2	367	-0.08702	386	0.08352	0.17054	77.1	298.2	0.002211933

Note: D.P = D parameter, difference between the maxima and minima, S.A= surface area, slope= B.E.T Slope from SESAMI Analysis

Urbach Plot

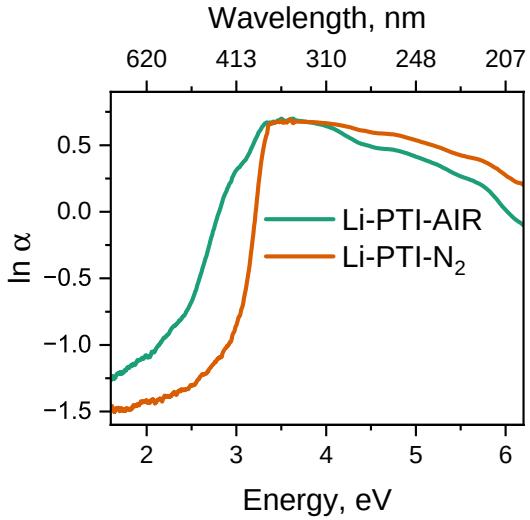
Wavelength, nm
620
413
310
248
207
0.5
0.0
−0.5
−1.0
−1.5
ln α
Li-PTI-AIR
Li-PTI-N2
2
3
4
5
6
Energy, eV

Diffuse Reflectance Spectroscopy

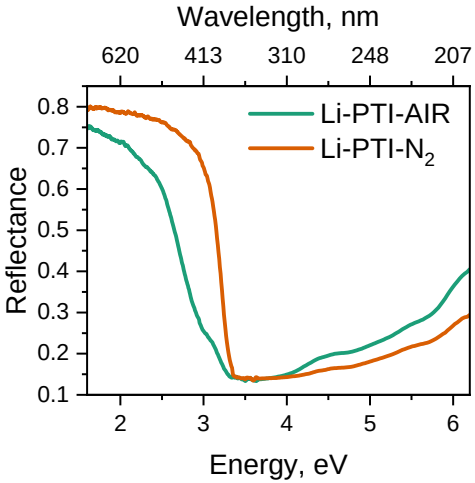

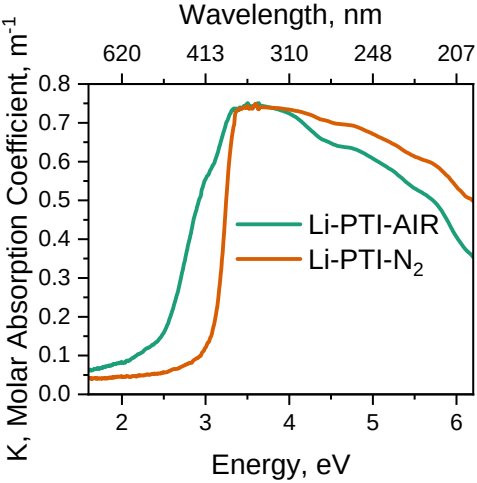

Diffuse Reflectance Spectroscopy

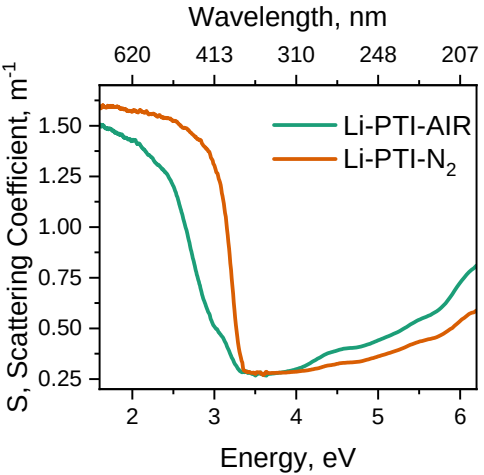

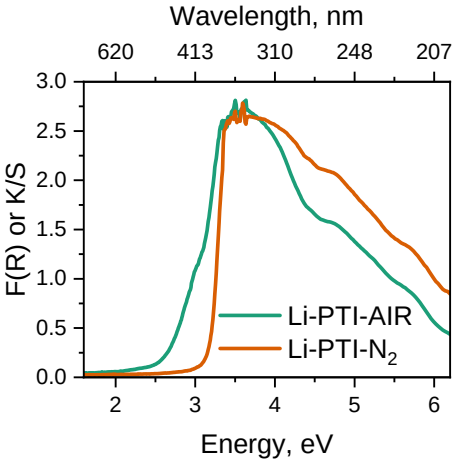

Kubelka-Monk Plots

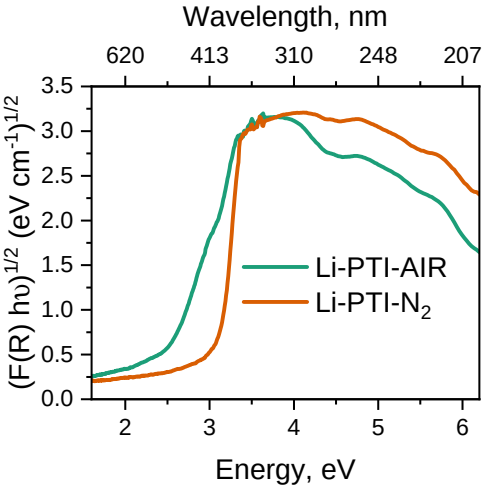

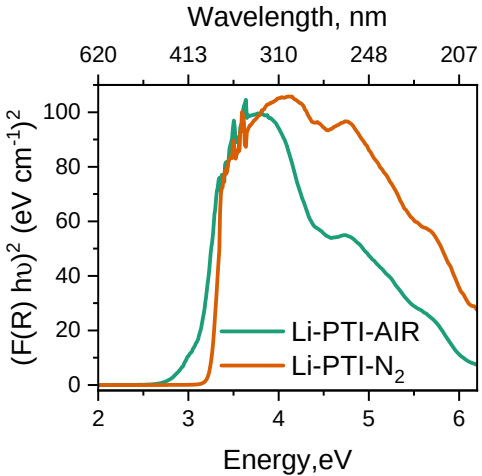

Derivative Kubelka-Monk Plots

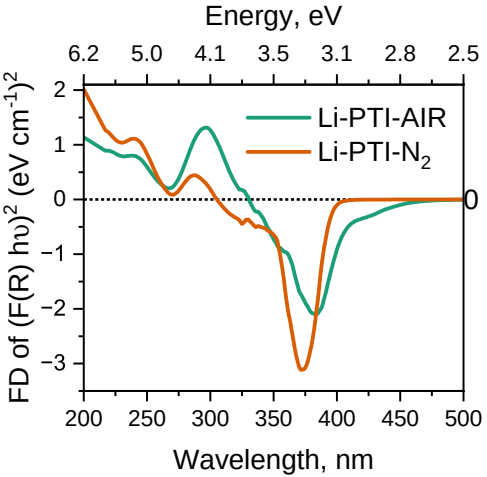

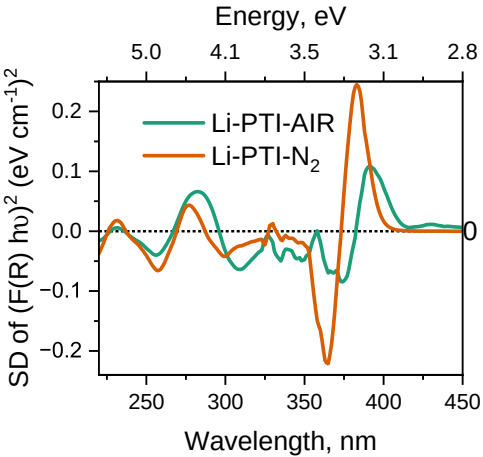

UV-Visible Diffuse Spectroscopy Analysis

Sample	Band Gap, eV						U.E meV	R.I
	Tauc Plot			K-M Plot				
	L.R	F.D	S.D	L.R	F.D	S.D	L.R	
Li-PTI-AIR	2.88	3.67	3.12	3.08	3.24	3.17	447	2.3259
Li-PTI-N_2	3.16	3.28	3.21	3.28	3.33	3.24	184	2.3038

L.R = Linear Regression; F.D = First Derivative; S.D = Second Derivative;
U.E= Urbach Energy; R.I= Refractive Index

Optical Conductivity

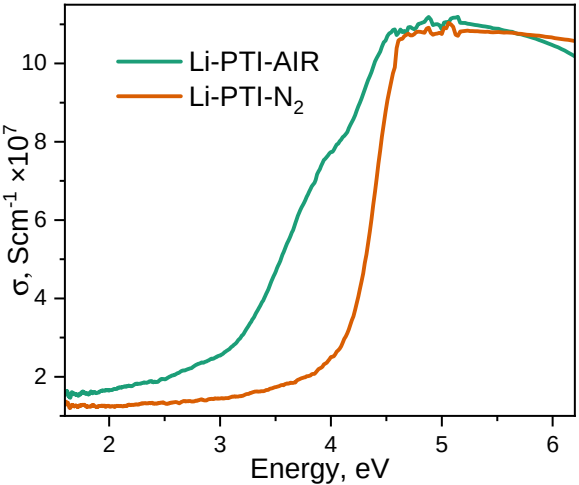

Derivative Diffuse Reflectance Spectroscopic Analysis

	Min	Intensity	Max	Intensity	D Parameter	S.A	Slope	D.P /S.A
Li-PTI-AIR	374	-0.08471	391	0.10879	0.1935	159.1	421.1	0.001216216
Li-PTI-N2	365	-0.22116	383	0.24477	0.46593	77.1	298.2	0.006043191

Note: D.P = D parameter, difference between the maxima and minima, S.A= surface area, slope= B.E.T Slope from SESAMI Analysis

Survey Spectrum

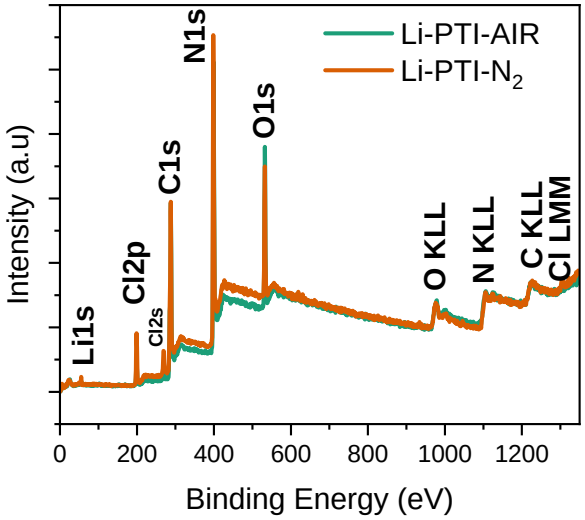

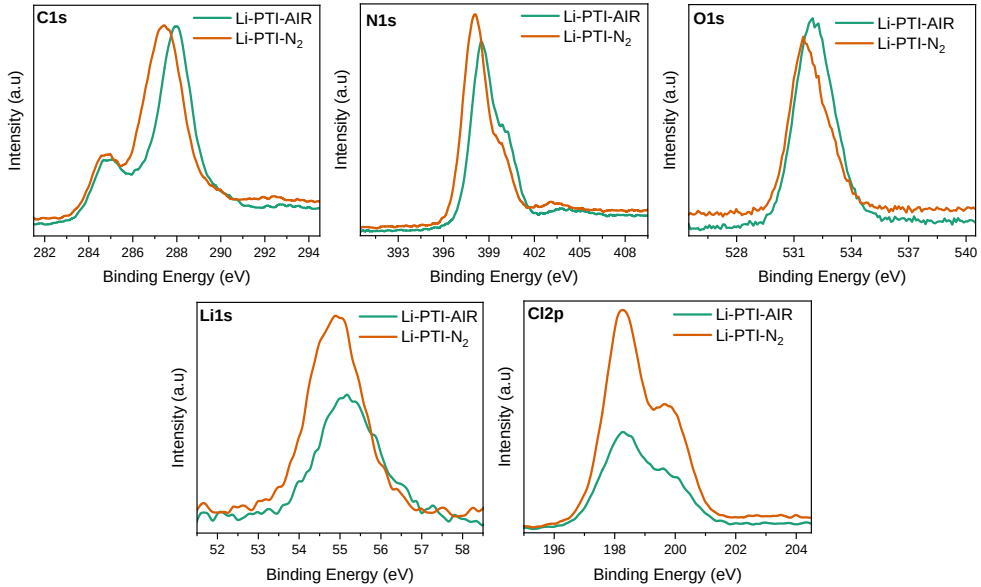
C1s
Li-PTI-AIR
Li-PTI-N2
Intensity (a.u)
282 284 286 288 290 292 294
Binding Energy (eV)
N1s
Li-PTI-AIR
Li-PTI-N2
Intensity (a.u)
393 396 399 402 405 408
Binding Energy (eV)
O1s
Li-PTI-AIR
Li-PTI-N2
Intensity (a.u)
528 531 534 537 540
Binding Energy (eV)
Li1s
Li-PTI-AIR
Li-PTI-N2
Intensity (a.u)
52 53 54 55 56 57 58
Binding Energy (eV)
Cl2p
Li-PTI-AIR
Li-PTI-N2
Intensity (a.u)
196 198 200 202 204
Binding Energy (eV)

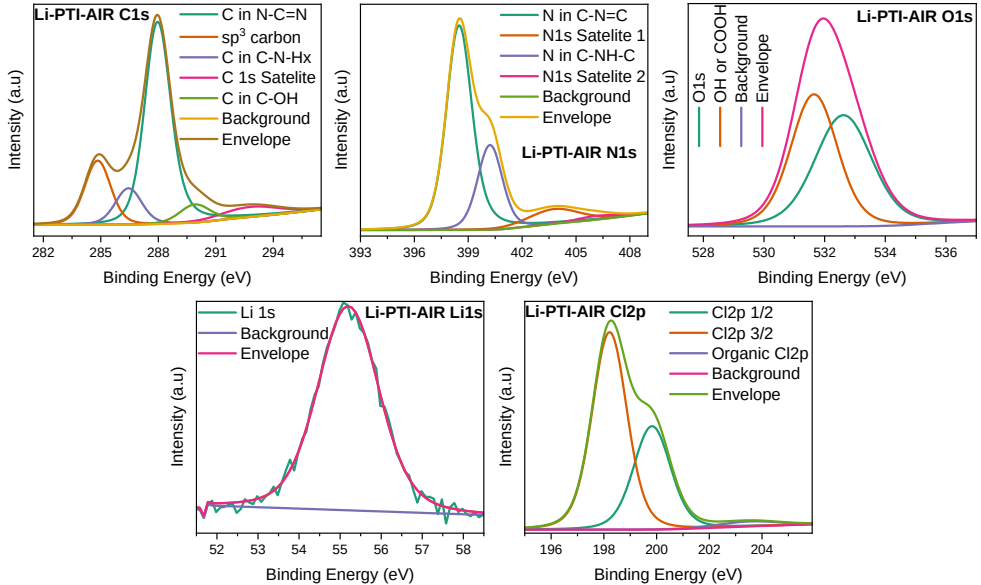
Li-PTI-AIR C1s
C in N-C=N
sp3 carbon
C in C-N-Hx
C 1s Satelite
C in C-OH
Background
Envelope
Intensity (a.u)
282 285 288 291 294
Binding Energy (eV)
N in C-N=C
N1s Satelite 1
N in C-NH-C
N1s Satelite 2
Background
Envelope
Li-PTI-AIR N1s
Intensity (a.u)
393 396 399 402 405 408
Binding Energy (eV)
Li-PTI-AIR O1s
O1s
OH or COOH
Background
Envelope
Intensity (a.u)
528 530 532 534 536
Binding Energy (eV)
Li 1s
Background
Envelope
Li-PTI-AIR Li1s
Intensity (a.u)
52 53 54 55 56 57 58
Binding Energy (eV)
Li-PTI-AIR Cl2p
Cl2p 1/2
Cl2p 3/2
Organic Cl2p
Background
Envelope
Intensity (a.u)
196 198 200 202 204
Binding Energy (eV)

XPS Analysis

Peak Assignment	Pos.	FWHM	L.Sh	Area	At%	Total%	STD
sp^3	284.84	1.58	LA(1.3, 243)	21587.92	7.12		
C in C−N−Hx	286.45	1.63	LA(1.3, 243)	12588.65	4.15		
C in N−C=N	287.93	1.58	LA(1.03, 1.24, 243)	72891.11	24.05	24.05	1.027
C1s Satelite 1	289.92	1.88	LA(1.3, 243)	7238.43	2.39		
C1s Satelite 2	292.81	3.52	LA(1.3, 243)	7496.19	2.47		
Cl 2p	198.22	1.55	LA(1.3, 243)	9093.26	1.31	2.04	0.9582
Cl 2p	199.83	1.66	LA(1.3, 243)	5085.45	0.73		
Cl 2p Satelite	203.51	2.75	LA(1.3, 243)	403.76	0.06		
Li 1s	55.2	1.75	LA(1.3, 243)	2120.57	12.32	12.32	0.8024
N in C=N−C	398.46	1.65	LA(1.03, 1.24, 243)	125115.52	22.93	31.66	0.9872
N in C−NH−C	400.21	1.62	LA(1.3, 243)	47623.52	8.73		
N1s Satelite 1	403.77	3.34	LA(1.3, 243)	17019.93	3.12		
N1s Satelite 2	406.16	2.64	LA(1.3, 243)	3436.77	0.63		
OH	531.65	1.81	LA(1.3, 243)	43601	4.91	4.91	0.9849
O1s	532.62	2.22	LA(1.3, 243)	45030.7	5.07		

Table 8: Spectral Features of Li-PTI-AIR

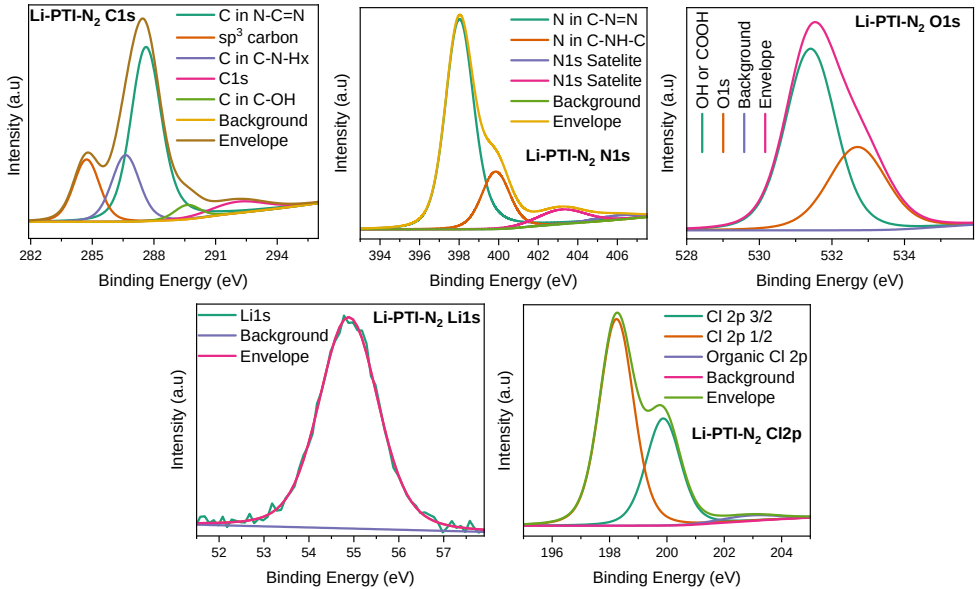
Li-PTI-N2 C1s
C in N-C=N
sp3 carbon
C in C-N-Hx
C1s
C in C-OH
Background
Envelope
Intensity (a.u)
282 285 288 291 294
Binding Energy (eV)
N in C-N=N
N in C-NH-C
N1s Satelite
N1s Satelite
Background
Envelope
Li-PTI-N2 N1s
Intensity (a.u)
394 396 398 400 402 404 406
Binding Energy (eV)
Li-PTI-N2 O1s
OH or COOH
O1s
Background
Envelope
Intensity (a.u)
528 530 532 534
Binding Energy (eV)
Li1s
Background
Envelope
Li-PTI-N2 Li1s
Intensity (a.u)
52 53 54 55 56 57
Binding Energy (eV)
Cl 2p 3/2
Cl 2p 1/2
Organic Cl 2p
Background
Envelope
Li-PTI-N2 Cl2p
Intensity (a.u)
196 198 200 202 204
Binding Energy (eV)

XPS Analysis

Peak Assignment	Pos.	FWHM	L.Sh	Area	At%	Total%	STD
sp^3	284.72	1.48	LA(1.3, 243)	19911.7	6.03		
C in C−N−Hx	286.62	1.59	LA(1.3, 243)	22915.37	6.94		
C in N−C=N	287.58	1.72	LA(1.03, 1.24, 243)	69329.88	20.98	20.98	1.075
C1s Satelite 1	289.62	1.47	LA(1.3, 243)	4514.95	1.37		
C1s Satelite 2	292.08	3.15	LA(1.3, 243)	7697.58	2.33		
Cl 2p	198.25	1.4	LA(1.3, 243)	19428.81	2.57	3.91	0.8894
Cl 2p	199.88	1.41	LA(1.3, 243)	10142.75	1.34		
Cl 2p Satelite	202.89	2.39	LA(1.3, 243)	892.85	0.12		
Li 1s	54.89	1.54	LA(1.3, 243)	3061.93	16.32	16.32	0.8519
N in C=N−C	397.98	1.66	LA(1.03, 1.24, 243)	148330.77	24.94	31.36	1.103
N in C−NH−C	399.85	1.67	LA(1.3, 243)	38153.66	6.42		
N1s Satelite 1	403.18	2.83	LA(1.3, 243)	16451.63	2.77		
N1s Satelite 2	405.96	2.74	LA(1.3, 243)	4714.67	0.79		
OH	531.41	1.63	LA(1.3, 243)	44820.42	4.63	4.63	0.8725
O1s	532.71	1.89	LA(1.3, 243)	23808.86	2.46		

Table 9: Spectral Features of Li-PTI-N_2

Valence Band XPS Analysis

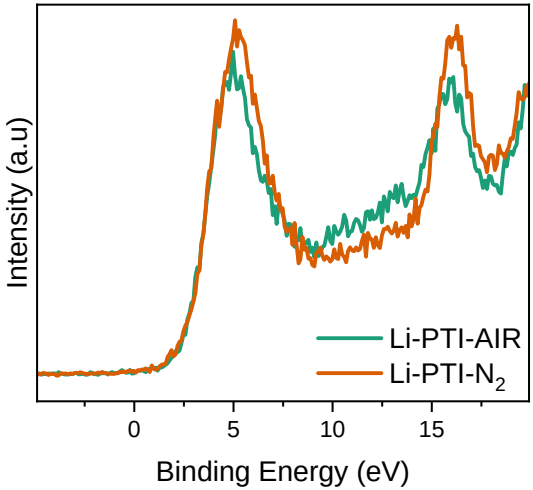

Valence Band XPS Analysis

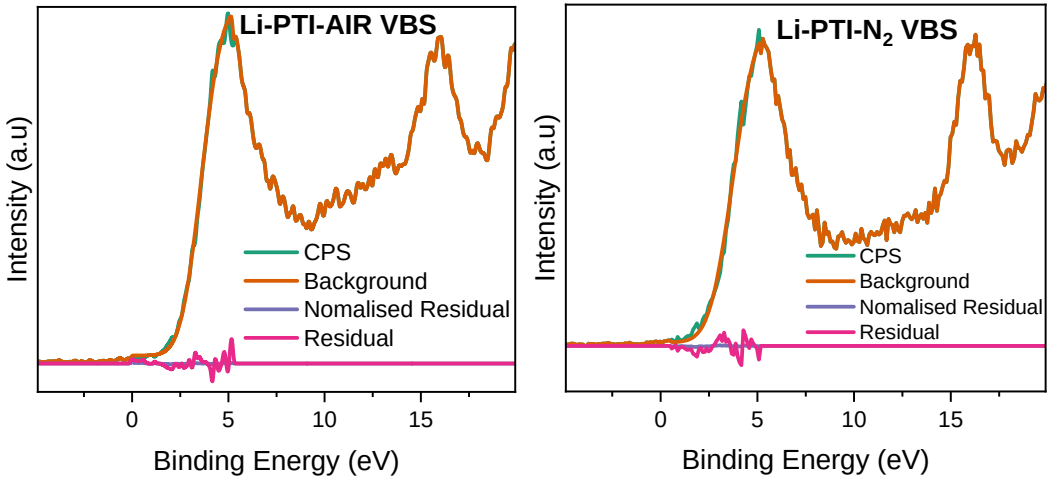

Derivative Valence Band XPS Analysis

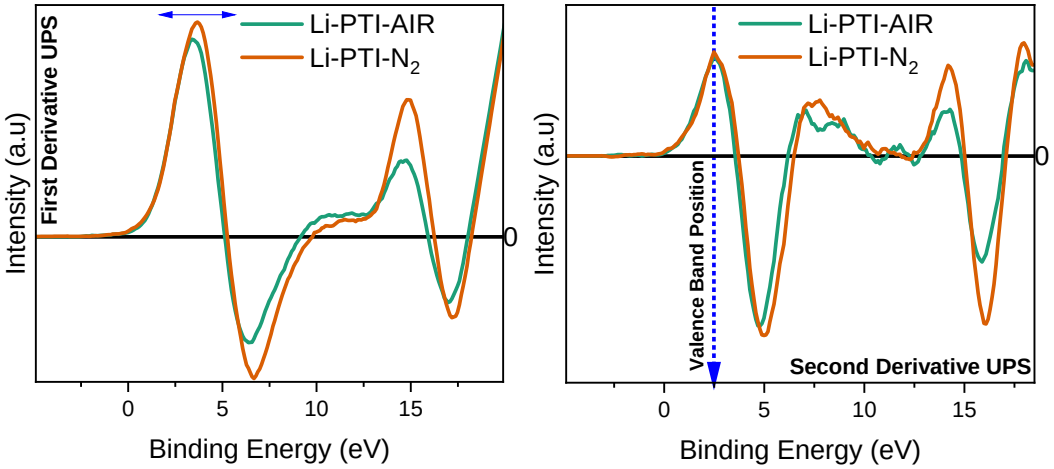

Valence Band XPS Analysis

	Highest Occupied Molecular Orbital (HOMO), eV				
Sample	**Second Derivative**	**Curve Fitting**			
		Position	**Original Value**	**FWHM**	**STD**
Li-PTI-AIR	2.48	2.41	2.4108	1.96	1.253
Li-PTI-N_2	2.48	2.39	2.3856	2.23	1.939

Energy Band Diagram Elucidation

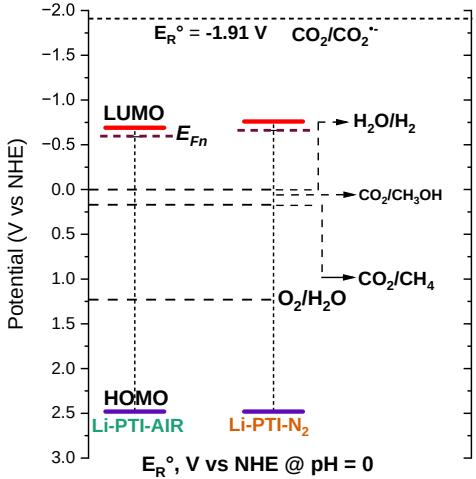

Energy Band Diagram Elucidation: pH Correction

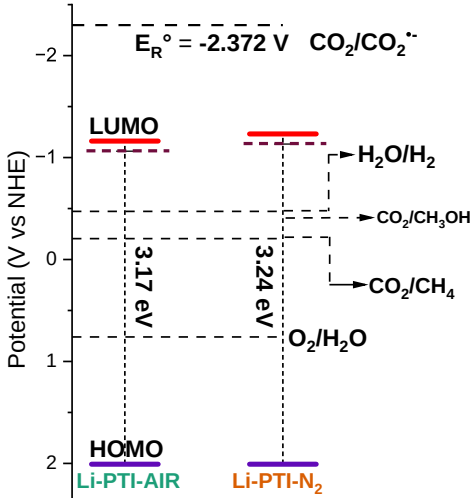

Band Position, Ionization Potential, and Electron Affinity

Sample	Bandgap	HOMO	LUMO	I.E	E.A	C	N	C/N
Li-PTI-AIR	3.17 eV	2.48 V	−0.69 V	6.92 eV	3.75 eV	25.05	31.66	0.7912
Li-PTI-N_2	3.24 eV	2.48 V	−0.76 V	6.92 eV	3.68 eV	20.98	31.36	0.6690

Table of Contents

Context

Synthesis of Melamine Cyanurate (CAM) Precursor

1. Eutectic synthesis using melamine cyanurate precursor:
   1. Preparation of a 1:1 mixture of melamine and cyanuric acid using Millipore water.
   2. Reflux and stirring of the mixture at 90 °C for 6 h.
   3. Cooling of the mixture followed by filtration to obtain melamine cyanurate crystals.
   4. Washing of the crystals with water and drying at 110 °C in a vacuum furnace overnight under 10^{-5} torr pressure.
2. Recrystallization of melamine cyanurate from an ethanol solution:
   1. Weighing of 0.5 g of melamine cyanurate powder and transferring it to a beaker.
   2. Addition of 50 mL of ethanol to the beaker and heating the solution on a hot plate until the melamine cyanurate dissolved.
   3. Constant stirring of the solution as it cooled.
   4. Filtration of the cooled solution through a piece of filter paper and transfer of the crystals to a Petri dish.
   5. Complete drying of the crystals.
3. Resulting product:
   1. Grounding of the crystals into a powder using a mortar and pestle.
   2. Storage of the powder in a 25 mL amber bottle labeled as CAM.

Synthesis of CAM-gCN

1. Recrystallization and sample preparation:
   1. Collection of recrystallized precursors.
   2. Grinding of the precursors in a mortar.
   3. Transfer of the ground precursors into an alumina boat with a lid using a spatula.
   4. Placement of the alumina crucible in a SIGMA Laboratory tubular furnace under N_2 atmosphere
   5. Heating for 4 h with a ramping rate of $2\,^{\circ}\mathrm{C\,min^{-1}}$ and a terminal temperature of 450 °C.
2. Post-heating process and storage:
   1. Transfer of the resulting fine yellow block of graphitic carbon nitride into a mortar.
   2. Grinding of the block well using a pestle.
   3. Transfer of the delicate yellow powder into a 25 mL storage amber glass vial with an airtight cap.
   4. Labeling of the vial as CAM-gCN.

Synthesis of CAM-gCN-$NiCl_2$-KCl

1. Experimental procedure for synthesis:
   1. Grinding of 2 g of recrystallized melamine cyanurate ($C_6H_9N_9O_3$) with 10 g of a nickel chloride and potassium chloride eutectic mixture (39.4:60.6 wt%) in a glove box under an inert atmosphere.
   2. Transfer of the resulting mixture into a Quarts boat with a lid.
   3. Introduction of the reaction mixture into a tubular furnace under a nitrogen atmosphere.
   4. Heating of the mixture at a ramping rate of $2\,^{\circ}C\,min^{-1}$ for 4 h until reaching a terminal temperature of 450 °C.
   5. Removal of the salt block from the reaction mixture through boiling distilled water washing and centrifugation at 10 000 rpm for 15 min.
   6. Drying of the obtained material in a vacuum oven at 110 °C overnight under a pressure of 10^{-5} torr.
2. Storage and labeling:
   1. Transfer of the resulting powder into a 25 mL amber bottle.
   2. Labeling of the bottle as CAM-gCN-$NiCl_2$-KCl.

Synthesis of CAM-gCN-$NiCl_2$-CsCl

1. Experimental procedure for synthesis:
   1. Grinding of 2 g of melamine cyanurate ($C_6H_9N_9O_3$), recrystallized from methanol, along with 10 g of a nickel chloride and caesium chloride eutectic mixture (50:50 wt
   2. Transfer of the resulting mixture into a Quarts boat with a lid.
   3. Introduction of the reaction mixture into a tubular furnace under a nitrogen atmosphere.
   4. Heating of the mixture at a ramping rate of 2 °C min^{-1} for 4 h until reaching a terminal temperature of 450 °C.
   5. Removal of the salt block from the reaction mixture through washing with boiling distilled water and centrifugation at 10 000 rpm for 15 min.
   6. Drying of the obtained material in a vacuum oven at 110 °C overnight under a pressure of 10^{-5} torr.
2. Storage and labeling:
   1. Transfer of the resulting powder into a 25 mL amber bottle.
   2. Labeling of the bottle as CAM-gCN-$NiCl_2$-CsCl.

X-ray Diffraction Analysis

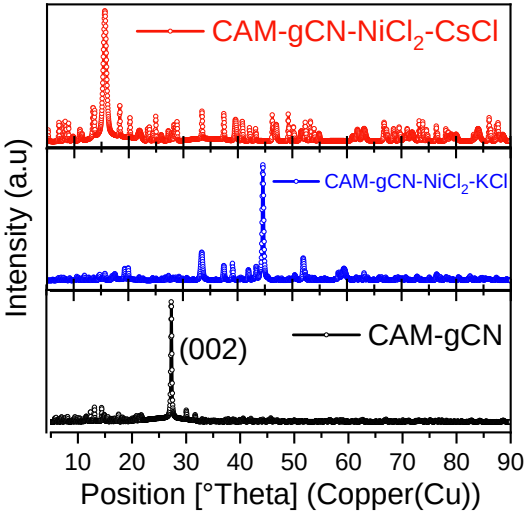

The B.E.T Surface Area

	B.E.T S.A	**C**
CAM-gCN	42.345	-623.684787
CAM-gCN-$NiCl_2$-CsCl	2.1652	-10.087368
CAM-gCN-$NiCl_2$-KCl	12.8343	-26.441754

Surface Area Analysis: BETSI vs. SESAMI Method

	Surface Area, m^2/g						
	B.E.T	**BETSI**	**SESAMI**	**C, SESAMI**	**qm, mol/kg**	**Pore Size, nm**	**t-plot M.A**
CAM-gCN	42.35	44	43.5	377.8	0.45	21.59	9.56
CAM-gCN-$NiCl_2$-CsCl	2.17	10	10.1	1002	0.10	104.76	18.85
CAM-gCN-$NiCl_2$-KCl	12.83	20	19.8	777.8	0.20	43.91	17.71

Physical Adsorption Characterization

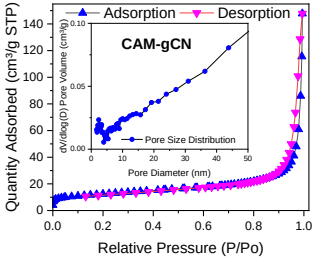

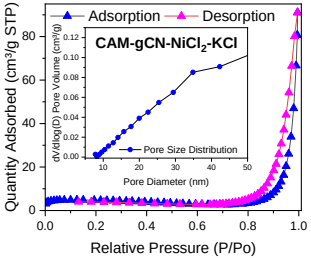

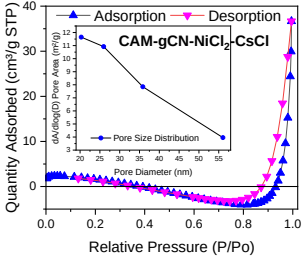

Surface Areas versus CH_4 Yield

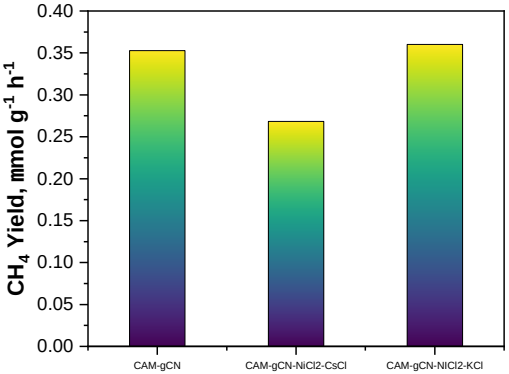

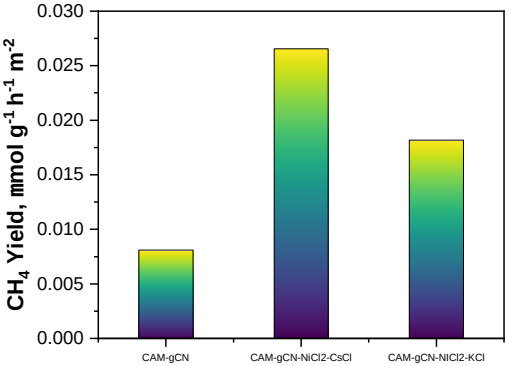

Surface Areas versus CH_3OH Yield

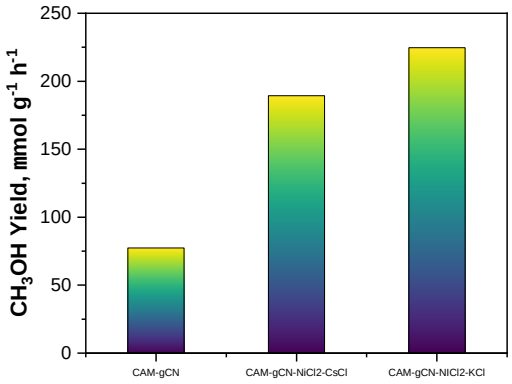

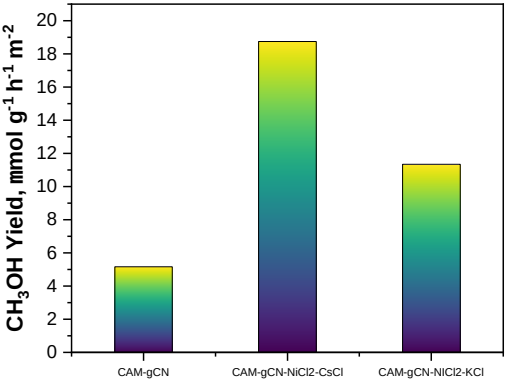

Surface Areas versus O_2 Yield

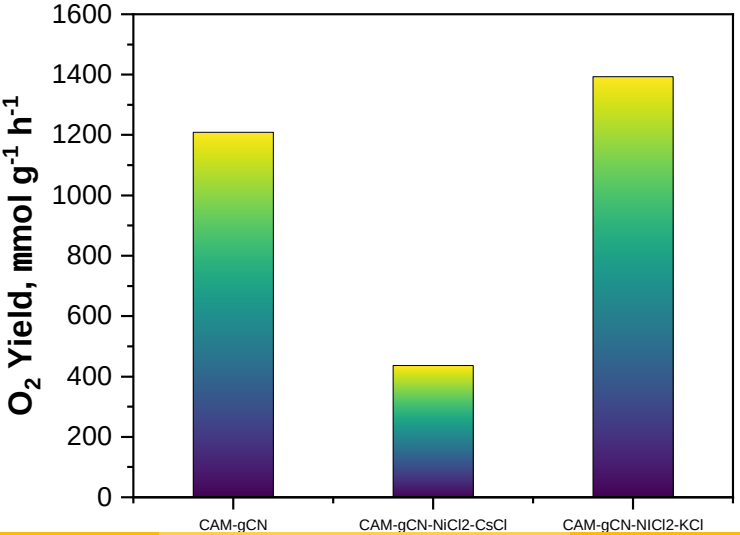

Derivative Isotherm Summation

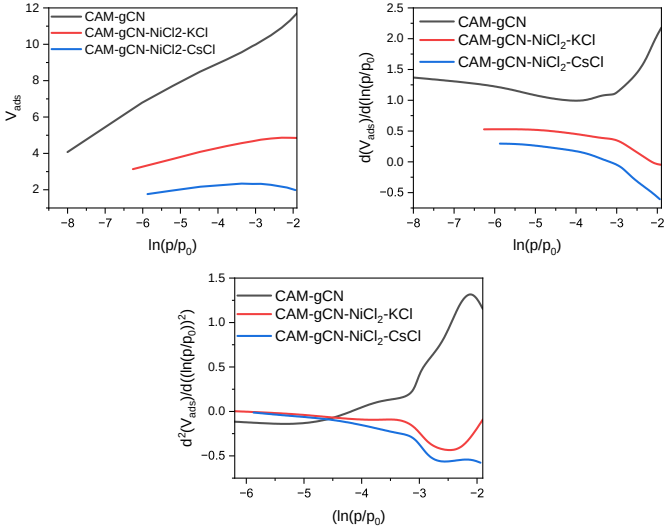

Derivative Isotherm Summation

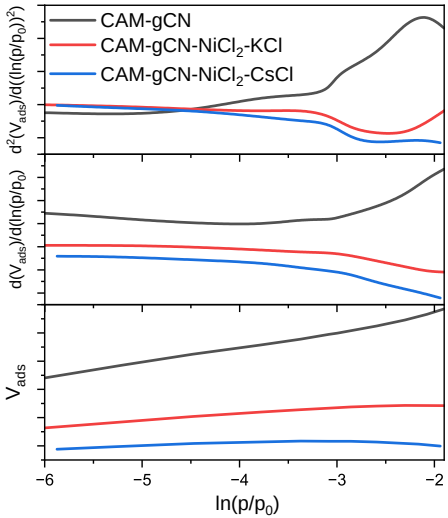

Field Emission Scanning Electron Microscopy (FESEM)

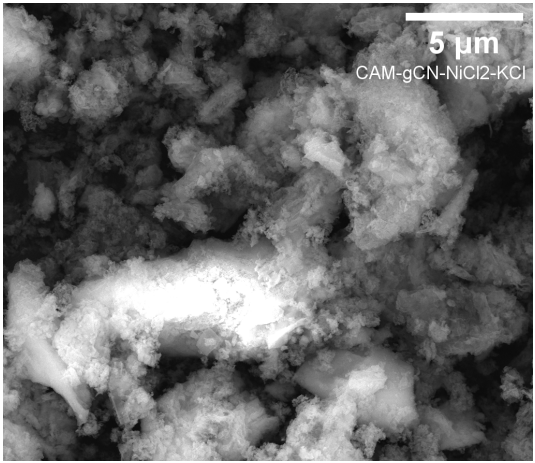

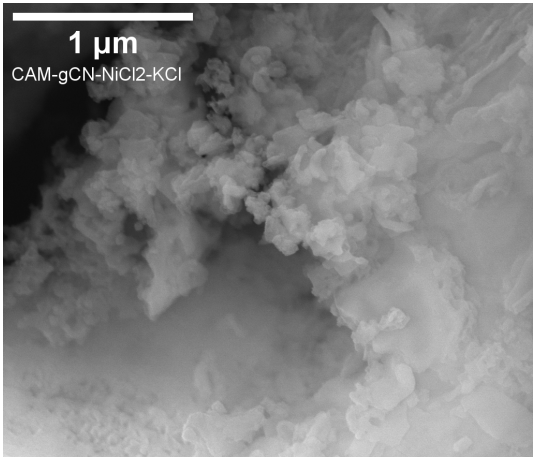

Field Emission Scanning Electron Microscopy (FESEM)

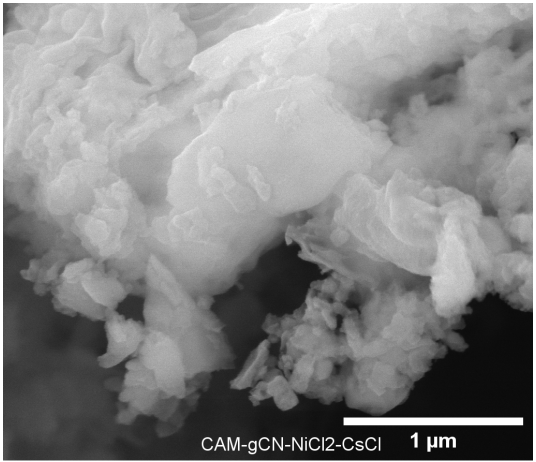

Energy-Dispersive X-ray Analysis (EDAX)

	Element	Weight %	MDL	Atomic %	Net Int.	Error %
CAM-gCN-$NiCl_2$-KCl	N K	27.9	1.81	32.6	40.2	14.5
	O K	15.9	0.72	16.3	55.0	13.6
	Cl K	7.1	0.12	3.3	374.8	4.0
	K K	0.1	0.14	0.0	2.7	62.6
	Ni K	17.5	0.39	4.9	250.3	3.6
CAM-gCN-$CsCl_2$-KCl	C K	25.9	2.05	37.9	40.5	14.7
	N K	24.9	1.66	31.3	40.8	14.5
	O K	17.6	0.65	19.4	71.7	13.2
	Cl K	10.0	0.12	4.9	565.8	3.8
	Ni K	21.4	0.39	6.4	333.7	3.3
	Cs L	0.3	0.48	0.0	3.8	56.9

Solid UV-Visible Spectroscopy

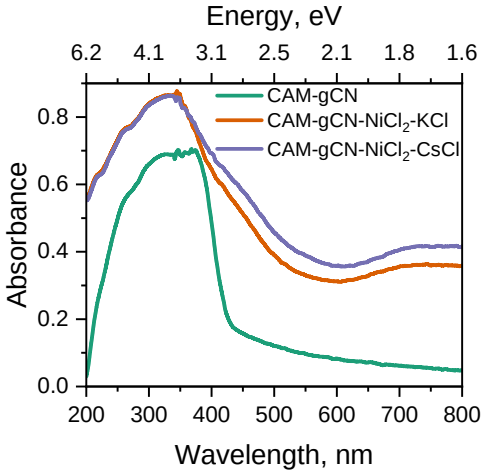

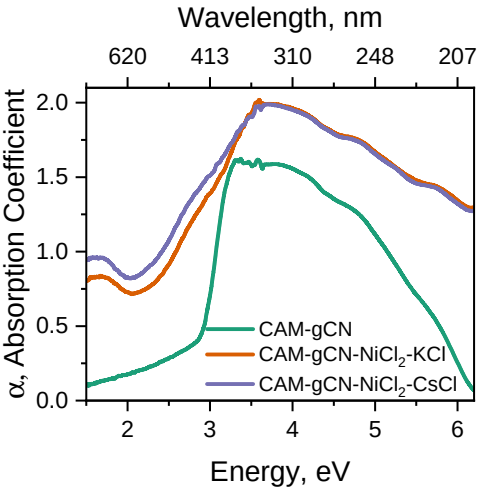

Tauc Plot Validation

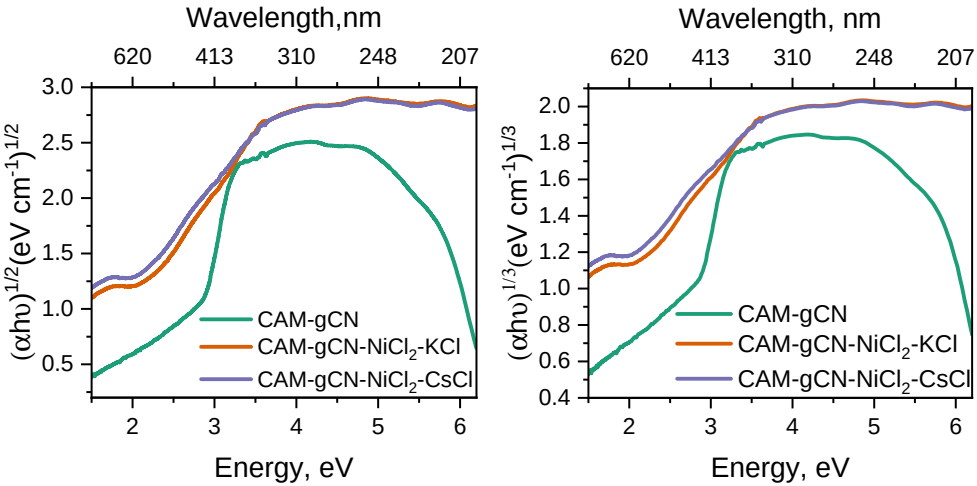

Tauc Plot Validation

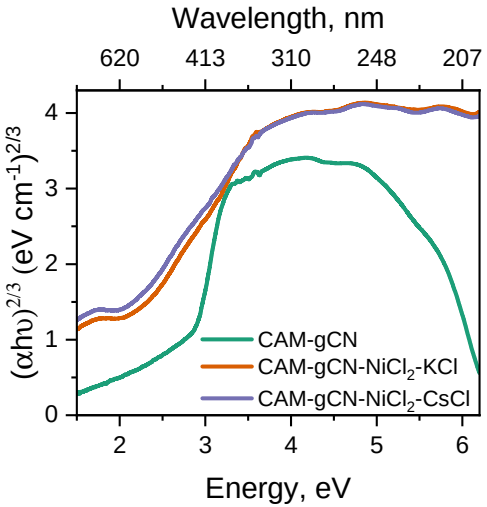

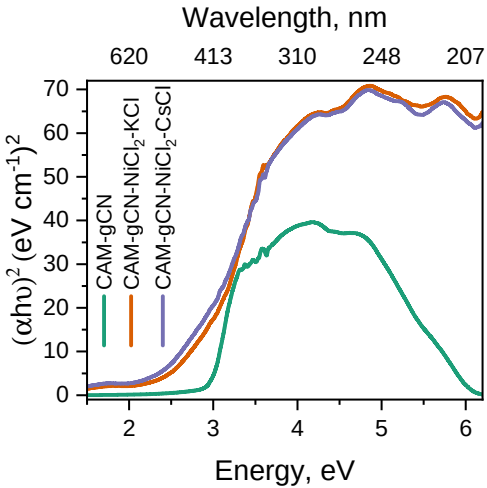

Derivative Tauc Plot

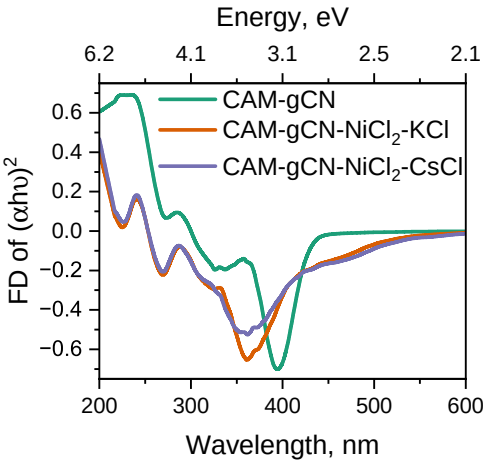

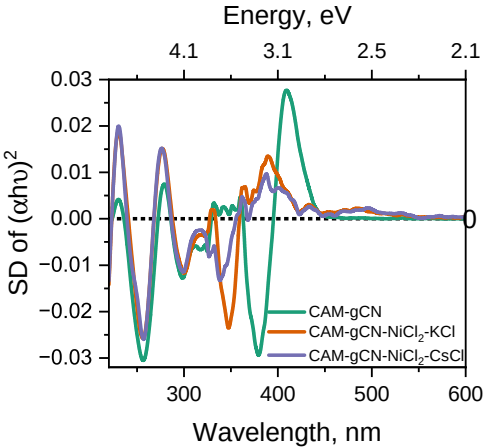

Derivative Tauc Plot Analysis

	Min	Intensity	Max	Intensity	D Parameter	S.A	Slope	D.P / S.A
CAM-gCN	379	-0.02948	409	0.02775	0.05723	43.5	377.8	0.001315632
CAM-gCN-$NiCl_2$-KCl	347	-0.02373	389	0.01358	0.03731	19.8	777.8	0.001884343
CAM-gCN-$NiCl_2$-CsCl	338	-1.33E-02	388	0.00978	0.02312	10.1	1002	0.002289109

Note: D.P = D parameter, difference between the maxima and minima, S.A= surface area, slope= B.E.T Slope from SESAMI Analysis

Urbach Plot

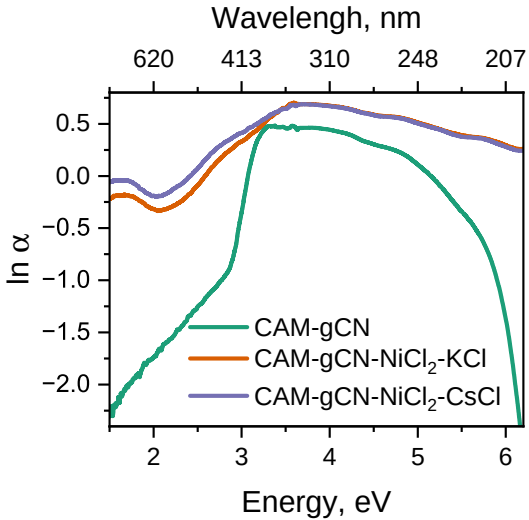
Wavelengh, nm
620
413
310
248
207
0.5
0.0
−0.5
−1.0
−1.5
−2.0
ln α
CAM-gCN
CAM-gCN-NiCl2-KCl
CAM-gCN-NiCl2-CsCl
2
3
4
5
6
Energy, eV

Diffuse Reflectance Spectroscopy

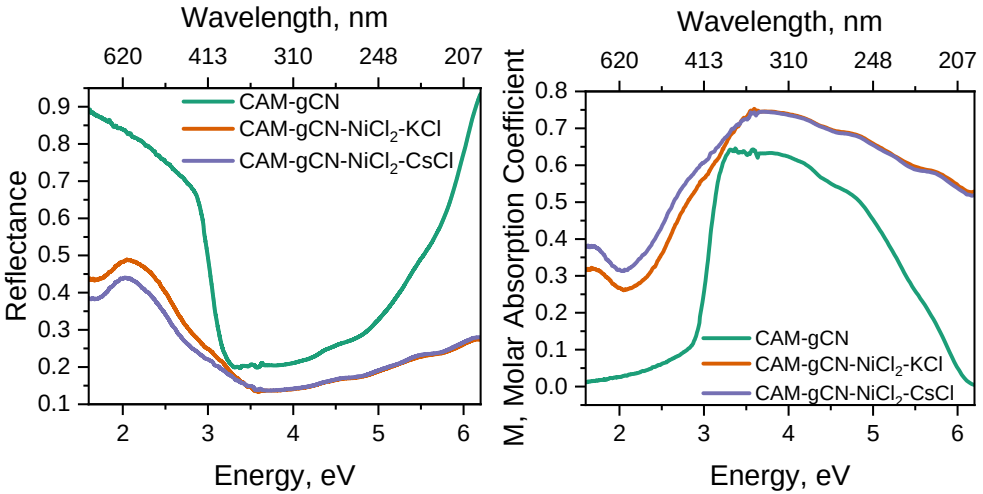

Diffuse Reflectance Spectroscopy

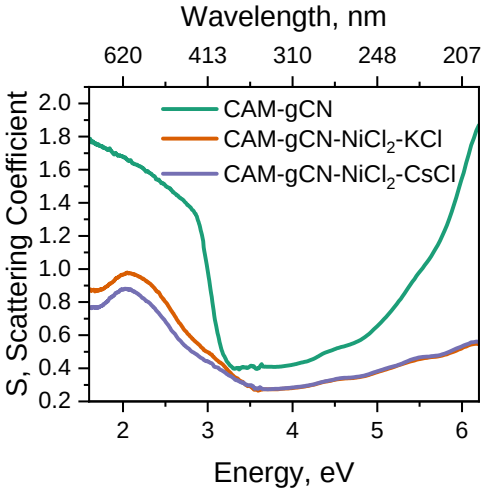

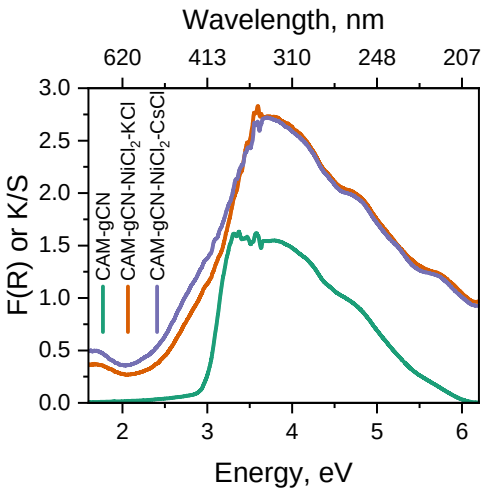

Kubelka-Monk Plots

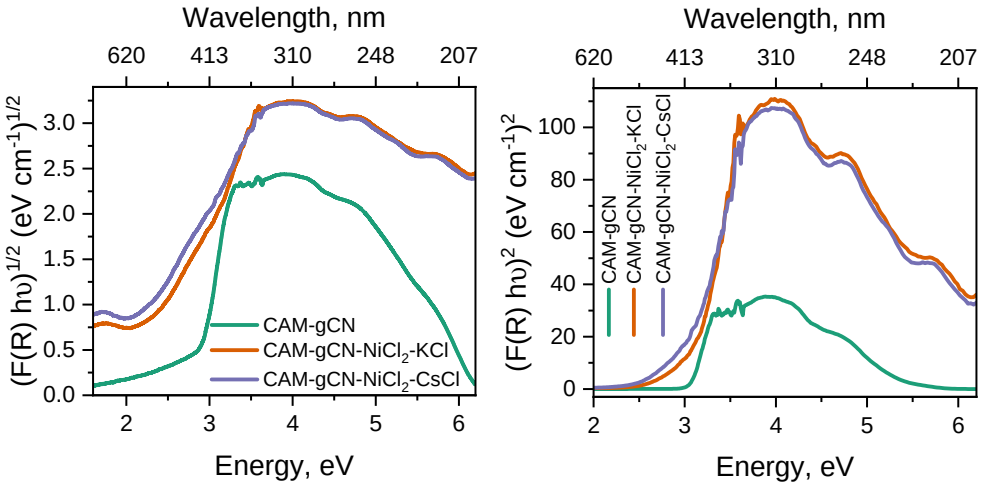

Derivative Kubelka-Monk Plots

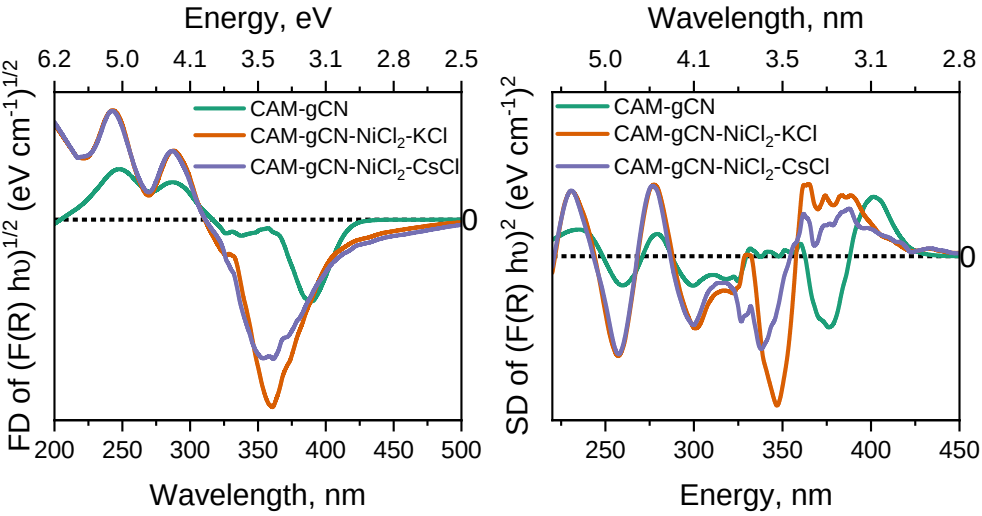

UV-Visible Diffuse Spectroscopy Analysis

Sample	Band Gap, eV						U.E meV	R.I
	Tauc Plot			K-M Plot				
	L.R	F.D	S.D	L.R	F.D	S.D	L.R	
CAM-gCN	2.96	3.14	3.03	3.06	3.19	3.08	229	2.3555
CAM-gCN-$NiCl_2$-KCl	2.82	3.42	3.19	3.43	3.12	3.4	1001	2.2564
CAM-gCN-$NiCl_2$-CsCl	2.66	3.42	3.2	2.98	3.43	3.2	1166	2.3163

L.R = Linear Regression; F.D = First Derivative; S.D = Second Derivative;
U.E= Urbach Energy; R.I= Refractive Index

Optical Conductivity

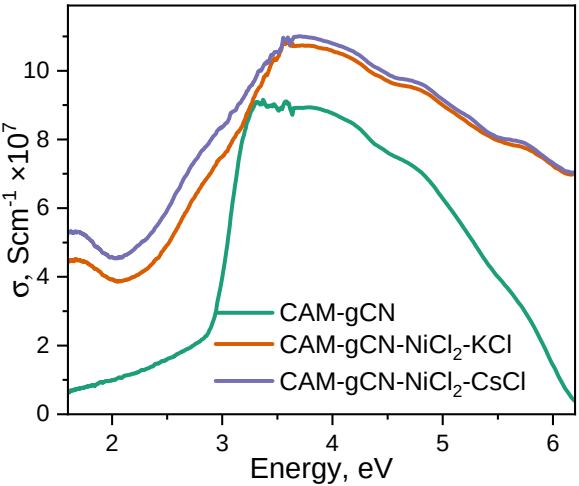

Derivative Diffuse Reflectance Spectroscopic Analysis

	Min	Intensity	Max	Intensity	D Parameter	S.A	Slope	D.P /S.A
CAM-gCN	376	-0.05251	401	0.04348	0.09599	43.5	377.8	0.002206667
CAM-gCN-$NiCl_2$-KCl	338	-0.06827	365	0.03192	0.12139	19.8	777.8	0.006130808
CAM-gCN-$NiCl_2$-CsCl	347	-0.11024	388	0.05312	0.14529	10.1	1002	0.014385149

Note: D.P = D parameter, difference between the maxima and minima, S.A= surface area, slope= B.E.T Slope from SESAMI Analysis

XPS Analysis

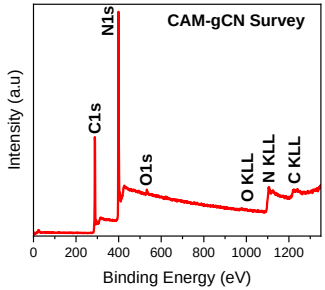
CAM-gCN Survey
N1s
C1s
O1s
O KLL
N KLL
C KLL
Intensity (a.u)
0
200
400
600
800
1000
1200
Binding Energy (eV)

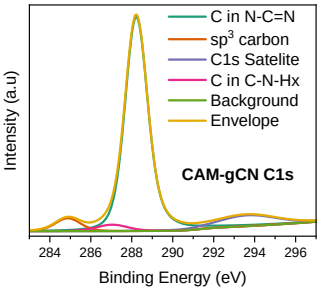
C in N-C=N
sp3 carbon
C1s Satelite
C in C-N-Hx
Background
Envelope
CAM-gCN C1s
Intensity (a.u)
284
286
288
290
292
294
296
Binding Energy (eV)

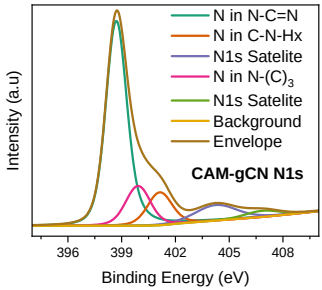
N in N-C=N
N in C-N-Hx
N1s Satelite
N in N-(C)3
N1s Satelite
Background
Envelope
CAM-gCN N1s
Intensity (a.u)
396
399
402
405
408
Binding Energy (eV)

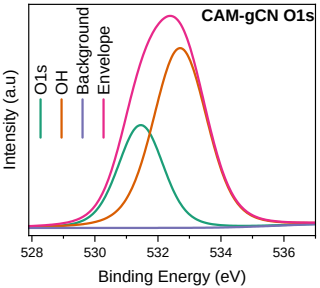
CAM-gCN O1s
O1s
OH
Background
Envelope
Intensity (a.u)
528
530
532
534
536
Binding Energy (eV)

Peak Assignment	Pos.	FWHM	L.Sh	Area	At%	Total%	STD
sp^3	284.88	1.45	LA(1.3, 243)	8946.39	2.26		
C in C−N−Hx	287.05	1.78	LA(1.3, 243)	5446.39	1.38		
C in N−C=N	288.19	1.28	LA(1.03, 1.24, 243)	139748.92	35.34	35.34	1.183
C1s Satelite 1	293.64	3.33	LA(1.3, 243)	17036.86	4.31		
N in C=N−C	398.67	1.36	LA(1.03, 1.24, 243)	251677.86	35.36	49.27	1.096
N in N−(C_3)	399.92	1.63	LA(1.3, 243)	54474.7	7.65		
N in C−N−Hx	401.13	1.61	LA(1.3, 243)	44595.35	6.26		
N1s Satelite 1	404.26	2.73	LA(1.3, 243)	35832.03	5.03		
N1s Satelite 2	406.84	2.31	LA(1.3, 243)	11858.5	1.67		
OH	531.46	1.69	LA(1.3, 243)	2802.28	0.24	0.24	0.8794
O1s	532.7	2	LA(1.3, 243)	5802.05	0.5		

Table 10: Spectral Features of CAM-gCN

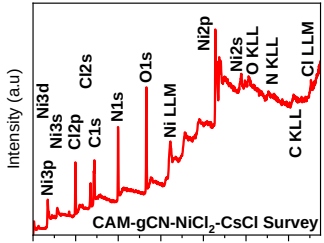
Intensity (a.u)
Ni3p
Ni3d
Ni3s
Cl2p
C1s
Cl2s
N1s
O1s
Ni LLM
Ni2p
Ni2s
O KLL
N KLL
C KLL
Cl LLM
CAM-gCN-NiCl2-CsCl Survey
0 200 400 600 800 1000 1200
Binding Energy (eV)

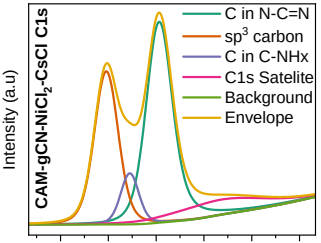
Intensity (a.u)
CAM-gCN-NiCl2-CsCl C1s
C in N-C=N
sp3 carbon
C in C-NHx
C1s Satelite
Background
Envelope
282 285 288 291 294 297
Binding Energy (eV)

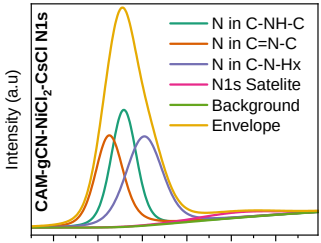
Intensity (a.u)
CAM-gCN-NiCl2-CsCl N1s
N in C-NH-C
N in C=N-C
N in C-N-Hx
N1s Satelite
Background
Envelope
396 398 400 402 404 406
Binding Energy (eV)

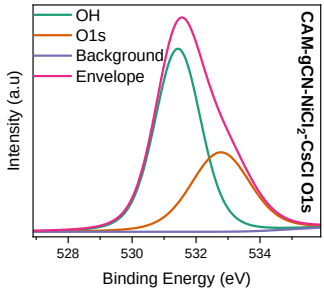
Intensity (a.u)
CAM-gCN-NiCl2-CsCl O1s
OH
O1s
Background
Envelope
528 530 532 534
Binding Energy (eV)

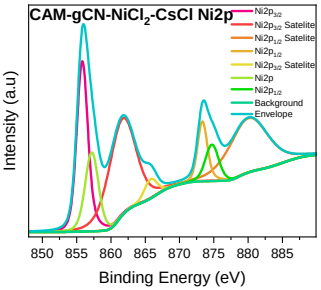
Intensity (a.u)
CAM-gCN-NiCl2-CsCl Ni2p
Ni2p3/2
Ni2p3/2 Satelite
Ni2p1/2 Satelite
Ni2p1/2
Ni2p3/2 Satelite
Ni2p
Ni2p1/2
Background
Envelope
850 855 860 865 870 875 880 885
Binding Energy (eV)

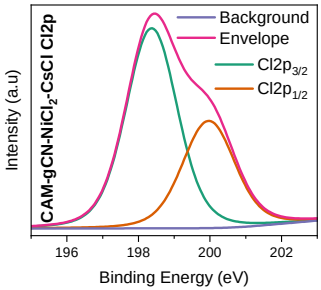
Intensity (a.u)
CAM-gCN-NiCl2-CsCl Cl2p
Background
Envelope
Cl2p3/2
Cl2p1/2
196 198 200 202
Binding Energy (eV)

Peak Assignment	Pos.	FWHM	L.Sh	Area	At%	Total%	STD
sp^3	284.87	1.77	LA(1.3, 243)	26175.63	13.05		
C in C−N−Hx	286.35	1.35	LA(1.3, 243)	6665.81	3.32		
C in N−C=N	288.15	1.91	LA(1.03, 1.24, 243)	39659.82	19.78	19.78	0.9326
C1s Satelite 1	292.07		LA(1.3, 243)	9559.53	4.77		
N in C=N−C	398.48	1.45	LA(1.03, 1.24, 243)	22605.93	6.26	20.72	0.918
N in C−NH−C	399.16	1.34	LA(1.3, 243)	24898.56	6.9		
N1s in C−N−Hx	400.08	1.93	LA(1.3, 243)	27305.05	7.56		
N1s Satelite	404.33	4.28	LA(1.3, 243)	3729.92	1.03		
Ni 2p 3/2	855.78	1.88	LA(1.03, 1.24, 243)	76375.89	1.72	3.58	0.9357
Ni 2p 3/2	857.21	2.3	LA(1.3, 243)	40287.69	0.91		
Ni 2p 3/2 Satelite	861.62	4.66	LA(1.3, 243)	100169.43	2.25		
Ni 2p 3/2 Satelite	865.79	2.2	LA(1.3, 243)	9442.57	0.21		
Ni 2p 1/2	873.3	1.66	LA(1.03, 1.24, 243)	23676.55	0.53		
Ni 2p 1/2	874.73	2.29	LA(1.3, 243)	18521.18	0.42		
Ni 2p 1/2 Satelite	880.03	6.68	LA(1.3, 243)	80807.16	1.82		
OH	531.43	1.7	LA(1.3, 243)	66218.8	11.27	11.27	1.152
O1s	532.77	2.19	LA(1.3, 243)	36937.88	6.29		
Cl 2p	198.37	1.69	LA(1.3, 243)	35288.42	7.7	11.92	1.023
Cl 2p	199.97	1.73	LA(1.3, 243)	19333.42	4.22		

Table 11: Spectral Features of CAM-gCN-$NiCl_2$-CsCl

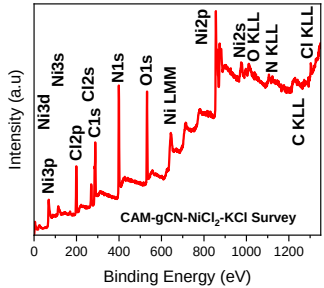
Intensity (a.u)
Ni3p
Ni3d
Ni3s
Cl2p
C1s
Cl2s
N1s
O1s
Ni LMM
Ni2p
Ni2s
O KLL
N KLL
Cl KLL
C KLL
CAM-gCN-NiCl2-KCl Survey
0 200 400 600 800 1000 1200
Binding Energy (eV)

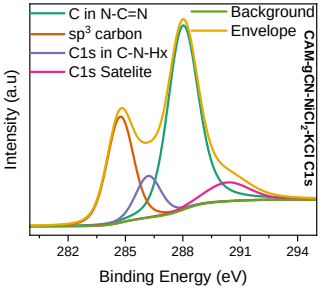
C in N-C=N
sp3 carbon
C1s in C-N-Hx
C1s Satelite
Background
Envelope
CAM-gCN-NiCl2-KCl C1s
Intensity (a.u)
282 285 288 291 294
Binding Energy (eV)

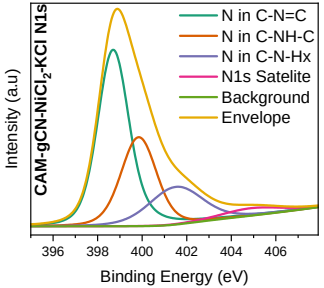
N in C-N=C
N in C-NH-C
N in C-N-Hx
N1s Satelite
Background
Envelope
CAM-gCN-NiCl2-KCl N1s
Intensity (a.u)
396 398 400 402 404 406
Binding Energy (eV)

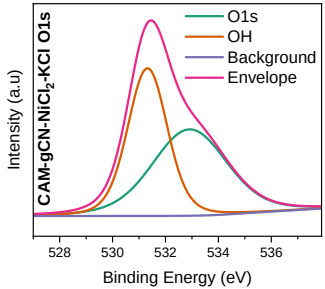
O1s
OH
Background
Envelope
CAM-gCN-NiCl2-KCl O1s
Intensity (a.u)
528 530 532 534 536
Binding Energy (eV)

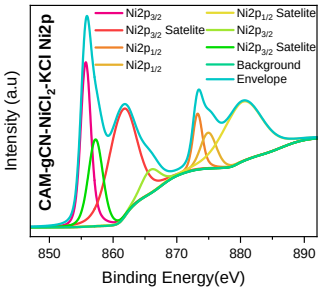
Ni2p3/2
Ni2p3/2 Satelite
Ni2p1/2
Ni2p1/2
Ni2p1/2 Satelite
Ni2p3/2
Ni2p3/2 Satelite
Background
Envelope
CAM-gCN-NiCl2-KCl Ni2p
Intensity (a.u)
850 860 870 880 890
Binding Energy(eV)

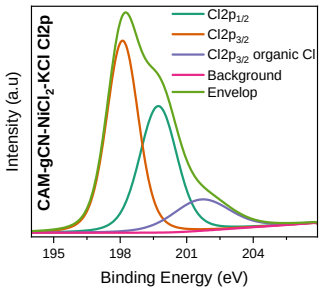
Cl2p1/2
Cl2p3/2
Cl2p3/2 organic Cl
Background
Envelop
CAM-gCN-NiCl2-KCl Cl2p
Intensity (a.u)
195 198 201 204
Binding Energy (eV)

Peak Assignment	Pos.	FWHM	L.Sh	Area	At%	Total%	STD
sp^3	284.73	1.62	LA(1.3, 243)	22193.62	9.77		
C in C-N-Hx	286.19	1.56	LA(1.3, 243)	8360.15	3.68		
C in N-C=N	287.97	1.84	LA(1.03, 1.24, 243)	46787.5	20.61	20.61	0.9505
C1s Satelite 1	290.34	2.72	LA(1.3, 243)	6605.52	2.91		
N in C=N-C	398.67	1.63	LA(1.03, 1.24, 243)	62371.5	15.26	28.76	0.9694
N in C-NH-C	399.85	1.87	LA(1.3, 243)	33797.03	8.27		
N1s in C-N-Hx	401.52	2.8	LA(1.3, 243)	21389.26	5.23		
N1s Satelite 2	404.86	3.14	LA(1.3, 243)	4748.98	1.16		
Ni 2p 3/2	855.67	1.87	LA(1.03, 1.24, 243)	68766.7	1.37	3.2	0.9221
Ni 2p 3/2	857.25	2.69	LA(1.3, 243)	48578.09	0.96		
Ni 2p 3/2 Satelite	861.47	5.11	LA(1.3, 243)	116346.18	2.31		
Ni 2p 3/2 Satelite	865.84	3.5	LA(1.3, 243)	17305.37	0.34		
Ni 2p 1/2	873.23	1.74	LA(1.03, 1.24, 243)	21755.92	0.43		
Ni 2p 1/2	874.94	2.95	LA(1.3, 243)	21996.04	0.44		
Ni 2p 1/2 Satelite	880.29	7.29	LA(1.3, 243)	90494.99	1.8		
OH	531.32	1.76	LA(1.3, 243)	48099.66	7.23	7.23	0.9721
O1s	532.91	3.32	LA(1.3, 243)	53016.83	7.97		
Cl 2p	198.11	1.68	LA(1.3, 243)	25696.39	4.95	8.81	0.9985
Cl 2p	199.72	1.99	LA(1.3, 243)	20016.17	3.86		
Cl 2p	201.68	3	LA(1.3, 243)	7464.45	1.44		

Table 12: Spectral Features of CAM-gCN-$NiCl_2$-KCl

Possible Structure

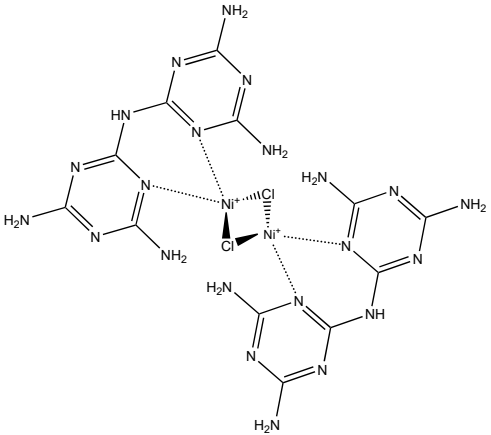

Potential coordination environment of a nickel cation with melam as bidentate ligand. Nickel is sharing two chloride ligands, thus formally exhibiting the oxidation state $+1$.

Possible Structures

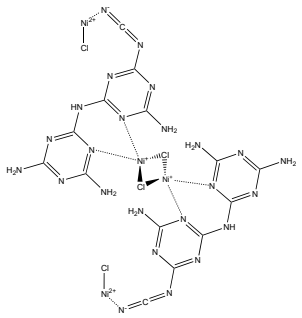

(a)

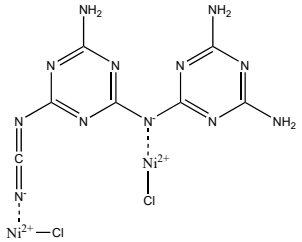

(b)

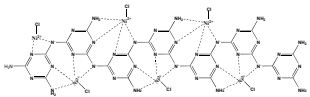

(c)

Hypothetical structures of Ni-CNx, assuming a molecular (a-b) and an oligomeric (c) arrangement of subunits. The melam units in (a) feature a coordinative and ionic bond towards nickel with oxidation states of $+1$ and $+2$, respectively. In (b) the melam is negatively charged featuring only ionic bonds and ox. state $+2$. (c) In the oligomeric form only ionic bonds persist; with nickel in ox. state $+2$.

Valence Band XPS Analysis

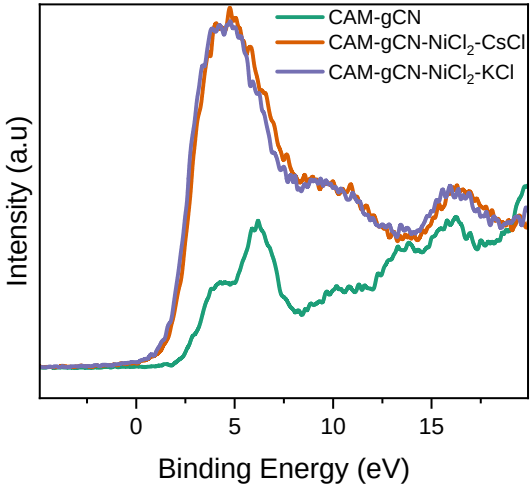

Valence Band XPS Analysis

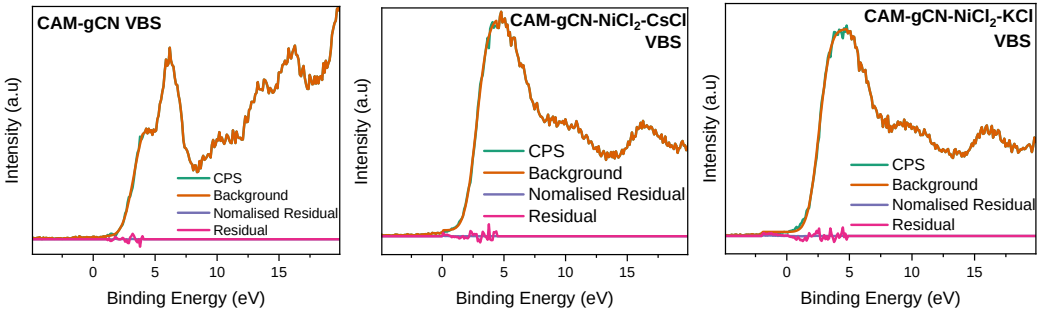

Derivative Valence Band XPS Analysis

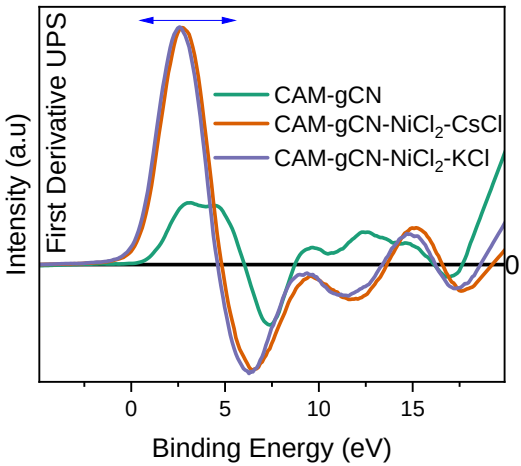

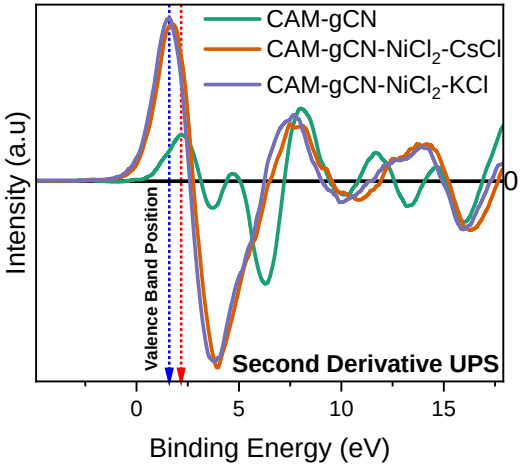

Valence Band XPS Analysis

	Highest Occupied Molecular Orbital (HOMO), eV				
Sample	**SD**	**Curve Fitting**			
		Position	**Original Value**	**FWHM**	**STD**
CAM-gCN	2.18	2.28	2.2832	1.53	1.368
CAM-gCN-$NiCl_2$-CsCl	1.78	1.74	1.7359	1.74	1.35
CAM-gCN-$NiCl_2$-KCl	1.58	1.57	1.5701	1.67	1.818

Energy Band Diagram Elucidation

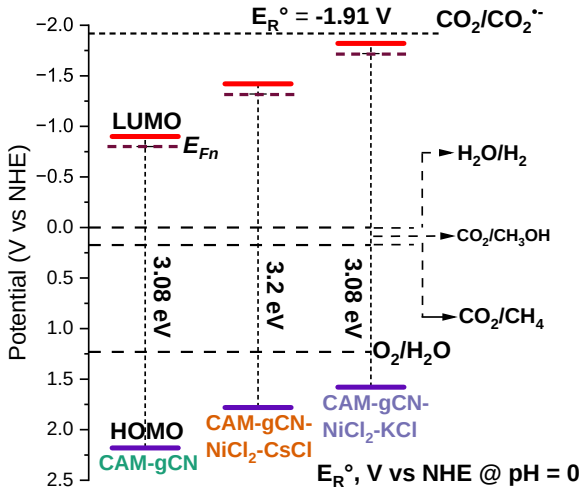

Energy Band Diagram Elucidation: pH Correction

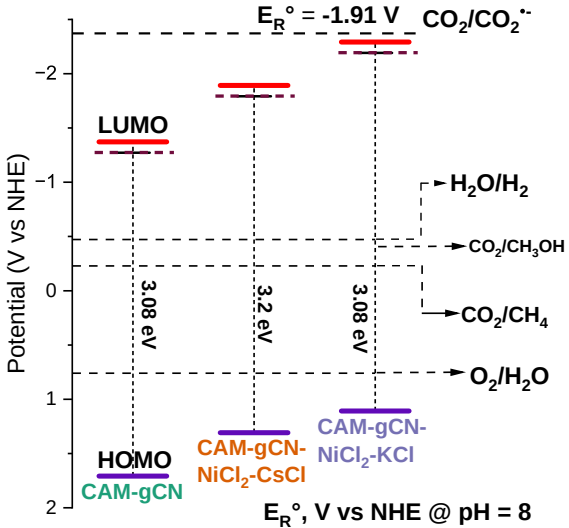

Band Position, Ionization Potential, and Electron Affinity

Sample	Bandgap	HOMO	LUMO	I.E	E.A	C	N	C/N
CAM-gCN	3.08 eV	2.18 V	−0.9 V	6.62 eV	3.54 eV	35.34	49.27	0.7173
CAM-gCN-$NiCl_2$-CsCl	3.2 eV	1.78 V	−1.42 V	6.22 eV	3.02 eV	19.78	20.72	0.9546
CAM-gCN-$NiCl_2$-KCl	3.08 eV	1.58 V	−1.82 V	6.02 eV	2.62 eV	20.61	28.76	0.7166

Publications

1. N. Hariprasad, SG Anju, EP Yesodharan, Sunlight induced removal of Rhodamine B from water through semiconductor photocatalysis: effects of adsorption, reaction conditions and additives. *Res. J. Mater. Sci*, 2320:6055, 2013.
2. N. Hariprasad, B. Viswanathan, Y. Suguna, Photocatalytic Reduction of Carbon Dioxide: Issues and Prospects. *Current Catalysis*, 5(2):79–107, 2016.
3. N. Hariprasad, M. V. Harindranathan Nair, B. Viswanathan, On the current status of the mechanistic aspects of photocatalytic reduction of carbon dioxide. *Indian Journal of Chemistry A*, 56(March 2017):251-269, 2017.
4. N. Hariprasad, B. Viswanathan, K.R. Krishnamurthy, M.V. Harindranathan Nair, Understanding Reaction Mechanism in Photon-Assisted Reduction of Carbon Dioxide. In *Photocatalytic Nanomaterials for Environmental Applications*, volume 27, pages 175-210. Materials Research Foundations, 2018.
5. N. Hariprasad, B. Viswanathan, K.R. Krishnamurthy, M.V. Harindranathan Nair, Hydrogen from photo-catalytic water splitting. In *Solar Hydrogen Production: Processes, Systems and Technologies*, volume 1, pages 419–486. Academic Press, Elsevier, 2019.

Publications

1. N. Hariprasad, M. V. Harindranathan Nair, B. Viswanathan, Revisiting the Fundamentals of Photon-Assisted Reduction of Carbon Dioxide: Insights into the Interfacial Reactions and Electron Transfer Mechanism. *Battery*, Special Issue: Energy Conversion and Storage: Recent Advances and Prospects, Invited Review Under Preparation
2. N. Hariprasad, M. V. Harindranathan Nair, B. Viswanathan, Unveiling the Synthesis Mechanisms of Carbon Nitride and its Derivatives. *J. Mater. Chem. C*, Invited Review

Conferences

1. A.A.B. Kirali, N. Hariprasad, B. Viswanathan, B. Marimuthu, Sucrose Conversion to Value-Added Products Using Metal-Supported Graphitic Carbon Nitride Surfaces, 3^{rd} International Conference On Recent Trends In Analytical Chemistry (ICORTAC-2023), University of Madras, June 26-28, 2023.
2. N. Hariprasad, M. V. Harindranathan Nair, B. Viswanathan, *Photocatalytic Reduction of Carbon Dioxide on Graphitic Carbon Nitride Surfaces*, Fourth International Conference on Advance Oxidation Process, BITS-Pilani K K Birla Goa Campus, Goa, December 17-20, 2016.
3. N. Hariprasad, B. Viswanathan, K.R. Krishnamurthy, M.V. Harindranathan Nair, *On the Role of Surface Functionalities in the Photon-Assisted Reduction of Carbon Dioxide over Graphitic Carbon Nitride (g-C_3N_4) Surfaces*, Conference on Advances in Catalysis for Energy and Environment, Tata Institute of Fundamental Research, Mumbai, January 10-12, 2018.
4. N. Hariprasad, B. Viswanathan, K.R. Krishnamurthy, M.V. Harindranathan Nair, *Photon-assisted reduction of carbon dioxide on graphitic carbon nitride surfaces*, 23^{rd} National Symposium on Catalysis (CATSYMP-23), Applied Catalysis in emerging Technologies for Chemicals, January 17-19, 2018, Catalysis Society of India-Bengaluru Chapter.
5. Hariprasad N., Anju S.G., Yesodharan E.P. and Suguna Yesodharan, *Sunlight Induced Removal of Rhodamine B from Water through Semiconductor Photocatalysis: Effects of Adsorption, Reaction Conditions and Additives*, 1st International Science Congress (ISC-2011) on Science and Technology for Sustainable Development, December 8-9, 2012, Bon Maharaj Engineering College, Vrindavan, Mathura, U.P, India.

Table of Contents

Thank you for your attention! Any questions?